Unclassified

SECURITY CLASSIFICATION OF THIS PAGE (When Data Entered)

AD-A158 884

DTIC FILE COPY

REPORT DOCUMENTATION PAGE

READ INSTRUCTIONS BEFORE COMPLETING FORM

1. REPORT NUMBER: N00014-85-C-0141-TR5

2. GOVT ACCESSION NO.

3. RECIPIENT'S CATALOG NUMBER

4. TITLE (and Subtitle): ACOUSTICAL SCATTERING FROM AN ELASTIC SPHERE IN WATER: SURFACE WAVE GLORY, RESONANCES, AND THE SOMMERFELD-WATSON TRANSFORMATION FOR AMPLITUDES

5. TYPE OF REPORT & PERIOD COVERED: Technical Report

6. PERFORMING ORG. REPORT NUMBER

7. AUTHOR(s): Kevin L. Williams

8. CONTRACT OR GRANT NUMBER(s): N00014-85-C-0141 and N00014-80-C-0838

9. PERFORMING ORGANIZATION NAME AND ADDRESS:
Department of Physics
Washington State University
Pullman, WA 99164-2814

10. PROGRAM ELEMENT, PROJECT, TASK AREA & WORK UNIT NUMBERS:
Program Element: 61153N
Task Area: RR011-08-01
Work Unit: NR384-934

11. CONTROLLING OFFICE NAME AND ADDRESS:
Physics Division Office (Code 412)
Office of Naval Research
Arlington, VA 22217

12. REPORT DATE: August 1985

13. NUMBER OF PAGES: 161 + xi

14. MONITORING AGENCY NAME & ADDRESS (if different from Controlling Office)

15. SECURITY CLASS. (of this report): Unclassified

15a. DECLASSIFICATION/DOWNGRADING SCHEDULE

16. DISTRIBUTION STATEMENT (of this Report)

Approved for public release; distribution unlimited

17. DISTRIBUTION STATEMENT (of the abstract entered in Block 20, if different from Report)

18. SUPPLEMENTARY NOTES

Doctoral dissertation of K. L. Williams completed August, 1985. Chapters 2 and 3 are to appear in the Journal of the Acoustical Society of America as papers co-authored by P. L. Marston.

19. KEY WORDS (Continue on reverse side if necessary and identify by block number)

Acoustic Scattering, Rayleigh Waves, Resonance Scattering Theory, Backscattering, Sommerfeld-Watson Transformations, Inverse Scattering, Sonar Calibration, Physical Acoustics, Underwater Acoustics, Computer Programs

20. ABSTRACT (Continue on reverse side if necessary and identify by block number)

See reverse side.

DTIC ELECTE SEP 9 1985 S D

DD FORM 1 JAN 73 1473 EDITION OF 1 NOV 65 IS OBSOLETE
S/N 0102-LF-014-6601

Unclassified

SECURITY CLASSIFICATION OF THIS PAGE (When Data Entered)

20. The scattering of acoustical waves from fluid-load elastic spheres with $10 < ka < 100$ (where k is the wavenumber of the acoustic wave in the liquid and a the radius of the sphere) is studied. The main emphasis is on understanding the scattered pressure near backscattering. By carrying out a Sommerfeld-Watson Transformation (SWT) it is shown that this pressure includes contributions from specular reflection, transmitted bulk waves, and surface waves. It is shown experimentally that surface wave contributions to near backscattering display a J_0 Bessel function angular dependence characteristic of weak axial focusing along the backscattered direction; i.e., glory scattering. This focusing is modeled by alternate methods which agree and which complement each other. One method allows a simple picture of the glory phenomena while the others (which includes the SWT) are more mathematically rigorous. The absolute value of individual Rayleigh and whispering gallery surface wave contributions is found by this modeling to be equal to $A J_0(kb\gamma)$ ~~In this expression~~ γ is the angle relative to backscattering and b and A are parameters which depend on the surface wave contribution being examined and are determined by the models. The theoretical results ~~for A and b~~ are tested experimentally using the Rayleigh surface wave contribution to scattering from a tungsten carbide sphere. The SWT results are also used to find the far field backscattering pressure as a function of ka. These results ~~in turn~~ are used to better understand and interpret the recently developed Resonance Scattering Theory (RST) as applied to acoustical scattering. It is shown that surface wave contributions to backscattering may be summed in a way analogous to the frequency response of a Fabry-Perot resonator.

ACOUSTICAL SCATTERING FROM AN ELASTIC SPHERE IN WATER: SURFACE WAVE GLORY, RESONANCES, AND THE SOMMERFELD-WATSON TRANSFORMATION FOR AMPLITUDES

By

KEVIN LEE WILLIAMS

A dissertation submitted in partial fulfillment of
the requirements for the degree of

DOCTOR OF PHILOSOPHY

Accession For
NTIS GRA&I X
DTIC TAB
Unannounced
Justification
Distribution
Availability Codes
Avail and/or
Dist Special
A-1

WASHINGTON STATE UNIVERSITY
Department of Physics

August 1985

DTIC
COPY
INSPECTED

85 09 06 046

To the Faculty of Washington State University:

The members of the Committee appointed to examine the dissertation of KEVIN LEE WILLIAMS find it satisfactory and recommend that it be accepted.

Chair

Acknowledgments

I would like to express my gratitude to the three professors who have most influenced my current abilities in physics and/or viewpoint on physicists: Professor Philip L. Marston, Professor James L. Park, Professor George E. Duvall. I am especially indebted to Professor Marston, my thesis advisor. He has a special combination of theoretical and experimental talents which he is very willing to share with his students. On the other hand, he has allowed me the freedom to attack problems in my own way. It is for this willingness to share but care not to interfere that I thank him most. I thank Professor Park for helping me realize, through his excellent classroom instruction and discussions, that physics is indeed a human creation. Finally, I thank Professor Duvall for forcing me more than once to ask myself whether I really understood.

I thank the Office of Naval Research for the financial support which allowed the research of this dissertation to be carried out.

ACOUSTICAL SCATTERING FROM AN ELASTIC SPHERE IN WATER: SURFACE WAVE GLORY, RESONANCES, AND THE SOMMERFELD-WATSON TRANSFORMATION FOR AMPLITUDES

Abstract

by Kevin Lee Williams, Ph.D.
Washington State University, August 1985

Chair: Philip L. Marston

The scattering of acoustical waves from fluid-load elastic spheres with $10 < ka < 100$ (where k is the wavenumber of the acoustic wave in the liquid and a the radius of the sphere) is studied. The main emphasis is on understanding the scattered pressure near backscattering. By carrying out a Sommerfeld-Watson Transformation (SWT) it is shown that this pressure includes contributions from specular reflection, transmitted bulk waves, and surface waves. It is shown experimentally that surface wave contributions to near backscattering display a J_0 Bessel function angular dependence characteristic of weak axial focusing along the backscattered direction; i.e., glory scattering. This focusing is modeled by alternate methods which agree and which complement each other. One method allows a simple picture of the glory phenomena while the others (which includes the SWT) are more mathematically rigorous. The absolute value of individual Rayleigh and whispering gallery surface wave contributions is found by this modeling to be equal to $A\,J_0(kb\gamma)$. In this expression γ is the angle relative to backscattering and b and A are parameters which depend on the surface wave contribution being examined and are determined by the models. The theoretical results for A and b are tested experimentally using the Rayleigh surface wave contribution to scattering from a tungsten carbide sphere. The SWT results are also used to find the far field backscattering pressure as a

function of ka. These results in turn are used to better understand and interpret the recently developed Resonance Scattering Theory (RST) as applied to acoustical scattering. It is shown that surface wave contributions to backscattering may be summed in a way analogous to the frequency response of a Fabry-Perot resonator.

TABLE OF CONTENTS

Page

ACKNOWLEDGMENTS iii

ABSTRACT iv

LIST OF TABLES viii

LIST OF ILLUSTRATIONS ix

Chapter

1. INTRODUCTION 1

1.1 Overview 2

References to Chapter 1 24

2. AXIALLY-FOCUSED (GLORY) SCATTERING DUE TO SURFACE WAVES GENERATED ON SPHERES: MODEL AND EXPERIMENTAL CONFIRMATION USING TUNGSTEN CARBIDE SPHERES 27

2.1 Introduction 28

2.2 Model of angular dependence 32

A) Angular dependence using GTD, RST, and virtual ring-like sources 32

B) Angular dependence using Legendre polynomial expansions 36

C) Specializing angular dependence model to a tungsten carbide sphere 37

2.3 Experimental test of angular dependence 41

2.4 Discussion 48

Appendix to Chapter 2

Location of the focal circle 50

References to Chapter 2 52

Page

3. BACKSCATTERING FROM AN ELASTIC SPHERE: SOMMERFELD-WATSON TRANSFORMATION AND EXPERIMENTAL CONFIRMATION 55

3.1 Introduction 56
3.2 The Sommerfeld-Watson Transformation 57
3.3 Experimental confirmation of Rayleigh backscattering amplitudes 73
3.4 Discussion 81

Appendices to Chapter 3

A) Alternate expressions for B_n/D_n and B_ν/D_ν 84
B) Evaluation of contour integrals at infinity 87
C) Saddle point analysis for incident plane wave 89
D) Saddle point analysis for specular reflection 91

References to Chapter 3 93

4. RESONANCE SCATTERING THEORY REVISITED VIA THE SOMMERFELD-WATSON TRANSFORMATION FOR SCATTERING FROM ELASTIC SPHERES . . . 96

4.1 Introduction 97
4.2 The backscattering form function via SWT and RST 99

A) PWS and SWT form functions 100
B) Interpreting RST using f_{SR} 113

4.3 Resonance conditions from RST and the SWT 117

A) A first look 117
B) A more formal approach 120

References to Chapter 4 123

APPENDIX—COMPUTER PROGRAMS 125

ZNU and ZKA 126
SLOPE3 137
WS 138
OLVER 146
CHIVER 158

LIST OF TABLES

Page

CHAPTER 2

I. RST Rayleigh resonance values 38

CHAPTER 3

I. SWT Rayleigh poles 74

LIST OF ILLUSTRATIONS

Page

CHAPTER 1

1. Spherical coordinate system 4
2. Armico iron sphere—backscattering form function and echo structure 8
3. Surface wave picture using GTD 10
4. Rayleigh wave particle displacement 14
5. Tungsten Carbide sphere—backscattering form function and RST labeling 17
6. Transmitted wave glory rays 19
7. Angular dependence of transmitted wave glory 21

CHAPTER 2

1. Tungsten Carbide sphere echo structure-oscilloscope trace . . . 29
2. Surface wave "ray" diagram from GTD 33
3. Rayleigh wave group ad phase velocity dispersion curves 39
4. Simplified diagram of scattering experiment 42
5. Angular dependence of Rayleigh wave glory at ka = 60 44
6. ka vs γ_m^{-1}—experimental and theoretical results 46
7. Angular dependence of Rayleigh wave glory at ka = 32.3 47

A.1. Horizontal position of virtual source F_R 51

Page

CHAPTER 3

1. Spherical coordinate system 59

2. Contour Γ in λ plane 60

3. Contour $\overline{\Gamma}$ in λ plane 62

4. Contours Γ_s, Γ_1, Γ_2 in λ plane 63

5. Surface wave "ray" diagram 71

6. Simplified diagram of scattering experiment 76

7. On-axis Rayleigh wave backscattering amplitudes 77

CHAPTER 4

1. Spherical coordinate system 101

2. Coupling parameters and on-axis amplitudes 105

3. Rayleigh form function contribution $|f_R(x,\pi)|$ 107

4. Form function magnitude—f_b vs f_{SR} for $0 < ka \leq 80$ 108

5. Form function magnitude—f_b vs f_{SR} for $30 \leq ka \leq 50$ 110

6. Form function magnitude—f_b vs f_{SRWG} for $0 < ka \leq 80$ 111

7. Form function magnitude—f_b vs f_{SRWG} for $30 \leq ka \leq 80$ 112

8. f_{SR}, η_1^m, $Re(x_{n1})$ for $10 \leq ka \leq 80$ 115

9. f_{SR}, η_1^m, $Re(x_{n1})$ for $35 \leq ka \leq 65$ 116

DEDICATION

To my wife and my parents who have always given their spiritual, physical, and financial support.

Chapter 1

INTRODUCTION

1.1 Overview

Many times in physics, results derived from investigating "canonical problems" are important in understanding more difficult situations. A particular example of this is the scattering of waves incident on a sphere. This problem is of interest in such areas as electromagnetics, acoustics, geophysics, and particle physics. Because of this, it has been the subject of much analysis.[1] As early as 1863 Clebsh addressed the problem of acoustical wave scattering from a rigid sphere. In the ensuing years from 1863 to World War II many people examined various versions of the problem in many different fields. Reference 1 is a survey of many of these analyses up to 1941. Formal solutions to the various problems, in terms of an infinite Partial Wave Series (PWS) of spherical functions, are obtainable by using the separation of variables technique in solving the differential equations. In many cases the PWS results give little physical insight into the problem at hand. This is particularly true if the sphere is much larger than the wavelength of the plane wave. This is equivalent to saying the dimensionaless parameter ka of the sphere is much larger than one where k is the wavenumber of the plane wave and a is the sphere's radius. Much of the work even to this day revolves around obtaining a better understanding of observable physical phenomena by applying various mathematical techniques to the PWS results when $ka \gg 1$. From this type of analysis one can obtain results equivalent to those of less rigorous methods such as geometrical optics. For the problem we shall study (see below) we will first use the less rigorous methods directly since they have less of a tendency to mask the physics of the situation. We will then attack the problem by beginning with the PWS results which are also given below. Finally we will examine the interpretation of a recently developed theory which uses the PWS directly. In the paragraphs below we

shall specify the problem we will examine, give a short summary of its PWS solution and discuss work which had been carried out up till 1983 which was important to analysis in this dissertation.

The problem we wish to study is the scattering of an acoustical plane wave incident from an nonviscous fluid onto an isotropic elastic sphere. We are most interested in the total pressure external to the sphere in the range $10 < ka < 100$. The PWS solution for this pressure was found first by Faran in 1951.[2,3] Related work up to that point is summarized in Reference 2.

To solve the problem, Faran wrote the vector displacement $\vec{u}$ in the elastic solid in terms of a scalar potential ψ and a vector potential $\vec{A}$. In terms of these potentials the vector displacement $\vec{u}$ is given by

$$\vec{u} = -\nabla\psi + \nabla \times \vec{A} \tag{1}$$

where ∇ is the del operator. The potentials in turn must satisfy the equations

$$\nabla^2\psi = \frac{1}{c_L^2}\frac{\partial^2\psi}{\partial t^2} \tag{2}$$

$$\nabla \times \nabla \times \vec{A} = \frac{1}{c_S^2}\frac{\partial^2\vec{A}}{\partial t^2} \tag{3}$$

where c_L and c_S are the longitudinal and shear elastic wave speed respectively. Assuming a plane wave incident as shown in Fig. 1 symmetry considerations allow one to show that there will only be an A_ϕ component to $\vec{A}$ and that ψ and A_ϕ will have no ϕ dependence. Therefore solving Eq. (2) and (3) by the method of separation of variables one finds that ψ and A_ϕ may both be written as an infinite PWS with

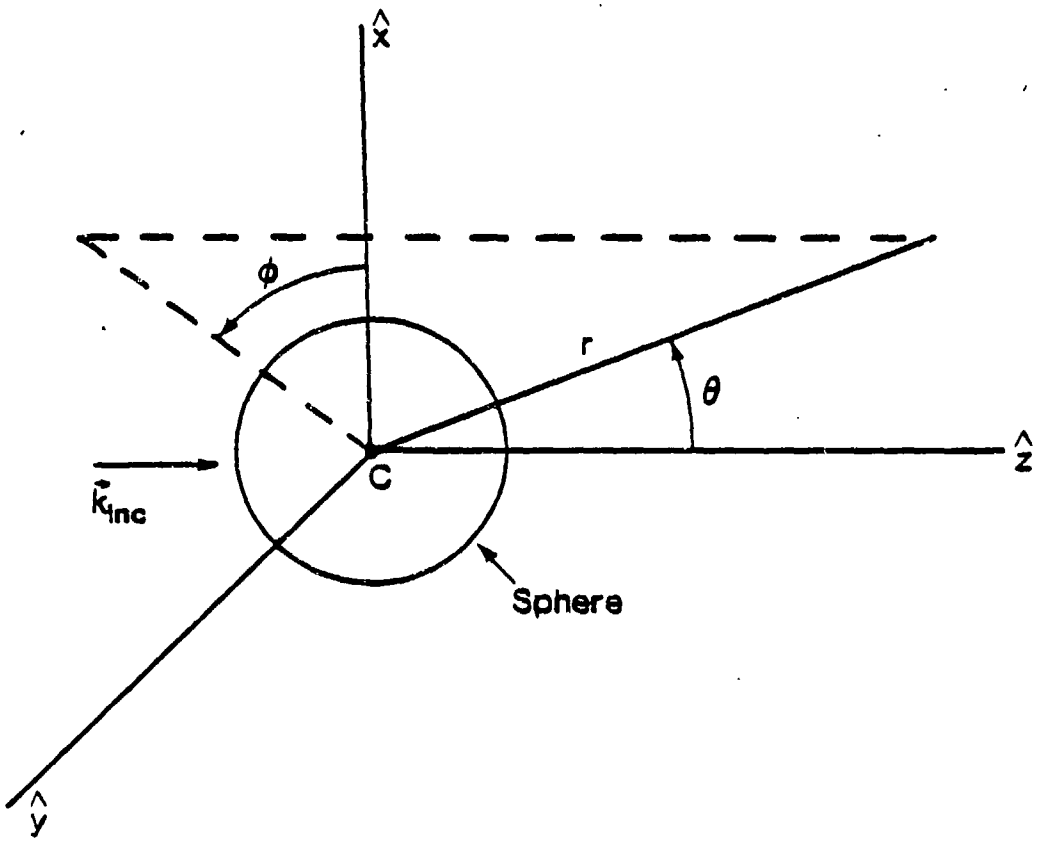

The r, θ, φ coordinate system shown above was used in writing the partial wave series (PWS) solution to plane wave scattering from an elastic sphere. The plane wave is assumed to be traveling in the +z direction.

Fig. 1.

$$\psi(r,\theta,t) = \sum_{n=0}^{\infty} a_n j_n(k_L a)\, P_n(\cos\theta) e^{-i\omega t} \tag{4}$$

$$A_\phi(r,\theta,t) = \sum_{n=0}^{\infty} b_n j_n(k_S a)\, P_n^1(\cos\theta) e^{-i\omega t} \tag{5}$$

where ω is the angular frequency of the incident plane wave, a_n and b_n are unknown constants, j_n is the spherical Bessel function, k_L and k_s are the longitudinal and shear wavenumbers, a is the radius of the sphere, and P_n and P_n^1 are the Legendre and associated Legendre functions respectively.

The pressure in the liquid satisfies the equation

$$\nabla^2 p = \frac{1}{c^2} \frac{\partial^2 p}{\partial t^2} \tag{6}$$

where c is the acoustic wave speed for the liquid. The vector displacement in the liquid is given by

$$\vec{u} = \frac{1}{\rho\omega^2} \nabla p \tag{7}$$

where ρ is the density of the liquid and ω is the angular frequency of the acoustic wave in the liquid. The total pressure p is given by the incident pressure p_i of the plane wave plus the scattered pressure p_s; i.e., $p = p_i + p_s$. Assuming an unit amplitude incident plane wave p_i can be written as

$$p_i(r,\theta,t) = \sum_{n=0}^{\infty} (i)^n (2n+1) j_n(kr) P_n(\cos\theta) e^{-i\omega t} \tag{8}$$

whereas the scattered pressure is a combination of outgoing spherical waves and is given by

$$p_s(r,\theta,t) = \sum_{n=0}^{\infty} c_n\, h_n^{(1)}(kr) P_n(\cos\theta) e^{-i\omega t} \tag{9}$$

In Eq. (8) and (9) k is the wavenumber for the pressure waves in the liquid. In Eq. (9) $h_n^{(1)}$ is the spherical Hankel of the first kind and the c_n are unknown constants.

Now to find the a_n, b_n, and c_n we must apply the appropriate boundary conditions. The boundary conditions are; the displacement u_r (the radial component of $\vec{u}$) is continuous across the boundary, the pressure in the liquid must equal the normal component of the stress in the solid sphere at the boundary, and the tangential (shear) stress components for the solid must vanish at the boundary. The mathematical form of these boundary conditions may be found in Ref. 2. We shall not carry out Faran's analysis to find the a_n, b_n, and c_n. We simply quote the result for the total pressure external to the sphere in a form appropriate for our purposes. The total pressure is

$$p(r,\theta) = \sum_{n=0}^{\infty} i^n(2n+1)[j_n(kr) + \frac{B_n(ka)}{D_n(ka)} h_n^{(1)}(kr)]P_n(\cos\theta) \qquad (10)$$

In the equation above, B_n and D_n are 3 x 3 determinant whose elements are given in Appendix A of Chapter 3. In Eq. (10) the time dependence $e^{-i\omega t}$ is not shown explicitly.

In 1962 Robert Hickling, using Faran's results, published an article in which he carried out a computer analysis of the far field backscattered pressure from elastic spheres made of several different materials.[4] The spheres had ka in the range $0 \leq ka \leq 60$. The case of backscattering (i.e., $\theta = \pi$) is particularly important in such areas as sonar and non-destructive testing. The analysis of this dissertation emphasizes the development of an understanding of the scattering pressure near $\theta = \pi$.

Hickling obtained the steady state backscattering pressure as a function of the dimensionaless parameter ka of the spheres. A diagram

equivalent to his steady state results for Armico iron is given in Fig. 2a. He used these steady state results along with Fourier transform techniques to determine the backscattering echo from an Armico iron sphere which was subjected to a tone burst. Redrawn in Fig. 2b is Hickling's result for the case of a 5 cycle pulse incident on an Armico iron sphere with ka = 24.5. The figure reveals a decaying pulse train. About a year before Hickling's analysis Hampton and McKinney had published an experimental paper in which, among other things, they had subjected an aluminum sphere to a short acoustic pulse of the form used by Hickling in his computer analysis. A pulse train type echo was clearly evident.[5] Also evident after reading both articles is the fact that much of the phenomena seen were incompletely understood. In fact the PWS solution is not a particularly well equipped vehicle through which to understand the physical origins of the echoes. We turn now to work that allows an alternate avenue through which to understand the backscattered pressure from the elastic sphere. It should be reaffirmed that we are examining work which was relevant to the methods used in the current dissertation and make no claim that the present summary is exhaustive.

In the middle 1950's Joseph Keller and associates developed a new theory of scattering[6,7] which they called the Geometrical Theory of Diffraction (GTD). The theory is based on the postulate that fields propagate along rays as in geometrical acoustics, but introduces diffracted waves. Like geometrical acoustics it is applicable to scattering from a sphere with ka >> 1. An article by Levy and Keller in 1959 is of particular interest since it applied GTD to acoustical scattering from impenetrable spheres and cylinders. For the problems discussed in the 1959 paper the diffracted rays propagated in part along the surface of the scattering object and were therefore called surface waves. The GTD surface wave picture is developed in

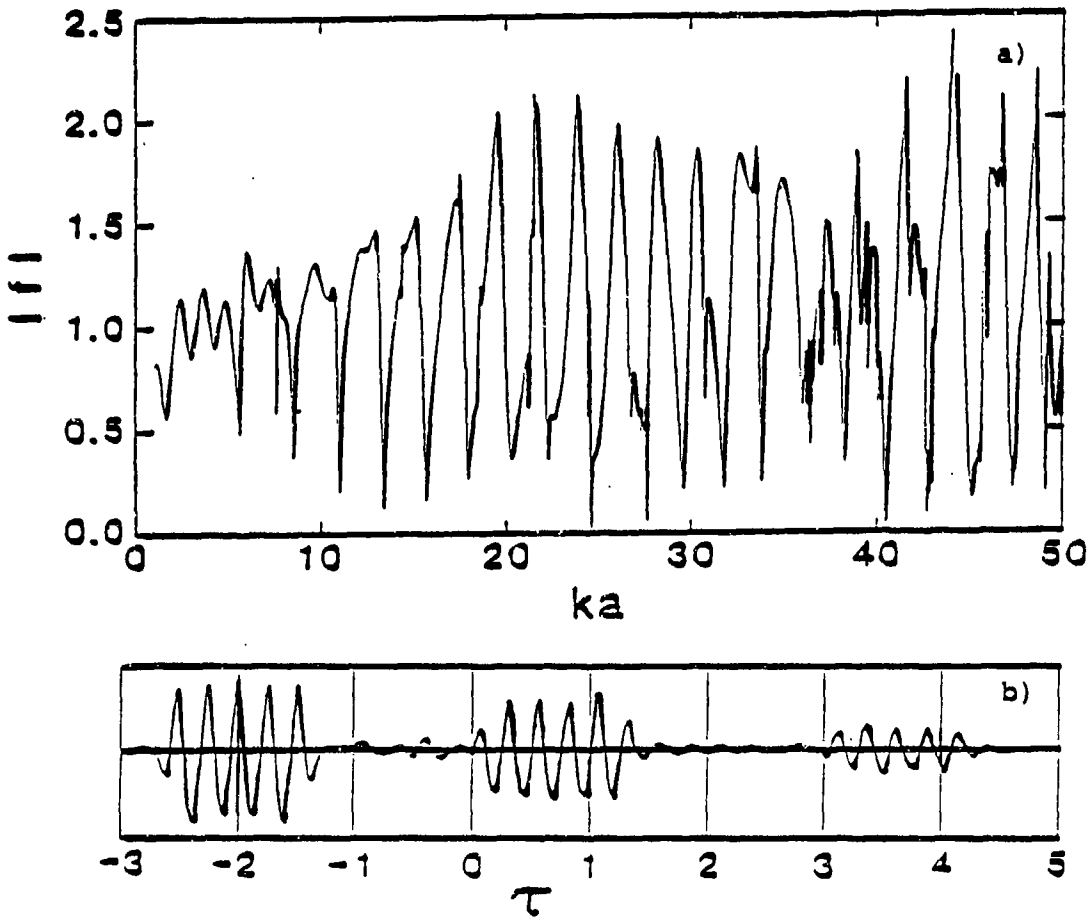

Calculations of the backscattered pressure from an Armico iron sphere: a) The backscattering form function as a function of ka. This figure was calculated using the program CHIVER given in the appendix, b) Using the results used to generate figure Fig. 2a and Fourier transformation techniques, Hickling obtained the backscattering response to a 5 cycle tone burst shown here. The horizontal time scale is referenced to the center of a pulse traveling in water from $(r = \infty, \theta = \pi) \rightarrow (r = 0) \rightarrow (r = \infty, \theta = \pi)$ and the nondimensional time unit $\tau = ct/a$.

Fig. 2.

Levy's paper by first using ideas similar to those of geometrical acoustics. A typical trajectory for a diffracted ray in going from a source point Q to a receiver P is shown in Fig. 3. The surface ray is launched at the point Q_1 whose location can be determined by phase matching conditions (cf. Chapter 2). The surface wave reradiates energy into the fluid continuously as it travels around the sphere (indicated by the dotted rays in Fig. 3). At the point Q_2 energy is reradiated into the liquid in the direction of the receiver P. The surface wave picture developed by use of geometrical arguments was recalculated more rigorously later in Levy's paper by using the Sommerfeld-Watson transformation (SWT).

The SWT consists of rewriting the PWS solution of the problem under study in terms of a contour integral. The contour is then deformed to surround poles in the complex plane which eventually lead to surface wave contributions. The contour can be also be separated and further deformed to pass through saddle points of the complex integral. A saddle point analysis then gives contributions to scattering which are familiar from geometrical acoustics; for example, specular reflection. The SWT was first used by Watson and then further developed by many others.[1]

In Levy's paper the SWT analysis occupies only a few pages and contains little detail since it was not the primary goal of the paper to understand all of the many effects which can be seen. In contrast to this Nussenzveig, in a 1965 paper,[8] embarked on a very detailed analysis of scalar plane wave scattering from a sphere using boundary conditions appropriate for an acoustically soft sphere. He used a modified SWT analysis to investigate the PWS solution for a wavefunction which could be interpreted as either the velocity potential for an acoustically soft sphere or as the Schrodinger wave function for a hard-core potential. At the time of his paper the SWT was

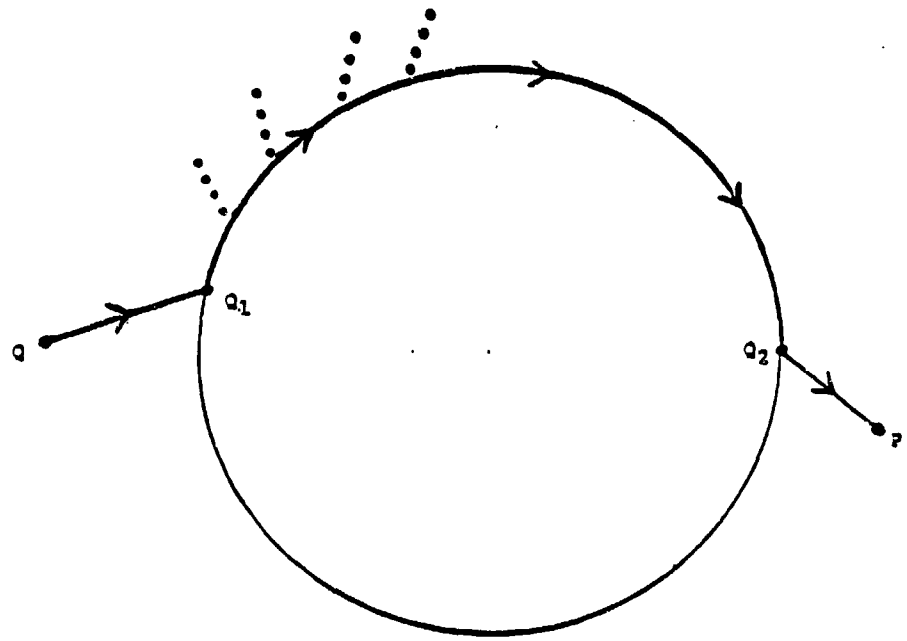

A typical trajectory for a diffracted ray of the GTD in going from the sender Q to receiver P. A surface wave is launched at point Q_1. As indicated by the dotted lines the surface wave continuously reradiates energy into the fluid. At the point Q_2 energy is radiated in the direction of P. As drawn here the ray is similar to ones used later in this dissertation. In Levy's paper[6] rays were assumed to be launched onto the sphere tangentially.

Fig. 3.

being used in particle physics in connection with Reggi's work on complex angular momentum.[8]

Later, in 1969, Nussenzveig authored two papers which treated a sphere with boundary conditions appropriate for the acoustical problem of a liquid sphere embedded in another liquid. The second of these papers was concerned partly with understanding a scattering effect known as glory. The term glory refers to a weak axial focusing of scattered waves along either the forward or backward scattering directions.[11] More will be said about glory scattering later in this introduction.

The results of Nussenzveig's papers included surface wave contributions in agreement with the ideas of the GTD. One obvious next step in studying scattering from a sphere would seem to be a generalization of Nussenzveig's papers to the case studied by Faran; i.e., an isotropic elastic sphere embedded in a nonviscous liquid. One could foresee a possible profitable interaction between experimental results such as Hampton's[5] and theoretical results of the SWT. This dissertation, in fact, represents a partial fulfillment of this next step.

It may at first seem curious that the generalization and interaction between experiment and theory described above did not happen before now. However, part of the reason for the delay can be found by realizing that there is another similar problem which is in some ways easier to study. That is the problem of plane wave scattering from an isotropic elastic cylinder in a liquid. In the same time frame as the studies discussed above, other investigators were developing equivalent results for cylinders.[12,13] Indeed, in 1968 (a year before Nussenzveig's study of the glory in Ref. 10) Doolittle, Überall, and Ugincius, published a SWT analysis of scattering from an elastic cylinder.[13] Some of the work (by them as well as other researchers) leading

up to this analysis is referenced in the introduction of Ref. 13. Elastic cylinders with $ka < 100$ (where a is now the radius of the cylinder) became the objects of study through which people increased their understanding of the surface waves of the SWT (at least in acoustics research). Thus the delay in obtaining SWT results for an elastic sphere. Doolittle et al. separated the surface waves they found on cylinders into two groups; "Franz-like" waves whose energy resided mostly in the liquid around the cylinder and which were present in the rigid and soft cylinder cases, "Rayleigh-like" waves whose energy resided mainly in the elastic cylinder. Investigations carried out over the next five years showed that the "Rayleigh-like" surface waves could be further split by identifying one Rayleigh wave whose phase velocity went asymptotically as $ka \to \infty$ to the phase velocity of the Rayleigh surface wave known to exist on a flat interface between a liquid and a solid (the possible existence of a unique type of surface wave along the flat interface between a vacuum and a solid was first demonstrated[14] 100 years ago by Rayleigh in 1885 hence the name) and a number of "whispering gallery" surface waves whose phase velocities went asymptotically to the phase velocities of the shear or longitudinal waves of the solid.[12] These whispering gallery waves correspond in the limit that $ka \to \infty$ to shear or longitudinal surface waves which are found to exist when a plane wave is incident from a liquid onto a flat interface between the liquid and a solid at the shear critical angle θ_S or longitudinal critical angle θ_L. These critical angles are related to the relative acoustical velocities of waves in the liquid and the solid. Reference 12 discusses the above identifications in some detail.

Before proceeding it is appropriate to further characterize the Rayleigh surface wave since it will prove to be a central character in the analysis which follows. The particle displacement for a Rayleigh wave is a

unique combination of shear and longitudinal displacement. The amplitude of the shear and the longitudinal particle displacements decay exponentially as one proceeds away from the liquid solid interface. The decay constants, however, are different. The phase velocity of the Rayleigh wave on a flat interface is slightly less than the shear wave phase velocity of the solid. A discussion of the flat interface Rayleigh wave can be found in Ref. 15. Figure 3.8 of that reference shows the combined particle displacements of a Rayleigh wave as a function of the observer's distance from the interface. That figure has been redrawn here as Fig. 4. In 1969 Rulf published an article examining Rayleigh waves on cylinders.[16] His work indicated that the Rayleigh wave velocity on the surface of a cylinder is a function of the ka of the cylinder. This velocity went asymptotically to the flat surface Rayleigh wave phase velocity as $ka \to \infty$. Similar behavior will be found in Chapter 2 for the Rayleigh wave when seen on spheres.

Experimentally, backscattered echoes resulting when a short tone burst was incident on an aluminum cylinder showed a decaying pulse train similar to that shown before for the Armico iron sphere.[17] The SWT results allowed one to identify some of these echoes as due to specular reflection and bulk waves transmitted within the cylinder and others as due to repeated circumnavigations of the cylinder by surfaces waves which periodically radiated energy in the backscattering direction.[17] In short, the SWT analysis for elastic cylinders allowed an interpretation of the echo structure not obvious by use of the PWS alone. The same sort of ideas should be applicable to elastic spheres. However, one might expect new phenomena due to the increased symmetry of the sphere.

The SWT analysis was also found to be useful in understanding steady state results. In 1977 Uberall, Dragonette, and Flax published a paper on the

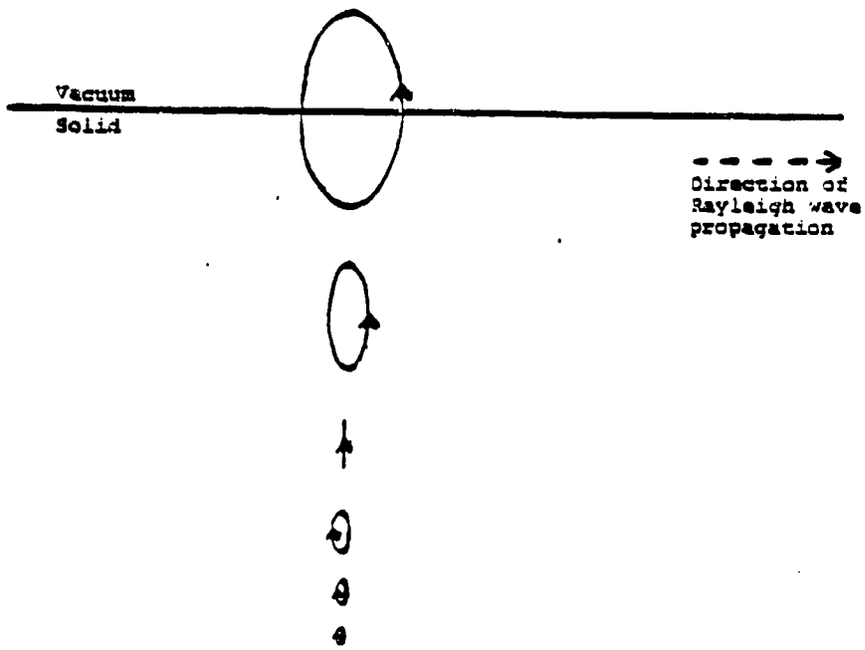

The combined particle displacement of a Rayleigh surface wave as a function of the observer's distance from the Vacuum-Solid interface.

Fig. 4.

relation between surface waves (also known as creeping waves) and normal modes of vibration of a curved body.[18] Each term of the PWS solution to a problem can be identified as a multipole. Each term may resonate (i.e., diverge) at several ka values. Uberall et al. argued that for a cylinder the resonance of the nth term of the PWS occurred at ka values where n cycles of a particular surface wave fit on the body. These ideas had been useful in particle physics where it was termed Reggi pole analysis. These ideas eventually led Flax to propose in 1978 an acoustical and electromagnetic scattering theory which examined PWS results directly and used nuclear scattering theory ideas. This theory was termed Resonance Scattering Theory (RST).[19]

RST achieves a separation between rapidly varying "resonances" portions of the PWS for the scattered signal and a slowly varying background. In particular, for an acoustical plane wave scattered from fluid-loaded elastic bodies such as cylinders[20] or spheres[21] the RST was used to interpret the rapid fluctuations in the backscattered pressure as the ka of the body is varied (cf. Fig. 2a). One of the important numerical tasks in RST is to find the complex "resonance" ka values which locate the poles of the scattering amplitude. Two basic ideas are then used in interpreting scattered pressures. For a <u>sphere</u> these ideas translate into the following statements[21]: (a) each of the many resonance ka's can be labeled with the integers n and ℓ and at the $(n,\ell)^{th}$ resonance $(n + 1/2)$ wavelengths of the ℓth surface wave fit onto the circumference of the sphere, (b) that any rapid fluctuation in the backscattered pressure is due to in-phase adding of a specific surface wave [(n,ℓ) resonance] and these fluctuations are thus associated in a simple fashion with the set of multipole resonances for the sphere. Two of the major goals of the last chapter of this dissertation are to examine the limitations of these ideas.

An example of the type of results which can be developed through the use of the RST ideas is shown in Fig. 5. In that figure (which is equivalent to Fig. 8 of Ref. 21) the absolute value of backscattering form function (related to the backscattering pressure, cf. Chapter 3) for a tungsten carbide sphere is shown. Also shown are some of the resonance ka values. Their positions are indicated by arrows and they are labeled by the (n,ℓ) pairs whose meaning was discussed in the last paragraph. Rapid fluctuations in the form function are found to occur at ka values close to specific (n,ℓ) pairs. In Chapter 4 we investigate, through the use of the SWT, the specific case depicted in Fig. 5 in order to better understand the caution which should be exercised in using the RST labeling of the backscattering form function.

It is interesting to note in passing the similarity between the structure found in Figs. 2a and Fig. 5. It would seem that appropriate rescaling of the ka axis of Fig. 2a would yield results which could be overlaid on the tungsten carbide result with good agreement. This might suggest similar physical reasons for the structure.

It should be emphasized again that in the case of a sphere that the RST attempts to interpret the FWS results such as shown in Fig. 2a in terms of the surface wave picture developed through the SWT without ever doing the SWT. Once the reader has examined the SWT analysis for the fluid-loaded elastic sphere given in Chapter 3 of this dissertation he will probably appreciate this goal of RST. However, once he has read the last chapter it is hoped that he appreciates the need for caution when trying to reach this goal.

The reader should not get the idea that the era between Nussenzveig's papers[9,10] of 1969 and Gaunaurd's[21] paper in 1983 was devoid of fruitful research on acoustical scattering from elastic spheres. For example, in the seventies and early eighties other researchers used Fourier transform

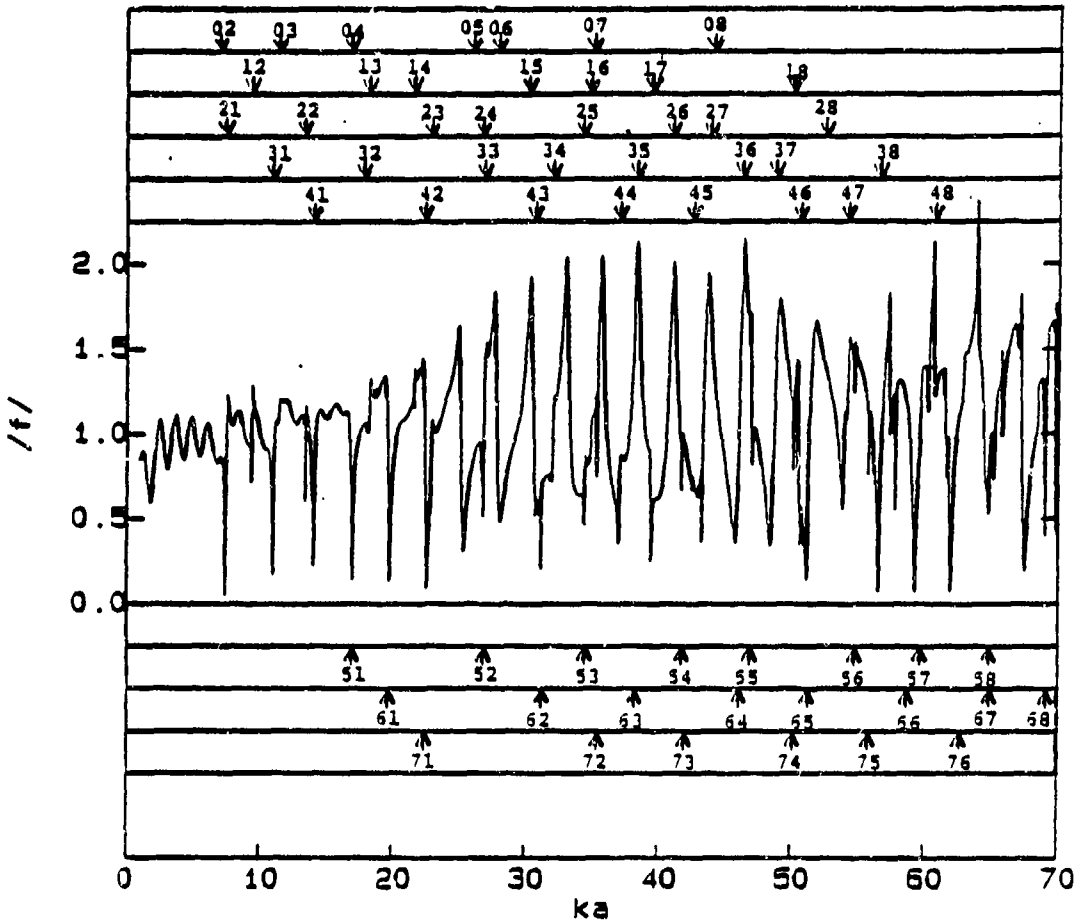

The backscattering form function of a tungsten carbide sphere as a function of ka. Also indicated by the arrows are the real part of the RST resonances for $n = 0-7$ and $\ell = 1-8$. The RST resonance locations were taken from Table IV of Ref. 21 and the figure is similar to Fig. 4 of the same reference.

Fig. 5.

techniques to obtain steady state results analogous to Fig. 5 from transient experimental data.[22-24] However, we neglect discussing these and other works in any detail since they are not of direct relevance to the development of this dissertation.

Further discussion of RST as applied to spheres can be found in Refs. 25 and 26. These references along with Ref. 21 were the latest research results available on acoustical scattering from elastic spheres with $0 < ka < 100$ when the research in this dissertation was initiated in 1983.

At this point it is appropriate to discuss the avenue through which this dissertation topic was arrived at since it influenced greatly the direction of the research. The phenomena of acoustical glory backscattering (which was mentioned earlier in connection with Nussenzveig's papers) had been under study[27-29] in the years preceding 1983. The spheres being studied experimentally and theoretically had ka values typically much larger than 100. At these ka values the radiation damping of surface waves has for the most part caused them to be of little importance to backscattering. The most important waves are those of geometrical acoustics; i.e., reflected and transmitted waves whose progress can be ascertained by ray tracing techniques. In the research of Ref. 27-29 the term glory rays was used to describe rays whose corresponding waves were weakly focused along the backscattering axis; i.e., glory scattering. A few glory rays are shown in Fig. 6 along with a couple of rays whose waves are not focused. The rays labeled by $n = 3,4,5$ are glory rays. The value of n gives the number of ray chords within the sphere. For instance the ray with $n = 3$ is transmitted within the sphere then internally reflected twice before being transmitted along the backscattering axis which gives three chords within the sphere. The rays labeled 0 and 2 are not glory rays. Ray 0 is the specular reflection from the

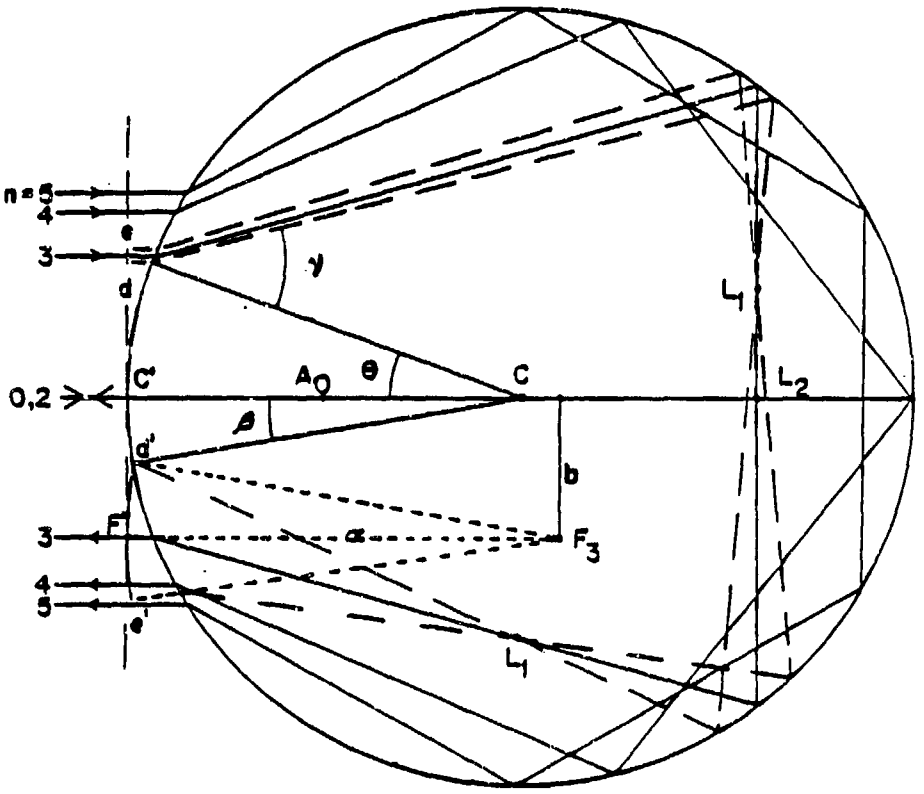

Several rays tracing transmitted wave propagation within the sphere are shown. The parameter n indicates the number of ray chords within the sphere. The rays labeled $n = 3,4,5$ are associated with waves weakly focused along the backscattering axis; i.e., they are glory rays. The waves associated with rays labeled $n = 0, 2$ are not focused.

Fig. 6.

front of the sphere while Ray 2 is the ray which is transmitted within the sphere, reflected from the back of the sphere, and then retransmitted along the backscattering axis. To properly model the weak axial focusing of rays such as 3, 4, and 5 one must use diffraction techniques.[28,29] One finds that glory scattering is characterized by a $J_0(kb\gamma)$ angular dependence in pressure amplitude for small angles γ away from the backscattering axis where J_0 is the zeroth order Bessel function. The parameter b is shown in Fig. 6 for the $n = 3$ glory ray and its significance is discussed in detail in Refs. 27-29 as well as Chapter 2. The J_0 angular dependence was confirmed experimentally by use of backscattering echoes resulting from tone bursts incident on a fused silica sphere with $ka \approx 457$. Because of the different propagation times the tone burst experiments allowed isolation in time of various glory ray contributions. A comparison between the theoretical and experimental angular dependence for a glory ray with $n = 4$ is shown in Fig. 7. The model also allowed calculation of the absolute pressure amplitude along the backscattering axis (when $\gamma = 0$) for any glory ray. These model predictions were tested experimentally for several glory rays and were found to give answers within 5 percent of experimental results.

It is interesting to ascertain whether surface wave contributions which are important at lower ka's can be shown experimentally to display weak axial focusing. Next, if surface waves do display glory scattering can one develop a model of surface wave glory which allows one to predict the absolute pressure amplitude along the backscattering axis?

At about the same time that the last reference on transmitted wave glory was submitted[29] the RST article by Gaunaurd[21] was published. It was felt that research which would be necessary to answer the questions above on surface wave glory might also be useful in developing a better understanding

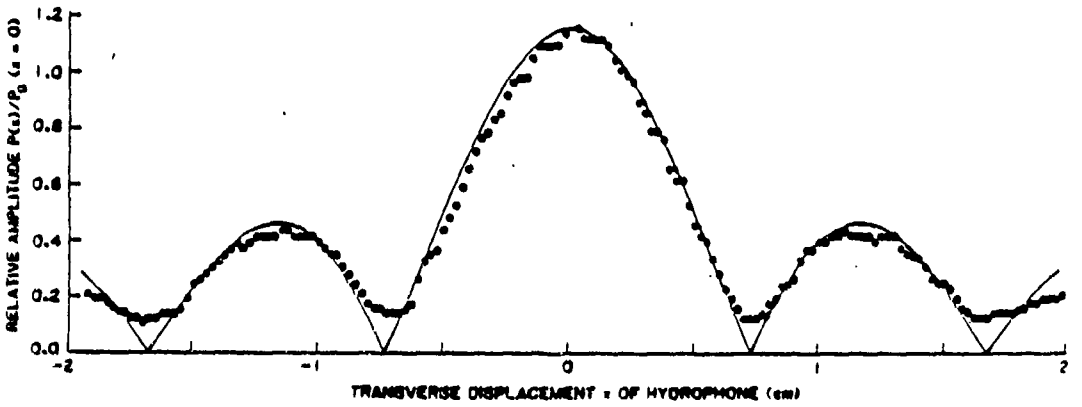

The result of a comparison of the experimental angular dependence found as a receiver hydrophone was displaced away from the backscattering axis vs. the theoretical $J_0(kb\gamma)$ dependence predicted. The dots are experimental results and the curve theoretical results. The glory ray being tested in this case had $n = 4$. Along the horizontal axis $x = 0$ corresponds to $\gamma = 0$ and $|x| = 2$ corresponds to $\gamma \approx .055$ radians.

Fig. 7.

of RST. In the course of answering the questions on surface wave glory scattering and trying to understand RST the historical perspective which has formed a large part of this introduction was developed.

The next three chapters address the issues put forth above. Some comments on the general structure of each chapter are useful. Each chapter is in reality a paper which has been submitted to the Journal of the Acoustical Society of America. As such, each has its own introduction section, appendices, references, figure numbers, and equation numbers. The papers which form Chapters 2 and 3 have been accepted for publication at the present time while the paper which forms Chapter 4 has only recently been submitted. Also included as a separate appendix are the computer programs which were developed for the calculations carried out in Chapters 2 through 4. This appendix contains text which introduces each program and briefly discusses any cautions deemed appropriate.

In Chapter 2 a theoretical model for surface wave glory is developed via two different routes. The first uses GTD, RST, and some of the ideas and results used in the transmitted wave glory model. This method allows a simple intuitive picture to be formed of the production of surface wave glory. The second method uses a slightly different form of the (PWS) in Eq. (9). The use of the SWT is intentionally avoided in Chapter 2. However, it is through the use of the SWT (which is carried out in Chapter 3) that one can obtain a theoretical prediction of the on-axis pressure amplitude of the surface wave glory. In Chapter 2 the model developed for angular dependence of the surface wave glory is experimentally tested using tungsten carbide spheres with $30 < ka < 100$. The agreement between experiment and theory is good.

In Chapter 3 the SWT is performed and the relation between SWT results and those of Chapter 2 are discussed. The SWT of Chapter 3 concentrates

mainly on contributions from the specular reflection and surface waves at small backscattering angles. The SWT is a more rigorous method through which one can predict the possible experimental observation of glory. It confirms the physical model used in Chapter 2 and for the first time predicts the absolute backscattering amplitude associated with one or more circumnavigations of the surface wave around the sphere; i.e., it predicts the amplitude of various surface wave contributions to the decaying pulse train seen in tone burst experiments. This prediction is tested experimentally in Chapter 3 using tungsten carbide spheres. Again, the agreement is good.

Finally in Chapter 4 the RST ideas discussed previously in this introduction are reexamined using the SWT results of Chapter 3. The chapter uses the specific case of the backscattering form function of a tungsten carbide sphere (cf. Fig. 5). The main effect of this analysis is on the interpretation of RST. The results show that care is needed when using the labeling of Fig. 5 to understand fluctuations in the backscattering form function. It is also shown that RST ka resonances only approximate the ka values at which surface waves add-in phase. However, the error in this approximation is usually negligible.

1.2 References

1. Nelson A. Logan, "Survey of some early studies of the scattering of plane waves by a sphere," Proc. IEEE 53,773-785 (1965).
2. James J. Faran, "Sound scattering by solid cylinders and spheres," Ph.D. Thesis, Harvard University, Cambridge, Massachusetts (1951).
3. J. J. Faran, "Sound scattering by solid cylinders and spheres," J. Acoust. Soc. Am. 23, 405 (1951).
4. Robert Hickling, "Analysis of echoes from a solid elastic sphere in water," J. Acoust. Soc. Am. 34, 1584-1592 (1962).
5. L. D. Hampton and C. M. McKinney, "Experimental study of the scattering of acoustical energy from solid metal spheres in water," J. Acoust. Soc. Am. 33, 664-673 (1961).
6. B. R. Levy and J. B. Keller, "Diffraction by a smooth object," Commun. Pure Appl. Math. 12, 159-209 (1959).
7. J. B. Keller, "Rays, waves, and asymptotics," Bull. Am. Math. Soc. 84, 727-750 (1978).
8. H. M. Nussenzveig, "High frequency scattering by an impenetrable sphere," Ann. Phy. 34, 23-95 (1965).
9. H. M. Nussenzveig, "High frequency scattering by a transparent sphere. I. Direction reflection and transmission," J. Math. Phys. 10, 82-124 (1969).
10. H. M. Nussenzveig, "High frequency scattering by a transparent sphere. II. Theory of the rainbow and glory," J. Math. Phys. 10, 125-176 (1969).
11. H. C. Van de Hulst, Light Scattering by Small Particles (Wiley, New York, 1957).

12. H. Überall, "Surface waves in acoustics," in Physical Acoustics, edited by W. P. Mason and R. N. Thurston (Academic, New York, 1973), Vol. 10, pp. 1-60.

13. R. O. Doolittle, H. Überall, and P. Ugincius, "Sound scattering by elastic cylinders," J. Acoust. Soc. Am. 43, 1-14 (1968).

14. Lord Rayleigh, "On waves propagated along the plane surface of an elastic solid," Proc. London Math. Soc. XVII, 4-11 (1885).

15. H. F. Pollard, Sound Waves in Solids (Pion Limited, London, 1977).

16. B. Rulf, "Rayleigh waves on curved surfaces," J. Acoust. Soc. Am. 45, 493-499 (1969).

17. W. G. Neubauer, P. Ugincius, and H. Überall, "Theory of creeping waves in acoustics and their experimental demonstration," Zeitschrift fur Naturforschung 24b, 691-700 (1969).

18. H. Überall, L. R. Dragonette, and L. Flax, "Relation between creeping waves and normal modes of vibration of a curved body," J. Acoust. Soc. Am. 61, 711-715 (1977).

19. L. Flax, L. R. Dragonette, H. Überall, "Theory of elastic resonance excitation by sound scattering," J. Acoust. Soc. Am. 63, 723-731 (1978).

20. D. Brill and G. C. Gaunaurd, "Acoustic resonance scattering by a penetrable cylinder," J. Acoust. Soc. Am. 73, 1448-1455 (1983).

21. G. C. Gaunaurd and H. Überall, "RST analysis of monostatic and bistatic acoustic echoes from an elastic sphere," J. Acoust. Soc. Am. 73, 1-12 (1983).

22. W. G. Neubauer, R. H. Vogt, and L. R. Dragonette, "Acoustic reflection from elastic spheres. I. Steady-state signals," J. Acoust. Soc. Am. 55, 1123-1129 (1974).

23. L. R. Dragonette, R. H. Vogt, L. Flax, and W. G. Neubauer, "Acoustic reflection from elastic spheres and rigid spheres and spheroids. II. Transient analysis," J. Acoust. Soc. Am. 55, 1130-1137 (1974).

24. L. R. Dragonette, S. K. Numrich, and L. J. Frank, "Calibration technique for acoustic scattering measurements," J. Acoust. Soc. Am. 69, 1186-1189 (1981).

25. L. Flax, G. C. Gaunaurd, and H. Überall, "Theory of resonance scattering," in Physical Acoustics, edited by W. P. Mason and R. N. Thurston (Academic, New York, 1981), Vol. 15, pp. 191-294.

26. G. C. Gaunaurd, E. Tangles, H. Überall, and D. Brill, "Interior and exterior resonance in acoustic scattering. I: Spherical targets," Nuov. Cim. B 76, 153-175 (1983).

27. P. L. Marston and D. S. Langley, "Glory- and rainbow-enhanced acoustical backscattering from fluid spheres: Models for diffracted axial focusing," J. Acoust. Soc. Am. 73, 1464-1474 (1983).

28. P. L. Marston, K. L. Williams, and T. J. B. Hanson, "Observation of the acoustical glory: High frequency backscattering from an elastic sphere," J. Acoust. Soc. Am. 74, 605-618 (1983).

29. K. L. Williams and P. L. Marston, "Mixed-mode acoustical glory scattering from a large elastic sphere: Model and experimental verification," J. Acoust. Soc. Am. 7, 1555-1563 (1984).

Chapter 2

AXIALLY-FOCUSED (GLORY) SCATTERING DUE TO SURFACE WAVES GENERATED ON SPHERES: MODEL AND EXPERIMENTAL CONFIRMATION USING TUNGSTEN CARBIDE SPHERES

2.1 Introduction

An understanding of the echo structure and angular dependences for scattering from spheres (or other elastic objects ensonified along an axis of symmetry) may be facilitated by modeling the focusing of sound along the backward axis. We have previously studied this axially focused scattering from large elastic[1,2] or fluid[3] spheres where the focused waves were associated with rays transmitted through (and internally reflected from) the sphere's surface. The cases studied had $ka \geq 100$. In the present paper we demonstrate axially-focused scattering from tungsten carbide spheres in water having ka as low as 30. For this choice of material and low range of ka ($30 < ka < 100$), it is shown that surface waves on the sphere which radiate sound back into the water produce axially focused backscattering. The specific type of surface wave associated with the echoes studied is the one usually referred to as the Rayleigh wave;[4] however, our method of analysis should be useful for modeling the angular dependence of echoes associated with other waves such as "whispering gallery" waves.[4] Indeed, the form of the angular dependence demonstrated for the <u>surface wave contribution</u> to the pressure, as a function of backscattering angle, should be applicable to spherical elastic shells and to certain other shapes (such as spheroids or cylinders having hemispherical caps) when the object is ensonified along the axis of symmetry. The angular dependence found differs from that expected for surface wave contributions to the backscattering from right circular cylinders[5,6] (for which the direction of incident sound lies perpendicular to the axis of symmetry).

The backscattering echo in Fig. 1 was produced by a four cycle sinusoidal tone burst incident on a tungsten carbide sphere with $ka \approx 49.1$. The dominant contributions to the signal, after the specular reflection, are due to Rayleigh surface waves. We experimentally and theoretically

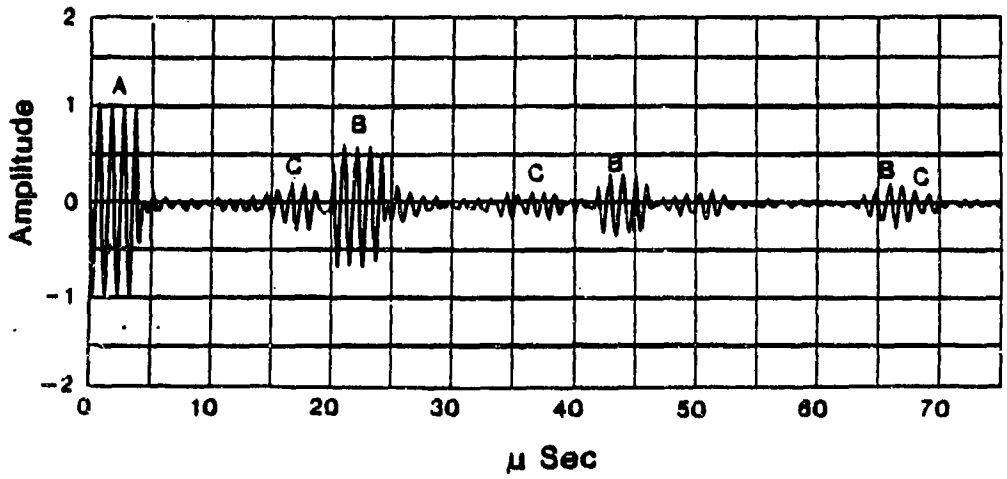

An oscilloscope trace of the backscattering echo from a tungsten carbide sphere ensonified by a tone burst. The ka of the sphere is approximately 49.1. The individual echoes are labeled as follows: A - specular reflection, B - Rayleigh surface wave echoes, C - echoes whose specific origin was not identified but which are conjectured to be other surface waves such as "Whispering Gallery" waves.

Fig. 1.

investigated the angular dependence of these Rayleigh echoes as one moves away from the backscattering direction. Our theoretical analysis uses the high frequency methods of the Geometrical Theory of Diffraction (GTD)[7] and Resonance Scattering Theory (RST).[4] The angular dependence found can be approximately modeled by $J_0(\beta\gamma)$ where β depends on the frequency of the tone burst (or equivalently the ka of the sphere) and γ is the angle relative to backscattering. This angular dependence is due to axial focusing and is characteristic of what has been called acoustical "glory."[1-3] The term "glory" comes from the enhancement of backscattered light from cloud droplets due to axial focusing.[3,8] Previous research on tungsten carbide spheres[9-12] does not directly address the affects of axial focusing.

In Section I we present a theoretical model of the $J_0(\beta\gamma)$ angular dependence of Rayleigh echoes via two different routes. The first uses GTD and RST together with results of our previous analysis[1-3] of virtual ring-like sources. This method allows a simple intuitive picture to be formed of the production of Rayleigh echoes. The second method uses the Partial-Wave Series (PWS) resulting from solving the steady-state scattering from a sphere. The approximate dependence, $J_0(\beta\gamma)$, also follows from the form of the PWS for spheres by way of a Sommerfeld-Watson Transformation (SWT) or a "modified" SWT (see e.g. Eq. (5.17) of Ref. 8). Our analysis given in Sec. I.A has the advantage that it relates β to the phase-velocity of the Rayleigh wave without further use of sophisticated analytical methods. In addition, our analysis may be extended to nonspherical objects (subject to restrictions noted in Sec. III) for which the PWS may not be known. In Sec. IC, the model is specialized to the particular case of tungsten carbide spheres.

We intentionally avoid the use of the SWT in Sec. I. However, it is through the use of the SWT that the ka dependence of the Rayleigh echo at

fixed γ may be determined. We return to the SWT analysis in a subsequent paper since the analysis for elastic spheres differs in significant details from the analysis for other spheres[8] or elastic cylinders.[13]

In Section II we test the angular dependence model on tungsten carbide spheres with $30 < ka < 100$. The experimental setup is similar to that used previously in transmitted wave studies on elastic spheres,[1,2] and so will be discussed only briefly. It is appropriate to comment on our use of tone bursts for comparison with the steady-state analysis given in Sec. I. This issue was addressed in earlier work[1,14] on axially-focused transmitted waves. It was found that though the scattered tone bursts should be distorted, the peak-to-peak amplitudes of the central cycle of a four-cycle burst should be given by a steady state analysis. It is anticipated that a detailed analysis of the shapes of transient Rayleigh echoes would lead to similar conclusions.

Tungsten carbide was particularly well suited as a target material for these experiments because (i) the Rayleigh-echo-amplitudes were significant for the range of ka examined and (ii) transmitted bulk-wave echoes were either insignificant in amplitude or well spaced in time from the Rayleigh echoes of interest. These properties are in part a consequence of tungsten carbide's large density ≈ 14 g/cm^3.

2.2 Model of angular dependence

A. Angular Dependence using GTD, RST, and Virtual Ring-Like Sources

The foundation of GTD was laid by Keller.[7,15,16] The GTD is useful in cases where the scattering body fulfills the condition $kd \gg 1$ where d is a characteristic dimension of the scatterer. It is based on the postulate that fields propagate along rays, but introduces diffracted rays. In the case of Rayleigh surface waves on a sphere it allows us to form the picture in Fig. 2. The "ray" AA' gets onto the sphere at angle θ_R. It proceeds around the sphere, along its surface, shedding energy continuously back into the water at angle θ_R as indicated by the dotted lines. Of particular interest is the fact that at one point (B') energy is shed along B'A'. This process continues and after circumnavigation of the sphere again more energy is shed in the backward direction. This process can be pictured for any number of trips around the sphere. A smaller amplitude echo will be seen after each trip because of the energy shedding, i.e. radiation damping.

The angle θ_R in Fig. 2 can be determined by the following phase matching criteria. For continual reinforcement of the Rayleigh wave the phase velocity of the wave c_R must match the component of the phase velocity in water c along the sphere's surface. This component is $c/\sin\theta_R$. Thus we can determine θ_R through the equation

$$\sin \theta_R = c/c_R \tag{1}$$

which is actually just Snell's law.

The above ideas explain qualitatively Fig. 1 though, as yet, they give no clue as to the angular dependence that will be seen as one moves away from

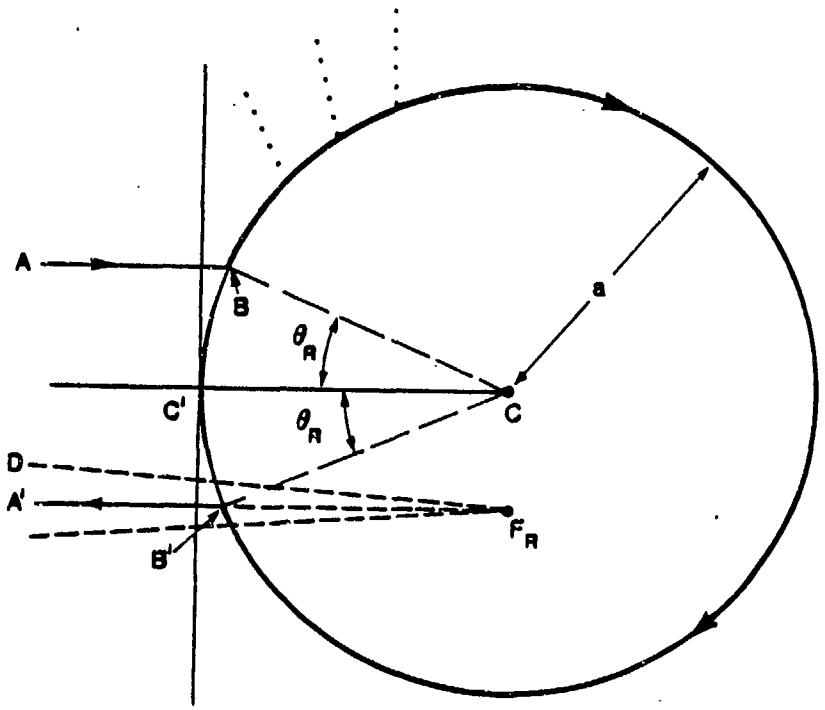

Surface wave "ray" diagram using the Geometric Theory of Diffraction (GTD). An incoming plane wave represented by AB allows the launching of a surface wave at B which circumnavigates the sphere while reradiating back into the surroundings. At point B' energy is radiated in the backward direction. This accounts for the echoes labeled B in Fig. 1. F_R is the virtual point source from which the ray A'B' and the dashed rays to either side appear to originate. When the diagram is rotated around the C'C axis, the point F_R traces out a virtual ring-like source.

Fig. 2.

the backscattering axis. To obtain the angular dependence of the Rayleigh echoes one must examine the dashed lines to either side of B'A'. These represent radiation damping slightly away from the backscattering direction. By tracing these rays as well as B'A' backward we arrive at F_R from which they appear to originate. (In the Appendix the horizontal position of F_R behind the vertical line through C' in Fig. 2 is found to be equal to a, the sphere's radius.) Next, because of the spherical symmetry of the situation, one can rotate the picture around the line CC' in which case the point F_R traces out a circle. Thus one sees that the Rayleigh waves appear to emanate from a ring-like source with radius $b = a \sin\theta_R$. When extended, the F_RD ray intersects the backscattering axis. Rays such as F_RD are responsible for the axial focusing when the CC' rotation is performed. (In the limit that the observation point goes to infinity F_RD goes to F_RA'.) Ring-like sources have been discussed in the previous work on acoustical glory due to transmitted waves in spheres.[1-3] These sources lead to an angular dependence for pressure amplitude which can be approximated as

$$p(\gamma) = p(\gamma=0)\,|J_0(kb\gamma)|\ , \quad \gamma \ll 1 \text{ radian} \tag{2}$$

where γ is the angular position of the observation point in the Fraunhofer or Fresnel region,[1] relative to the backscattering axis and the sphere's center. (See Eq. (16) of Ref. 1 where in the present case $z_n = z + a$, $\gamma \simeq \tan\gamma = h/z_n$, and h corresponds to x in Fig. 4 of the present paper.)

The results to this point lead one to expect the following form, in the backscattering region, for the pressure amplitude of individual Rayleigh echoes in Fig. 2

$$p_m = A_m(ka)\ J_0(\beta\gamma) \tag{3}$$

where the argument of the Bessel function combines Eqs. (1) and (2), and $\beta = kac/c_R$, and m is a natural number (0,1,2 . . .). In this expression m indexes which Rayleigh echo we are examining, i.e. $m = 0$ implies the first Rayleigh echo after the specular reflection etc. A_m is the on-axis amplitude of a particular Rayleigh echo and may be a function of ka. The phase velocity ratio may also be a function of ka.

Calculation of the on-axis amplitudes $A_m(ka)$ and the phases of Rayleigh echoes requires use of the SWT. However, knowledge of this parameter is not required in order to test the J_0 dependence of the Rayleigh echo. We therefore defer to a subsequent paper calculations of the A_m's and of the phases of the Rayleigh echoes.

To obtain angular dependence results to compare with experiment one must know the phase velocity ratio c/c_R as a function of ka. This dependence can be found through the results of RST. The form function of an elastic sphere is given by[9]

$$f = (2/ika) \sum_{n=0}^{\infty} (2n+1) \frac{B_n(ka)}{D_n(ka)} P_n(\cos\theta) \tag{4}$$

where θ denotes the scattering angle relative to forward scattering and B_n and D_n are determinants of 3×3 matrices whose elements are combinations of spherical Bessel and Hankel functions.[9] In RST one examines the PWS of Eq. (4) term by term. Resonances in each term are determined numerically. One finds the resonant ka values for the nth term by solving the equation

$$D_n(X_{n\ell}) = 0 \tag{5}$$

where $X_{n\ell}$ is the ℓth resonance of the nth term. Knowing the value of a particular resonance in the nth term allows one to approximate the phase

velocity of the surface wave corresponding to that resonance. The relation used to obtain the phase velocity at the resonance values $X_{n\ell}$ is[4,17]

$$c_p/c = \mathrm{Re}(X_{n\ell})/(n + 1/2) \tag{6}$$

The Rayleigh phase velocity c_R is given by c_p when $\ell = 1$. For the specific case of a tungsten carbide sphere the resonances corresponding to Rayleigh waves have been found[9] for $n = 0$ to 7; c_R/c as a continuous function of ka can be found by curve fitting the discrete values found via Eq. (6). Equation (3) with $c_R(ka)/c$ found using Eq. (6) represents the final results for the angular dependence predicted for Rayleigh wave echoes. It is evident that the reasoning above can also be applied to whispering gallery waves.

B. Angular Dependence using Legendre Polynomial Expansions

It is appropriate to discuss briefly an alternate route to the angular dependence found. If the form function of Eq. (4) is rewritten using $\gamma = \pi - \theta$, where γ is the angle relative to backscattering and here θ is the scattering angle relative to the forward direction, it becomes

$$f = (2/ika) \sum_{n=0}^{\infty} (-1)^n (2n+1) \frac{B_n(ka)}{D_n(ka)} P_n(\cos\gamma) \tag{7}$$

For small angles γ one can use the following expansion derived by Szego[8,18]

$$P_n(\cos\gamma) = (\gamma/\sin\gamma)^{1/2} J_0((n + 1/2)\gamma) + O(n^{-3/2}) \tag{8}$$

Close to a Rayleigh resonance[4] $ka = \mathrm{Re}\, X_{n,1}$ and the γ dependence of the nth partial wave amplitude is similar to that of Eq. (3). This follows by noting Eq. (6) gives $c_R/c = ka/(n+1/2)$ and hence that $\beta = kac/c_R = n+1/2$. Taking $\gamma/\sin\gamma \approx 1$ reduces the γ dependence of Eq. (8) to the form of Eq. (3),

$$P_n(\cos\gamma) \approx J_0(\beta\gamma) \tag{9}$$

C. Specializing Angular Dependence Model to a Tungsten Carbide Sphere

Earlier it was stated that the Rayleigh resonance ka's were known for a tungsten carbide sphere for the specific cases of $n = 0$ through 7. Unfortunately, for use in comparison with our experiment we need the Rayleigh resonant ka's for $n = 10$ through 30. Since these were not available, we developed a computer program which would find them. (The program was verified with the results given in Ref. 9 for $n = 4$ through 7.) The Rayleigh resonances for $n = 0$ through 30 are given in Table I. The elastic parameters used in the program are given in the caption to the table. The results for $n = 0$ through 3 are from Ref. 9, the rest of the resonances are from our program. Using these resonant ka's and Eq. (6) we obtained the phase velocity ratio as a continuous function of ka for ka from 0 to 85. We also calculated the group velocity ratio for the Rayleigh wave using[4,17]

$$c_g/c = d(\mathrm{Re}(X_{n1}))/dn \tag{10}$$

Curves for both the phase and group velocities are given in Fig. 3. Note that the group velocity ratio is essentially constant for $ka \geq 30$. We can use this result and integrate Eq. (10) obtaining

$$(c_g/c)n + G' = \mathrm{Re}(X_{n1})$$

where G' is an integration constant. Then writing G' as $G' = G + c_g/(2c)$ we have

$$(c_g/c)(n + 1/2) + G = \mathrm{Re}(X_{n1}) \approx ka$$

Table I. Roots of $D_n(X_{n\ell}) = 0$ corresponding to the Rayleigh wave resonances of a tungsten carbide sphere. n is the partial wave series index and X_{n1} the corresponding Rayleigh pole. The material parameters used for the tungsten carbide sphere were[a]: density = 13.80 g/cm^3, longitudinal wave speed = 6.860×10^5 cm/s, shear wave speed = 4.185×10^5 cm/s. Those for water were: density = 1 g/cm^3, longitudinal wave speed = 1.4760×10^5 cm/s.

n	X_{n1}[b]	n	X_{n1}[b]	n	X_{n1}[b]
0[a]	$-0.22\times10^{-5} + 10.31\times10^{-6}$	11	33.1196 - 10.2437	22	61.9253 - 10.3979
1[a]	0.055980 - 10.069192	12	35.7583 - 10.2583	23	64.5298 - 10.4126
2[a]	7.454188 - 10.080989	13	38.3910 - 10.2723	24	67.1333 - 10.4263
3[a]	11.031209 - 10.11226	14	41.0190 - 10.2866	25	69.7353 - 10.4399
4	14.0869 - 10.1342	15	43.6421 - 10.3013	26	72.3364 - 10.4563
5	16.9497 - 10.1519	16	46.2612 - 10.3149	27	74.9370 - 10.4673
6	19.7231 - 10.1685	17	48.8774 - 10.3286	28	77.5366 - 10.4810
7	22.4472 - 10.1847	18	51.4907 - 10.3433	29	80.1353 - 10.4946
8	25.1401 - 10.1997	19	54.1021 - 10.3569	30	82.7329 - 10.5083
9	27.8130 - 10.2144	20	56.7114 - 10.3706		
10	30.4712 - 10.2290	21	59.3189 - 10.3843		

[a]Reference 9.

[b]X_{n1} values for n = 4 to 30 have uncertainties of ±0.0005.

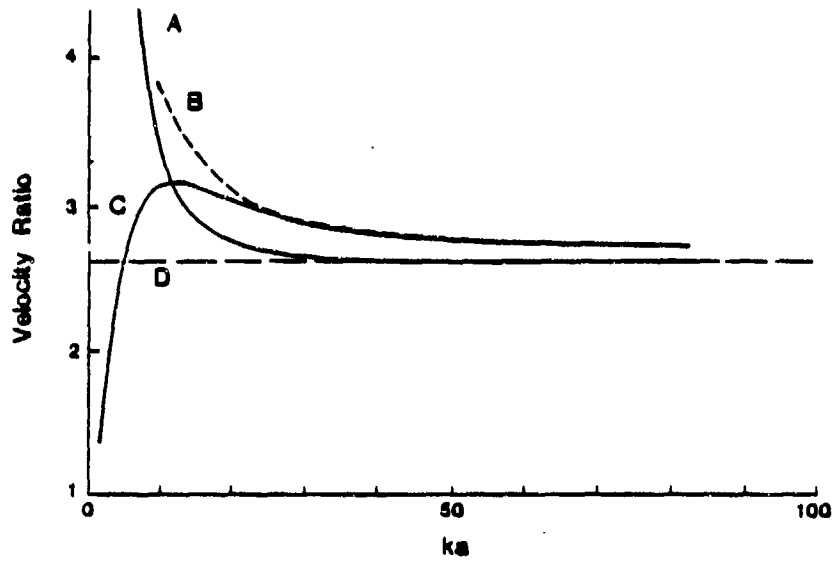

Rayleigh velocity ratios for a tungsten carbide sphere as a function of ka. The individual curves are: A - group velocity ratio, B - phase velocity ratio using Eq. (11), C - phase velocity ratio using Eq. (6), D - the phase velocity ratio for a Rayleigh wave propagating along a tungsten carbide-water plane interface.

Fig. 3.

Finally, using Eq. (6) and some algebraic manipulation we have the relation

$$c_R/c = (c_g/c)(1 - G/ka)^{-1} \tag{11}$$

between the phase velocity ratio and the group velocity ratio. G in this expression is a dimensionless constant. We emphasize that this is valid only if c_g/c is independent of ka.

A comparison between the exact curve for c_R/c and the approximate formula of Eq. (11) is shown in Fig. 3. For the case represented in Fig. 3, $c_g/c = 2.60$ for $ka \geq 30$ and G was chosen as 3.1. For $ka \geq 20$ agreement between Eq. (11) and the exact curve is good.

Also shown in Fig. 3 is the phase velocity ratio for a Rayleigh wave propagating along a flat tungsten carbide-water interface. This ratio was obtained by numerically solving a secular equation (below) for c_f, the complex phase velocity along a flat solid-liquid boundary. Let $u = (c_T/c_f)^2$ and $v = (c_T/c_L)^2$ where c_T and c_L are the transverse and longitudinal phase velocities respectively. The secular equation[19,20] is

$$(1-2u)^2 - 4u^2(u-1)^{1/2}(u-v)^{1/2} = -i(\rho_\ell/\rho_s)(u-v)^{1/2}[(c_T/c)^2 - u]^{-1/2}$$

where ρ_ℓ and ρ_s are the densities of the liquid and solid respectively. For the material parameters given in Table 1, this gives $c_f = (3.8154 - i0.0192) \times 10^5$ cm/sec for the Rayleigh root. The flat surface ratio shown in Fig. 3 is $\mathrm{Re}(c_f/c) \approx 2.60$ and both c_R/c and c_g/c were found to approach this value as $ka \to \infty$.

Using Eq. (11) and $\beta = kac/c_R$ one has

$$\beta = (c/c_g)(ka - G) \tag{12}$$

which can be substituted into Eq. (3) to give the normalized pressure amplitude of the mth Rayleigh echo when c_g/c is constant.

In the experiment to be described $p(\gamma)$ is determined as the receiver is moved away from the backscattering axis. These data were fitted to give the location of the first pressure null. This procedure is repeated for several ka values. Examining Eq. (3) one sees that the pressure null location corresponds to the point where the J_0 angular dependence first equals zero, i.e. when

$$(c/c_g)(ka - G)\gamma_m = 2.4048 \tag{13}$$

γ_m is the angle in radians corresponding to the pressure null. Equation (13) can be rewritten as

$$ka = (c_g/c)(2.4048)\gamma_m^{-1} + G \tag{14}$$

Since c_g/c and G are constants this relation implies that a plot of ka vs γ_m^{-1} should be a straight line. Furthermore the slope of that line depends on the value of c_g/c. The theoretical prediction above will be tested experimentally in the next section.

2.3 Experimental test of angular dependence

In this section the J_0 angular dependence model, as specialized in Sec. I.C to tungsten carbide, will be tested. The experimental apparatus has been discussed previously.[1,2] Here we note only the significant alterations to the apparatus which facilitate implementation of the current experimental test, and then proceed to the experimental procedure and results.

Figure 1 of Reference 1 is shown again in Fig. 4. This figure gives a conceptual description of the experiment. A piston-like transducer produces a short sinusoidal tone burst 4 cycles in duration. This tone burst is

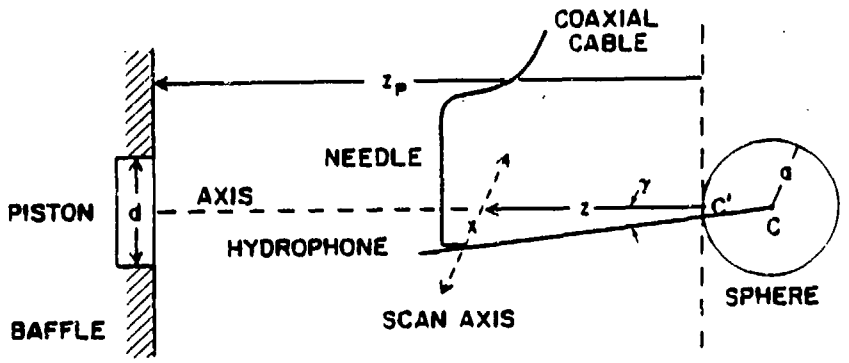

Simplified diagram of the scattering experiment. The hydrophone may be scanned along a line transverse to the symmetry axis defined by the source and the sphere. γ is the angle relative to backscattering. The diagram is not drawn to scale. In all the experiments described in Section II, $z_p = 160$ cm, while $z = 33$ cm for experiments with the 2.54 cm diameter tungsten carbide sphere and $z = 19$ cm for experiments with the 1.27 cm sphere.

Fig. 4.

scattered from a tungsten carbide sphere. The resulting echo is picked up by a needle hydrophone which may be positioned at small angles γ relative to the backscattering axis ($\tan\gamma = x/(z+a)$). In the present experiment the Panametrics model V309 sending transducer of Ref. 1 was replaced by either a Panametrics model V3261 or a Panametrics model V3260. These broadband transducers have lower resonance frequencies than the V309 (the V3261 has a 1 MHz resonance and the V3260 a 2.25 MHz resonance compared with 5MHz for the V309). In this experiment, which uses a 1.27 cm and 2.54 cm diameter tungsten carbide sphere, these transducers allow investigation in the ka range from 30 to 100. The only other significant changes in apparatus from Ref. 1 are the use of a digital signal averager (described in Ref. 2) and a new target mounting system. The main concern in designing a mounting system is to eliminate spurious echoes in the time window of the experiment (cf. Fig. 1).

The procedure used to test the model was to average the echo received at any angle γ over 256 bursts using the digital scope. Then the amplitude in volts of the central cycle of the first Rayleigh wave was determined. This voltage and the angle γ were recorded in a data file. The amplitude of the first Rayleigh wave was found via the process for at least 25 values of γ on either side of $\gamma = 0$. The computer normalized all data points by dividing by the amplitude at $\gamma = 0$ and plotted these normalized points on an amplitude vs γ graph. The computer next generated plots of the function $J_0(\beta\gamma)$ for several values of the constant β to find the value yielding the closest fit to the experimental results. An example of the results of this analysis is shown in Fig. 5. One immediately sees at least qualitative agreement between experiment and the model of Eq. (3).

The procedure above was repeated for 29 frequencies corresponding to ka values from 30 to 100. The 29 values of ka gave 29 different β values.

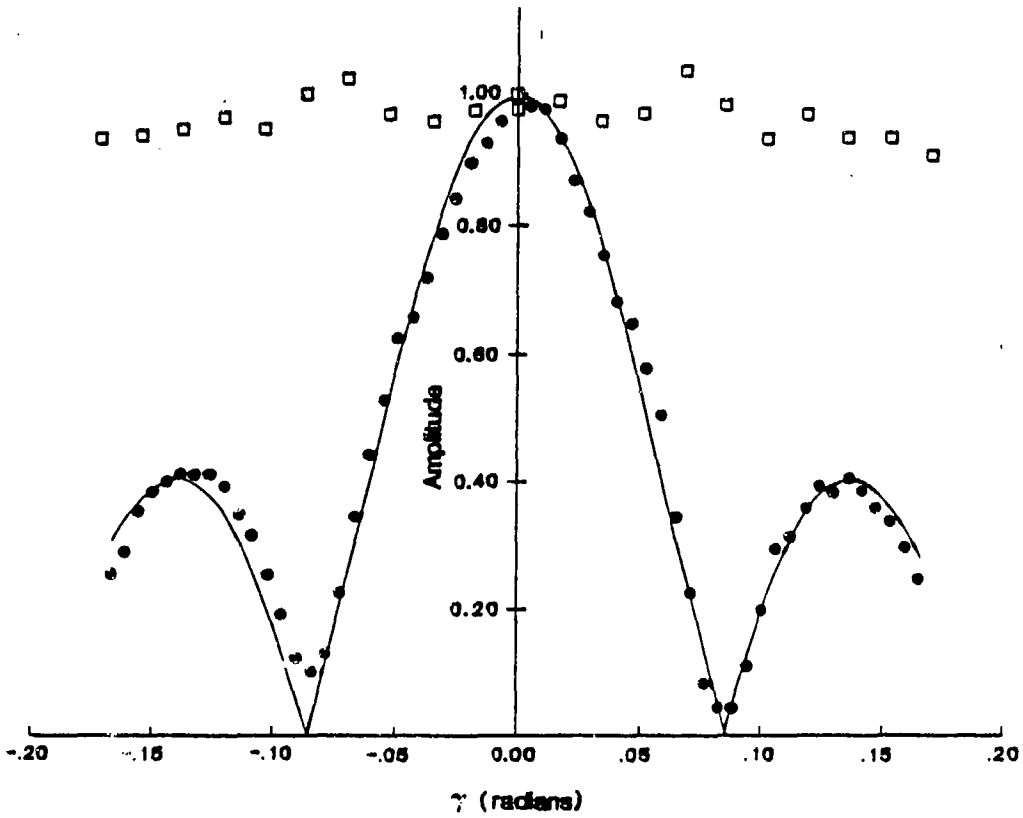

Experimental and theoretical results for ka = 60. The dots are experimental results of the angular dependence of the first Rayleigh echo amplitude normalized to the Rayleigh echo amplitude when γ, the backscattering angle, vanishes. The squares show experimental results for the specular reflection amplitude as a function of γ normalized to the specular reflection amplitude at $\gamma = 0$.

Fig. 5.

These β values were used to find the smallest angle γ_m for which $J_0(\beta\gamma_m)$ equaled zero, i.e. $\beta\gamma_m = 2.4048$. This gave 29 values of γ_m which were plotted on a graph of ka vs γ_m^{-1}.

To compare the experimental results for ka vs γ_m^{-1} with the theoretical prediction of Eq. (14) one needs the group velocity ratio for the sphere being used. The group velocity ratio can be obtained from the time spacing between Rayleigh waves. This spacing remained essentially constant at all ka values examined as it should if the group velocity remains constant as predicted in Fig. 3 for the ka range of interest. The experimental group velocity ratios found were 2.46 for the 2.54 cm sphere and 2.60 for the 1.27 cm sphere. One caveat should be noted. The constant G was found via an analysis using the elastic parameters in Ref. 9 as in Table I. The elastic parameters of our sphere should be close but not necessarily the same. This difference will probably have a small effect on G.

In Fig. 6 the experimental results for ka vs γ_m^{-1} are compared with the model prediction of Eq. (14). The theoretical lines used G = 3.1 and the approximate experimental values of c_g/c. Figure 6a shows the comparison for the 2.54 cm sphere and Fig. 6b shows the comparison for the 1.27 cm sphere. The agreement between model and experiment is good. This agreement confirms the theoretical model developed in Section I.

Figure 7 shows the data obtained at the lowest ka values examined; i.e., ka = 32.3. The data appear to have a small-amplitude structure superimposed on the $J_0(\beta\gamma)$ dependence. The cause of the structure was not determined.

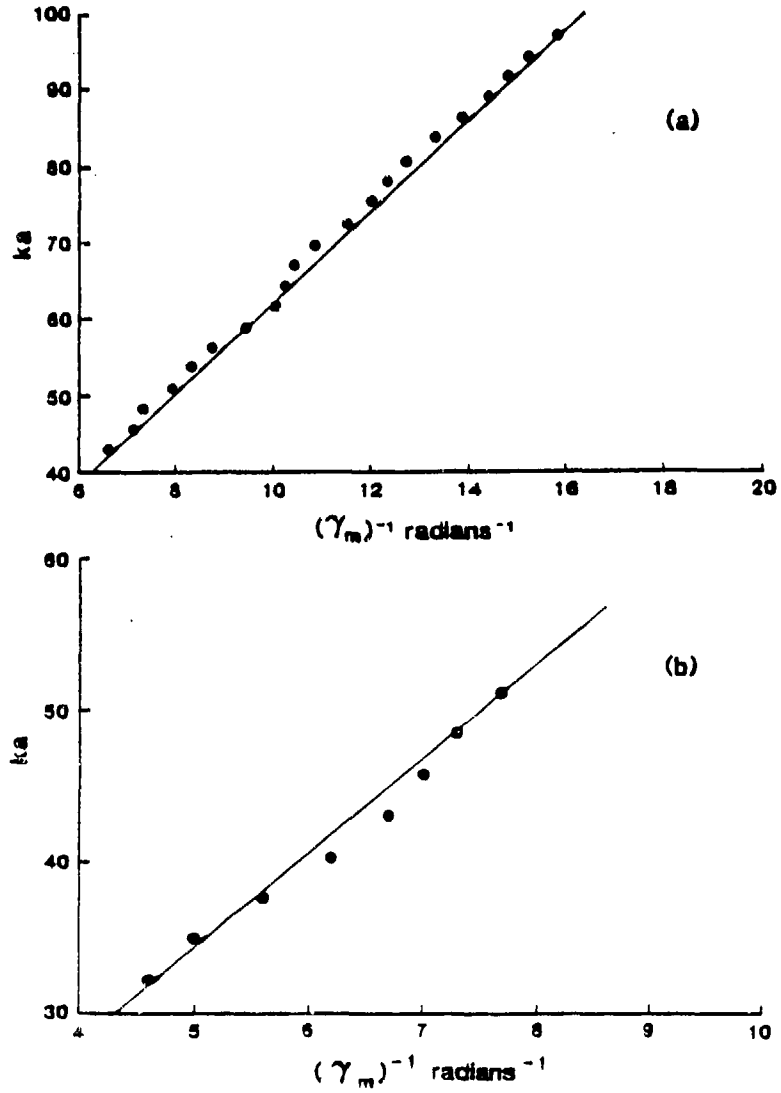

Experimental and theoretical results for ka vs γ_m^{-1} (defined in the text). Figure 6a are results for a 2.54 cm tungsten carbide sphere and Fig. 6b are for a 1.27 cm tungsten carbide sphere. The dots are experimental results and the lines are theoretical predictions using Eq. (14).

Fig. 6.

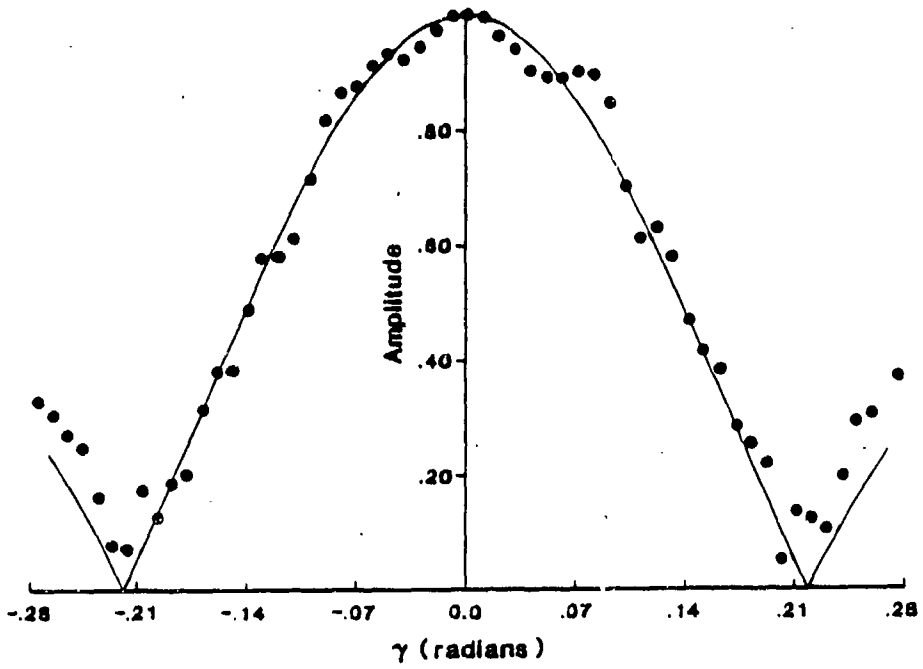

Experiment vs theory results analogous to Fig. 5 but at the lowest ka value tested; i.e. ka = 32.3. The dots are experimental results. The curve is given by $|J_0(\beta\gamma)|$ with β adjusted to fit the data. From Fig. 6(b) it is evident that this β gives a value for γ_m^{-1} which agrees with theory.

Fig. 7.

2.4 Discussion

We have presented a model of the axially-focused scattering due to surface waves generated on spheres. We have verified that the angular dependence of the pressure amplitude is $\approx J_0(\beta\gamma)$, which may have been anticipated from the SWT applied to other surface wave scattering problems.[8] We have related β to the surface wave's phase and group velocities and have verified the modeled β for the range of ka examined. The experiment demonstrates that axial focusing can be important down to ka's of at least 30. These results complement our earlier work on acoustical glory for large spheres ($ka \geq 100$) where the axial focusing was due to transmitted waves not surface waves.[1-3]

The model of axial focusing was derived using two methods. Both approaches led to the same angular dependence prediction; however, neither method gave a quantitative prediction of the on-axis amplitude of the surface wave echoes. This shortcoming can be eliminated via the use of the SWT as will be shown in a subsequent paper.

As an indication of the difference between the angular dependence of a focused and unfocused echo, data on the γ dependence of the unfocused specular reflection[3] from the 2.54 cm diameter tungsten carbide sphere were obtained. These data are shown as squares in Fig. 5. Only small fluctuations in the amplitude of the specular reflection are seen. This can be contrasted with the J_0 amplitude variation of the focused Rayleigh wave. (The origin of the small fluctuation in the specular reflection has not been determined.)

The arguments used here in our method of predicting the high-frequency angular dependence of surface wave echoes can be extended to non-spherical elastic objects possessing a symmetry axis. When the object is ensonified along its axis of rotational symmetry, axially-focused surface wave echoes

should be present in the near backward scattering direction. It is necessary that the phase matching criteria be met for the excitation of a surface wave and that the attenuation associated with circumnavigation be sufficiently small. The consequences of focusing are evident in previous measurements of the backscattering of tone bursts from a spheroid in air (Fig. 6 of Ref. 10). The creeping wave (i.e., Franz) echo was significantly larger when the spheroid was ensonified along its symmetry axis than when ensonified perpendicular to the symmetry axis.

Acknowledgments

This research was supported by the Office of Naval Research. The computer programs used to evaluate the roots of Eq. (5) were based on ones developed by B. L. Brim (also with O.N.R. support) for other purposes.[21] Evaluation of the required Hankel functions (with complex arguments) was partially facilitated with algorithms supplied by Professor J. A. Cochran of the Washington State University Department of Pure and Applied Mathematics. These algorithms were based, in part, on analysis done in Ref. 22.

Appendix: Location of the Focal Circle

In this appendix we calculate the horizontal distance α of the point F_R in Fig. 2 behind the vertical line through C'. In Fig. A1 a portion of Fig. 2 is redrawn. The surface wave is launched at point B. Radiation in the backscattering direction is represented by ray A'B' while radiation at an angle γ relative to backscattering is represented by A"B". The intersection of the backward extrapolated A"B" and A'B' in the limit $\gamma \to 0$ defines the location of the virtual focus F_R.

Inspection of Fig. A1 shows that $\delta = \gamma$. In the limit $\gamma \to 0$, it is evident that the distance between B' and B", denoted as (B'B"), becomes $a\delta$ where a is the sphere's radius. Inspection of Fig. A1 also shows that $(B''C'') \to (B'B'')\cos\theta_R$ as $\gamma \to 0$ and that $(B''C'') \to \alpha'\gamma$. Combining these results gives $\alpha' = a \cos \theta_R$. By definition, $\alpha = \alpha' + a(1-\cos\theta_R)$ which gives $\alpha = a$.

The result $\alpha = a$ could have been anticipated from the calculation of α in Ref. 2 of for the case of transmitted waves within an elastic sphere. If we examine Eq. (10) of Ref. 2 in the limit that n (the total number of chords of the transmitted wave within the sphere) goes to ∞ we find $\alpha \to a$.

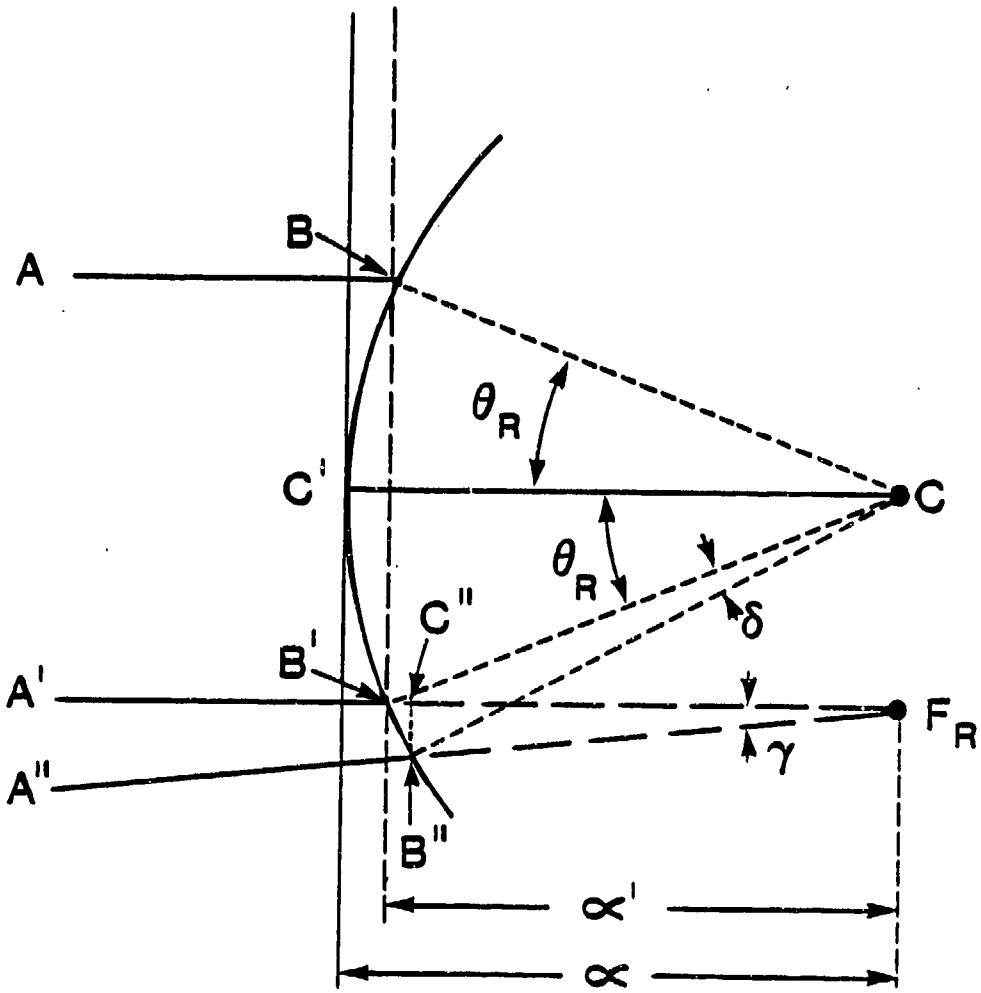

The region of Fig. 2 relevant to calculating the horizontal position of point F_R behind the vertical line through C' is shown.

Fig. A1.

References

1. P. L. Marston, K. L. Williams, and T. J. B. Hanson, "Observation of the acoustical glory: High frequency backscattering from an elastic sphere," J. Acoust. Soc. Am. 74, 605-618 (1983).
2. K. L. Williams and P. L. Marston, "Mixed-mode acoustical glory scattering from a large elastic sphere: Model and experimental verification," J. Acoust. Soc. Am. 76, 1555-1563 (1984).
3. P. L. Marston and D. S. Langley, "Glory and rainbow enhanced acoustic backscattering from fluid spheres: Models for diffracted axial focusing," J. Acoust. Soc. Am. 73, 1464-1475 (1983).
4. L. Flax, G. C. Gaunaurd, and H. Uberall, "Theory of resonance scattering" in Physical Acoustics, edited by W. P. Mason and R. N. Thurston (Academic, New York, 1981), Vol. 15, pp. 191-294.
5. G. V. Frisk and H. Uberall, "Creeping waves and lateral waves in acoustic scattering by large elastic cylinders," J. Acoust. Soc. Am. 59, 46-54 (1976).
6. J. W. Dickey and H. Uberall, "Acoustic high frequency scattering by elastic cylinders," J. Acoust. Soc. Am. 66, 275-283 (1979).
7. B. R. Levy and J. B. Keller, "Diffraction by a smooth object," Commun. Pure Appl. Math. 12, 159-209 (1959).
8. H. M. Nussenzveig, "High frequency scattering by a transparent sphere. II. Theory of the rainbow and glory," J. Math. Phys. 10, 125-176 (1969); the reader is cautioned that in Eq. (5.17), $\beta = ka$ and that the detailed results do not apply to the problem considered here.
9. G. C. Gaunaurd and H. Uberall, "RST analysis of monostatic and bistatic acoustic echoes from an elastic sphere," J. Acoust. Soc. Am. 73, 1-12 (1983).

10. L. R. Dragonette, R. H. Vogt, L. Flax, and W. G. Neubauer, "Acoustic reflection from elastic spheres and rigid spheres and spheroids. II. Transient analysis," J. Acoust. Soc. Am. 55, 1130-1137 (1974).

11. K. Numrich, L. R. Dragonette, and L. Flax, "Classification of submerged targets by acoustic means," in Elastic Wave Scattering and Propagation, edited by V. K. Varadan and V. V. Varadan (Ann Arbor Science Publishers, Michigan, 1982), pp. 149-171.

12. L. R. Dragonette, S. K. Numrich, and L. J. Frank, "Calibration technique for acoustic scattering measurements," J. Acoust. Soc. Am. 69, 1186-1189 (1981).

13. R. D. Doolittle, H. Uberall, and P. Ugincius, "Sound Scattering by Elastic Cylinders," J. Acoust. Soc. Am. 43, 1-14 (1968).

14. P. L. Marston, "Half-order derivative of a sine-wave burst: Applications to two dimensional radiation, photoacoustics, and focused scattering from spheres and a torus," J. Acoust. Soc. Am. 76, 291-295 (1984).

15. J. B. Keller and F. C. Karal, Jr., "Geometrical theory of elastic surface-wave excitation and propagation," J. Acoust. Soc. Am. 36, 32-40 (1964).

16. J. B. Keller, "Rays, Waves, and Asymptotics," Bull. Am. Math. Soc. 84, 727-750 (1978).

17. H. Uberall, J. George, A. R. Farhan, G. Mezzorani, A. Nagl, K. A. Sage, and J. D. Murphy, "Dynamics of acoustic resonance scattering from spherical targets: Application to gas bubbles in fluids," J. Acoust. Soc. Am. 66, 1161-1172 (1979).

18. G. Szego, Orthogonal Polynomials (American Mathematical Society, New York, 1939), Theorem 8.21.6.

19. H. Überall, "Surface Waves in Acoustics," in Physical Acoustics, edited by W. P. Mason and R. N. Thurston (Academic, New York, 1973), Vol. 10, pp. 1-60.

20. G. V. Frisk, J. W. Dickey, and H. Überall, "Surface wave modes on elastic cylinders," J. Acoust. Soc. Am. 58, 996-1008 (1975).

21. B. L. Brim, "Theoretical investigation of Brewster angle phenomenon for curved surfaces," M.S. project report, Washington State University, 1983 (unpublished).

22. J. A. Cochran and J. N. Hoffspiegel, "Numerical techniques for finding ν-zeros of Hankel functions," Math. Comp. 24, 413-422 (1970).

Chapter 3

BACKSCATTERING FROM AN ELASTIC SPHERE: SOMMERFELD-WATSON TRANSFORMATION AND EXPERIMENTAL CONFIRMATION

3.1 Introduction

Understanding the physical nature of the echo structure of elastic objects having simple shapes is an important step toward understanding echoes from complex elastic bodies. Studies on acoustical scattering from spheres and cylinders[1-11] date back to Rayleigh.[1] The plane wave scattering of an elastic sphere or cylinder may be written as an infinite partial-wave series (PWS).[2,3] At high frequencies the PWS converges slowly and the Sommerfeld-Watson transform (SWT) may be used to convert the PWS to a more rapidly convergent form.[3] Furthermore, the results of the SWT may be interpreted in terms of reflected and transmitted bulk waves and the scattering contributions of Franz, Rayleigh, and whispering gallery waves. In this way, the physical origins of the echo structure are elucidated. Detailed analysis using the SWT has been carried out on fluid-loaded elastic cylinders.[3,4] The "modified" SWT has been used to study the case of scalar plane wave scattering from a transparent sphere.[12,13] The transparent sphere analyses may be used as an aid in understanding acoustical scattering from fluid-loaded <u>fluid</u> spheres. In the present paper we carry out the SWT on a fluid-loaded <u>elastic</u> sphere. The analysis for elastic spheres differs in significant details from the analysis for other spheres[12,13] or elastic cylinders.[3,4]

Our SWT analysis concentrates on the specular reflection and Rayleigh wave contributions to scattering at small backscattering angles. Previously we have measured and modeled the angular dependence of the Rayleigh contributions to near backward scattering.[14] The SWT confirms the physical picture used and, for the first time, predicts the absolute backscattering amplitude associated with one or more circumnavigations of the Rayleigh wave around the sphere. Explicit expressions for the damping of Rayleigh waves on an elastic <u>sphere</u> due to radiation into the surrounding fluid are obtained.

The analysis may be extended to include whispering gallery waves. Though the emphasis of this paper is on the backward axially-focused scattering from spheres, the resulting physical picture should be applicable to to the objects of revolution ensonified along the symmetry axis.

To test the SWT, tungsten carbide spheres in water were ensonified by tone bursts having central frequencies such that $24 < ka < 80$ where a is the sphere's radius and k is the wavenumber. Measurements were made of the first and second Rayleigh contributions to the backscattered pulse train. Plots of the measured distinct Rayleigh amplitudes as a function of ka confirm the results of the SWT and illustrate the significance of radiation damping and axial focusing.

In Section I the SWT is performed. The criteria $ka \gg 1$ is assumed throughout the section. The physical picture which ensues from the analysis is discussed. The analytical prediction of the Rayleigh contributions to backscattering follows from the discussion. In Section II tungsten carbide spheres are used to experimentally confirm this prediction. Throughout the paper we relate results of the present analysis to the work of Ref. 14. Section III discusses the results.

3.2 The Sommerfeld-Watson Transformation

In this section the SWT is carried out on the total pressure field of a fluid-loaded elastic sphere ensonified by a plane wave. An expression for the form function f ensues from the initial analysis. Having obtained f, further analysis will concentrate on its interpretation. The main emphasis of the analysis will be on the specular reflection and Rayleigh contribution to f at small backscattering angles. However, extensions necessary to include other waves are delineated. Portions of the present analysis parallel the SWT analysis of a fluid-loaded elastic cylinder.[3]

Using the coordinate system shown in Fig. 1 and assuming a unit amplitude plane wave traveling in the +z direction the total pressure in the fluid surrounding the sphere is the real part of[11]

$$p(r,\theta,t) = e^{-i\omega t} \sum_{n=0}^{\infty} i^n(2n+1)(j_n(kr) + \frac{B_n}{D_n} h_n^{(1)}(kr))P_n(\mu) \qquad (1)$$

In this expression $\mu = \cos\theta$, $k = \omega/c$, c is the sound speed in the liquid, r and the scattering angle θ are defined in Fig. 1, j_n and h_n are spherical Bessel and Hankel functions, and P_n is the Legendre polynomial. B_n and D_n are 3 x 3 determinants whose elements are given in Appendix A. They are functions of x, x_S, x_L, ρ_o, ρ_E where $x = ka$; $x_S = xc/c_S$; c_S = shear sound speed in the elastic sphere; $x_L = xc/c_L$; c_L = longitudinal sound speed in the elastic sphere; ρ_o = density of the liquid; ρ_E = density of the solid.

The SWT consists of rewriting the PWS of Eq. (1) in terms of a contour integral using the relation[15]

$$\sum_{n=0}^{\infty} g(n + 1/2) = \tfrac{1}{2} \int_{\Gamma} g(\lambda) \frac{e^{-i\pi\lambda}}{\cos\pi\lambda} d\lambda \qquad (2)$$

The contour Γ is shown in Fig. 2. The contour surrounds the positive poles of $(\cos\pi\lambda)^{-1}$. Substituting Eq. (1) into Eq. (2), using $C_n = D_n j_n(kr) + B_n h_n^{(1)}(kr)$, and the substitution $\nu = \lambda - 1/2$ for compactness of notation, we have

$$p(r,\theta) = \int_{\Gamma} e^{-i\pi/4} \lambda(\frac{C_\nu}{D_\nu}) P_\nu(\mu) \frac{e^{-i\pi\lambda/2}}{\cos\pi\lambda} d\lambda \qquad (3)$$

We proceed by deforming the contour so p may be written as an integral over the poles of $1/D_\nu$ in the first quadrant (Section II discusses a pole finding procedure). The general location of the poles in the first quadrant is shown

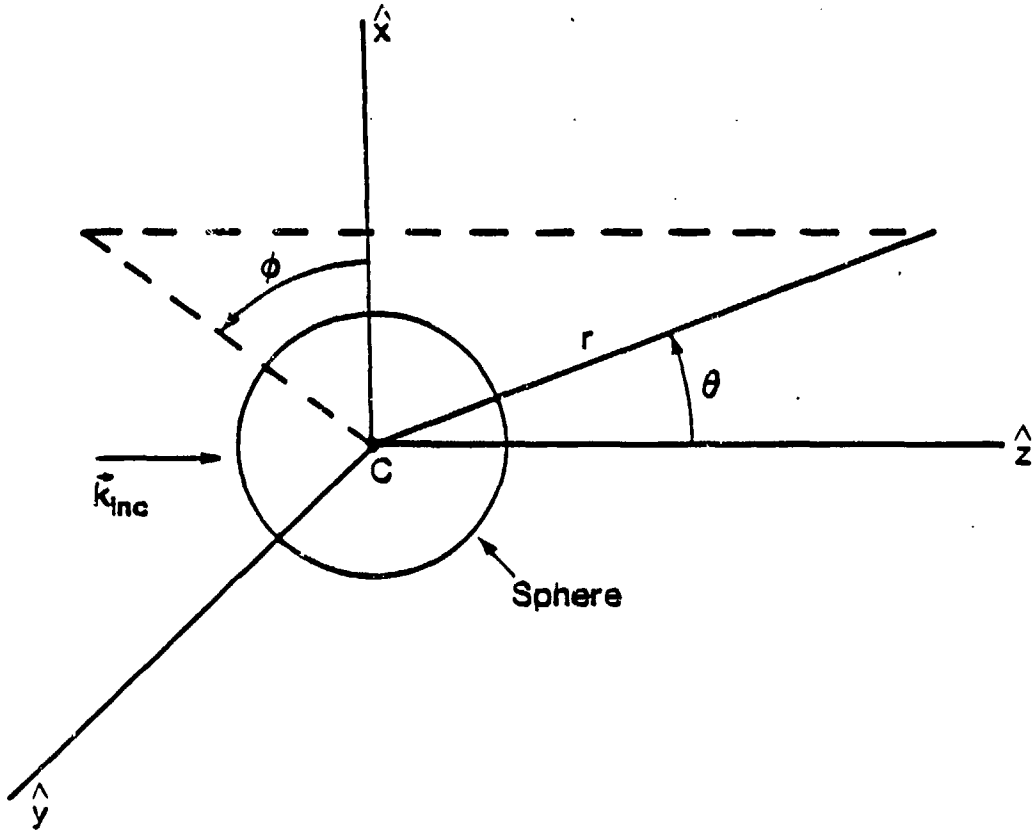

The r, θ, φ coordinate system shown above was used in writing the partial wave series (PWS) solution to plane wave scattering from an elastic sphere. The plane wave is assumed to be travelling in the +z direction.

Fig. 1.

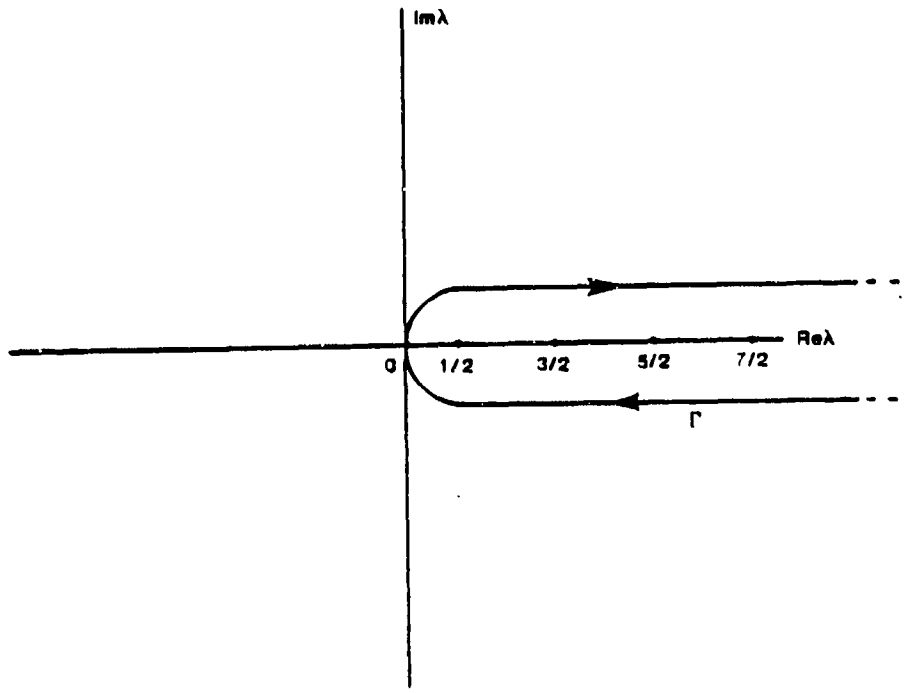

Contour used in rewriting the PWS solution as a contour integral in the complex λ plane. The half integer points along the real axes are poles of $(\cos\pi\lambda)^{-1}$. The residues of the integrand at these poles recaptures the PWS.

Fig. 2.

in Fig. 3. The location and identification of the poles as Rayleigh, whispering gallery, or Franz was checked using the specific case of an aluminum sphere with the same physical parameters as the aluminum cylinder which was addressed in Ref 3. Figure 3 also shows a contour $\bar{\Gamma} = (\Gamma', \Gamma_\infty^1, \Gamma_0, \Gamma_\infty^2, -\Gamma, \Gamma_\infty^3)$. There are no poles within the contour. Therefore the integral of Eq. (3) over this contour would vanish. In Appendix B we show that the contributions to the integral over $\bar{\Gamma}$ due to the paths at ∞ are negligible. With this result we can write p as $p = p_I + p_{II}$ where

$$p_{I,II} = \int_{\Gamma_{I,II}} e^{-i\pi/4} \lambda \left(\frac{C_\nu}{D_\nu}\right) P_\nu(\mu) \frac{e^{-i\pi\lambda/2}}{\cos\pi\lambda} d\lambda \tag{4}$$

and the respective contours are $\Gamma_I = \Gamma_0$ and $\Gamma_{II} = \Gamma'$. We limit the analysis which follows to p_I since it contains, among other things, the contributions of main concern to us; i.e., the specular reflection and Rayleigh surface waves. p_{II} is the "background integral" which has been argued to be small in the cylindrical case.[3,4] We will return briefly to p_{II} in Section III.

To evaluate p_I we first break Γ_0 into contours Γ_1 and Γ_2 shown in Fig. 4. This must be done as a preliminary to separating out the contributions to p_I from the incident, and bulk waves.[3] Then, in the Γ_2 integral, we use the relations[9,15]

$$e^{i\pi\nu} P_\nu(-\mu) + 2i\, e^{i\pi\nu} \cos\pi\lambda\, Q_\nu^{(1)}(\mu) = P_\nu(\mu) \tag{5}$$

$$Q_\nu^{(1)}(\mu) = \tfrac{1}{2}\left[P_\nu(\mu) + \left(\frac{2i}{\pi}\right) Q_\nu(\mu)\right] \tag{6}$$

where P_ν and Q_ν are Legendre functions of the first and second kind. The auxiliary function $Q_\nu^{(1)}$ is introduced because of useful properties[15] when

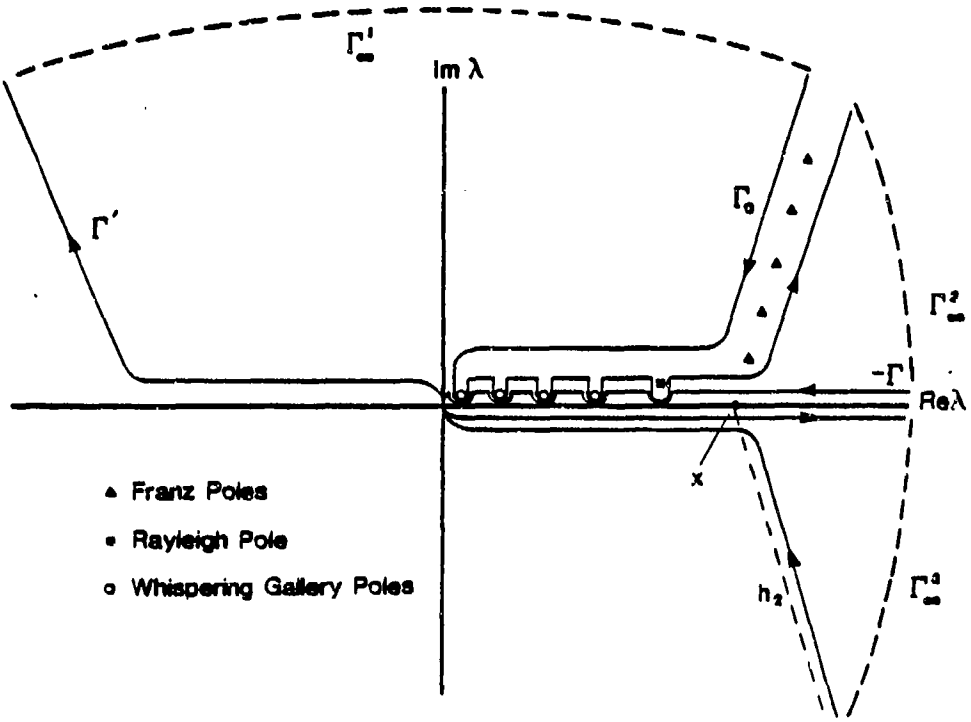

The contour $\bar{\Gamma} = (\Gamma', \Gamma^1_\infty, \Gamma_o, \Gamma^2_\infty, -\Gamma, \Gamma^3_\infty)$ is used to rewrite the contour integral for the pressure. The pressure can be written as a contour integral over Γ' and Γ_o.

Fig. 3.

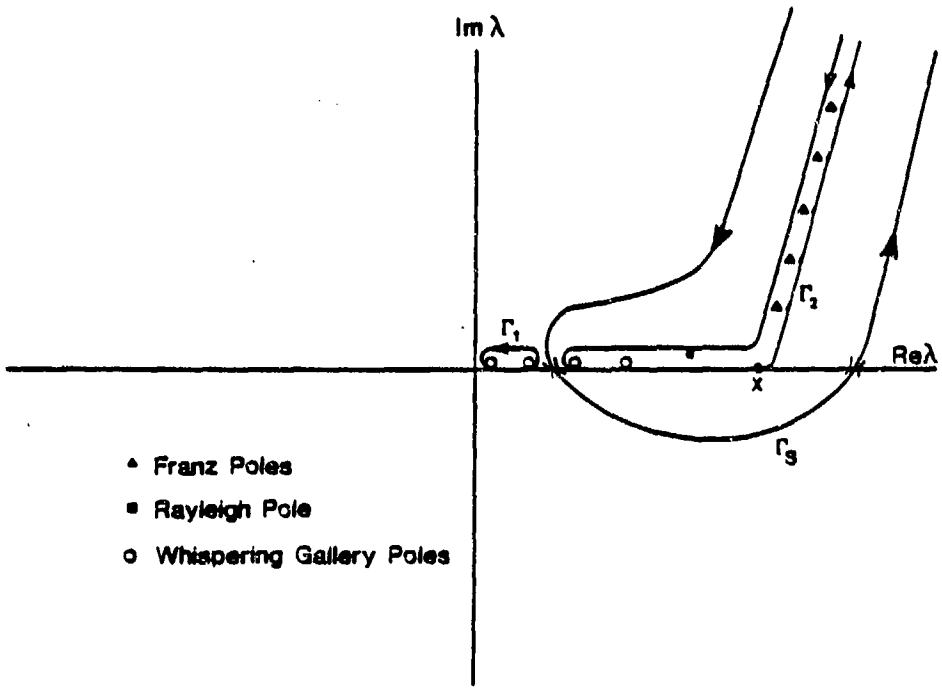

The contour Γ_o of Figure 3 can be separated into contours Γ_1 and Γ_2 shown. The contour Γ_s is used to find the contribution to the pressure from the incident plane wave and the specularly reflected wave.

Fig. 4.

$|\lambda| >> 1$ (see Appendix C). Substituting Eq. (5) into Eq. (4) we have $p_I = p_1 + p_2 + p_3$ where

$$p_1 = 2i \int_{\Gamma_2} e^{-i3\pi/4} F_1(\lambda) Q_\nu^{(1)}(\mu) e^{i\pi\lambda/2} d\lambda \tag{7}$$

$$p_2 = \int_{\Gamma_2} e^{-i3\pi/4} F_1(\lambda) P_\nu(-\mu) \frac{e^{i\pi\lambda/2}}{\cos\pi\lambda} d\lambda \tag{8}$$

$$p_3 = \int_{\Gamma_1} e^{-i\pi/4} F_1(\lambda) P_\nu(\mu) \frac{e^{-i\pi\lambda/2}}{\cos\pi\lambda} d\lambda \tag{9}$$

and $F_1(\lambda) = \lambda C_\nu / D_\nu$. Note that the integrand of p_1 no longer has the term $(\cos\pi\lambda)^{-1}$ and therefore it has no poles along the real axis.

We now examine the expression for $r >> ka^2$ (the far zone) and show that it leads to

$$p_I = e^{ikz} + \frac{ae^{ikr}}{2r} f \tag{10}$$

where f is a form function descriptive of the scattering for $ka >> 1$.

To aid in manipulating the expressions for p_1, p_2, and p_3 we rewrite $F_1(\lambda)$ using the relation

$$j_\nu(kr) = \tfrac{1}{2} (h_\nu^{(1)}(kr) + h_\nu^{(2)}(kr)) \tag{11}$$

and the result from Appendix A (Eq. (A4)) that

$$B_\nu/D_\nu = - \tfrac{1}{2} (1 + \frac{H_\lambda^{(2)}(x)}{H_\lambda^{(1)}(x)} \frac{\mathfrak{D}_\nu^-}{\mathfrak{D}_\nu^+}) \tag{12}$$

where $\mathfrak{D}_\nu^-$ and $\mathfrak{D}_\nu^+$ are given by Eq. (A5) and H_λ is a cylindrical Hankel

function. Substituting Eq. (11) and (12) into $C_\nu = D_\nu j_\nu(kr) + B_\nu h_\nu^{(1)}(kr)$ and using this result in the relation for $F_1(\lambda)$ gives

$$F_1(\lambda) = \frac{\lambda}{2}\left(h_\nu^{(2)}(kr) - \frac{H_\lambda^{(2)}(x)}{H_\lambda^{(1)}(x)}\frac{\mathfrak{D}_\nu^-}{\mathfrak{D}_\nu^+} h_\nu^{(1)}(kr)\right) \tag{13}$$

When this expression is substituted into Eqs. (7), (8), and (9) we find there is no contribution to these integrals due to the $h_\nu^{(2)}(kr)$ in Eq. (13) since Γ_1 and Γ_2 contain no poles of $h_\nu^{(2)}(kr)$ and since along Γ_2, $h_\nu^{(2)}(kr)$ vanishes exponentially as a function of λ over the portions of Γ_2 which go to ∞. (The latter assertion may be established using the methods of Appendix B. See also Ref. 4 and references therein for the cylindrical case.)

The above results give for p_1, p_2, and p_3

$$p_1 = -i\int_{\Gamma_2} e^{-i3\pi/4} F_2(\lambda,x)h_\nu^{(1)}(kr)Q_\nu^{(1)}(\mu)\, e^{i\pi\lambda/2}\, d\lambda \tag{14}$$

$$p_2 = -\tfrac{1}{2}\int_{\Gamma_2} e^{-i3\pi/4} F_2(\lambda,x)h_\nu^{(1)}(kr)P_\nu(-\mu)\,\frac{e^{i\pi\lambda/2}}{\cos\pi\lambda}\, d\lambda \tag{15}$$

$$p_3 = -\tfrac{1}{2}\int_{\Gamma_1} e^{-i\pi/4} F_2(\lambda,x)h_\nu^{(1)}(kr)P_\nu(\mu)\,\frac{e^{-i\pi\lambda/2}}{\cos\pi\lambda}\, d\lambda \tag{16}$$

where $F_2(\lambda,x) = \lambda H_\lambda^{(2)}(x)\mathfrak{D}_\nu^-/H_\lambda^{(1)}(x)\mathfrak{D}_\nu^+$. Since the integrand of p_1 contains no poles along the real axis we may deform Γ_2 into the path Γ_S shown in Fig. 4. Γ_S goes through the two saddle points found to exist for the integrand of p_1. The right-hand saddle point is found in Appendix C to lead to the incident wave $\exp(ikz)$. This and the approximation $h_\nu^{(1)}(kr) \simeq (kr)^{-1}\exp[i(kr - \nu\pi/2 - \pi/2)]$, which is valid for $kr \to \infty$, allows f in

Eq. (10) to be written as $f = f_1 + f_2 + f_3$ where

$$f_1 = \frac{2i}{ka} \int_{\Gamma_L} F_2(\lambda,x)\, Q_\nu^{(1)}(\mu)\, d\lambda \tag{17}$$

$$f_2 = \frac{1}{ka} \int_{\Gamma_2} F_2(\lambda,x)\, \frac{P_\nu(-\mu)}{\cos\pi\lambda}\, d\lambda \tag{18}$$

$$f_3 = \frac{1}{ika} \int_{\Gamma_1} F_2(\lambda,x)\, \frac{P_\nu(\mu)}{\cos\pi\lambda}\, d\lambda \tag{19}$$

In f_1 the contour Γ_L is only a portion of the contour Γ_S namely that portion which goes over the left-hand saddle point since the right-hand saddle point has already yielded the incident wave.

The problem now is to evaluate f and interpret the results. In examining f we will be particularly concerned about its form at small angles γ relative to backscattering where $\pi - \theta = \gamma$, $|\gamma| \ll 1$ rad. It can be verified via the analysis which follows, that as θ increases from 0 to π, the left-hand saddle point approaches the origin in the complex λ plane. This implies that for small angles relative to backscattering the Γ_1 contour encloses no poles and $f_3 = 0$. Therefore near backscattering we need only examine f_1 and f_2.

In the cylindrical case an analysis of an integral similar to f_1 has been carried out.[4] In Appendix A we use the methods of Ref. 4 to rewrite $\mathfrak{D}_\nu^-/\mathfrak{D}_\nu^+$ as $\mathfrak{D}_\nu^-/\mathfrak{D}_\nu^+ = R_{S\lambda} - U_\lambda$. This allows one to write $F_2(\lambda,x) = F_S + F_{tw}$ with $F_S = \lambda R_{S\lambda} H_\lambda^{(2)}(x)/H_\lambda^{(1)}(x)$ and $F_{tw} = -\lambda U_\lambda\, H_\lambda^{(2)}(x)/H_\lambda^{(1)}(x)$. With this separation we have $f_1 = f_S + f_{tw}$ where f_S and f_{tw} are given by Eq. (17)

with $F_2(\lambda,x)$ replaced by F_S and F_{tw} respectively. The motivation for this separation will be evident from the results which follow.

In Appendix D, f_S is evaluated via the saddle point method giving

$$f_S = -R_{S\lambda_s} e^{-i2ka\cos(\gamma/2)} \tag{20}$$

where $R_{S\lambda_s}$ is given by evaluating Eq. (A8) at the saddle point $\lambda_s = ka \sin\gamma/2$. In the limit $ka \to \infty$ one can show that $(-R_{S\lambda s})$ becomes the reflection coefficient of a plane wave incident onto a plane solid-liquid boundary at angle $\gamma/2$ with respect to the normal. In particular for $\gamma = 0$ one finds

$$\lim_{ka \to \infty} (-R_{S(\lambda_s=0)}) \to (\rho_E c_L - \rho_o c)/(\rho_E c_L + \rho_o c) \equiv R_p \tag{21}$$

For finite ka values $(-R_{S\lambda s})$ is therefore the coefficient for specular reflection from the sphere. Equation (20) also gives the propagation phase of the specular reflection measured <u>relative to</u> a wave traveling in liquid along the path $(r = \infty, \theta = \pi) \to (r = 0) \to (r = \infty, \theta = \pi - \gamma)$. We have previously obtained results analogous to Eq. (20) by different methods.[16,17] (In these previous results the phase of the specular reflection was given relative to a wave traveling in the liquid along the path $(r=\infty, \theta=\pi) \to (r=a, \theta=\pi) \to (r=\infty, \theta=\pi-\gamma)$).

Through further analysis which would involve a combination of the methods of Ref. 4, 16-18, one should be able to recapture from f_{tw} the contribution to scattering from <u>bulk waves transmitted within the sphere</u>. Since f_{tw} is not of direct relevance to the goals of the present paper we will not examine it in detail; analysis using the techniques of Refs. 16

and 18 suggests $|f_{tw}|$ is small for the experiments presented in Sec. II (a short discussion of this analysis is given in Sec. III).

A caveat concerning the evaluation of f_s should be noted. The asymptotic expressions used in the saddle point analysis of Appendix D breakdown near $\theta = 0$ and $\theta = \pi$. For $\theta \to \pi$ the problem lies in the asymptotic expression used for $Q_\nu^{(1)}(\mu)$. Nussensveig has shown in Refs. 12 and 15 that, for scattering from a fluid or soft sphere, the saddle point result for specular reflection remains uniformly valid up to $\theta = \pi$ even though the saddle point method is not valid near $\theta = \pi$. Using Nussensveig's methods one may show the same to be true for evaluation of f_s. For $\theta \to 0$ one cannot use either the asymptotic expressions for $Q_\nu^{(1)}(\mu)$ or the Debye expressions for the Hankel functions. In the neighborhood of $\theta = 0$ one must use Airy type expansions for the Hankel functions and new effects arise.[15] The above evaluation of f_s is therefore incomplete near forward scattering.

Using the method of residues[3,19,20] the integral expression for f_2 can be written as a sum over the Rayleigh, Franz, and whispering gallery poles which we designate as λ_R, λ_{WG}, λ_F respectively. Here $\lambda = \lambda_\ell$ is a root of the equation $\mathfrak{D}^+_{\lambda-\frac{1}{2}} = 0$. From the residue analysis one obtains

$$f_2 = \sum_{\ell=R,WG,F} f_{\lambda_\ell} \tag{22}$$

$$f_{\lambda_\ell} = \lambda_\ell \frac{2\pi i}{ka} \frac{H^{(2)}_{\lambda_\ell}(x)}{H^{(1)}_{\lambda_\ell}(x)} \frac{\mathfrak{D}^-_{\lambda_\ell-\frac{1}{2}}}{\dot{\mathfrak{D}}^+_{\lambda_\ell-\frac{1}{2}}} \frac{P_{\lambda_\ell-\frac{1}{2}}(\cos\gamma)}{\cos\pi\lambda_\ell} \tag{23}$$

where $\dot{\mathfrak{D}}^+_{\lambda_\ell-\frac{1}{2}}$ is the derivative of $\mathfrak{D}^+_{\lambda-\frac{1}{2}}$ with respect to λ evaluated at $\lambda = \lambda_\ell$ and the relation $\pi - \theta = \gamma$ was used. The procedure used to obtain Eq. (22) and (23) is analogous to that of Ref. 7. Further manipulation of f_{λ_ℓ} depends on the type of pole being examined. The primary difference in

further analysis is in the asymptotic expansions used for the Hankel functions in Eq. (23). For the Rayleigh and whispering gallery poles the Debye expansions

$$H_\lambda^{(1,2)}(x) = \left(\frac{2}{\pi}\right)^{1/2} \frac{\exp[\pm i(x^2-\lambda^2)^{1/2} \mp i\lambda \arccos(\lambda/x) \mp i\pi/4]}{(x^2 - \lambda^2)^{1/4}} \quad (24)$$

may be used since the poles are between x and $-x$ in the λ plane and $|\lambda_\ell - x| >> (\lambda_\ell)^{1/3}$ (cf. Fig. 3, also Appendix A of Ref. 15 for a relevant summary of asymptotic expansions). The Franz poles, however, are in a region of the λ plane where combination of asymptotic expansions must be used (Ref. 7, Appendix A). Since our main interest is in the Rayleigh-wave form function $f_{\lambda_R} \equiv f_R$ we particularize further analyses to that case. The whispering gallery contributions to f_2 have the same form and interpretation as we will find for f_R.

In rewriting f_R the relation[8]

$$(\cos\pi\lambda_\ell)^{-1} = 2i \sum_{m=0}^{\infty} \exp[i\pi(2m+1)(\lambda_\ell - 1/2)] \quad (25)$$

is useful. Also, for the near backscattering region ($|\gamma|<<1$ rad) of most interest to us, we can use the following approximation for the Legendre function[12,13,21] valid when $|\gamma|<<1$ rad, $|\lambda|>>1$, $|\mathrm{Re}\lambda|>>|\mathrm{Im}\lambda|$

$$P_{\lambda_\ell - \frac{1}{2}}(\cos\gamma) \approx J_0(\lambda_\ell \gamma) \quad (26)$$

where J_0 is the zeroth order Bessel function and the requirement $|\mathrm{Re}\lambda|>>|\mathrm{Im}\lambda|$ has been verified numerically for the Rayleigh zeros of aluminum, tungsten carbide, and fused silica. We assume $|\mathrm{Re}\lambda|>>|\mathrm{Im}\lambda|$ for the remainder of the analysis. Using Eqs. (24-26) gives the following approximation for the Rayleigh wave form function

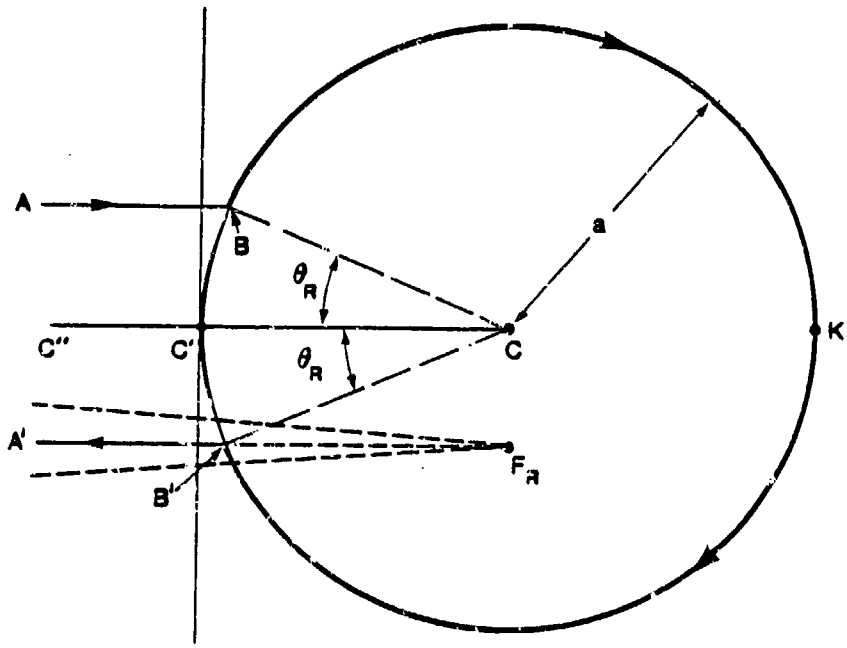

This figure shows the physical picture which ensues from the SWT analysis of the Rayleigh contributions to scattering. The incoming plane wave represented by AB allows the launching of a Rayleigh surface wave at B which circumnavigates the sphere while reradiating back into the surroundings. At point B' energy is radiated in the backward direction. F_R is the virtual point source from which ray A'B' and the dashed rays to either side appear to originate. When the diagram is rotated around the C'C axis, the point F_R traces out a virtual ring-like source.

Fig. 5.

$$f_R \approx -G_R\, e^{i\eta}\, J_0(\lambda_R\gamma) \sum_{m=0}^{\infty} \exp[i\pi(2m+1)(\lambda_R-\tfrac{1}{2})] \tag{27}$$

where

$$G_R = i\lambda_R \frac{4\pi}{ka} \frac{\mathcal{D}^-_{\lambda_R-\frac{1}{2}}}{\mathcal{D}^+_{\lambda_R-\frac{1}{2}}} \tag{28}$$

$$\eta = 2[-((ka)^2 - \lambda_R^2)^{1/2} + \lambda_R \cos^{-1}\frac{\lambda_R}{ka}] \tag{29}$$

The Rayleigh pole satisfies the condition $0 < \mathrm{Re}\,\lambda_R < ka$ and it will be convenient to define the parameters: $\beta_R = \mathrm{Im}(\lambda_R)$, $k_R a = \mathrm{Re}(\lambda_R)$ and $\theta_R = \arcsin(k_R/k)$. We may then write

$$\lambda_R = [illegible] + i\beta_R \tag{30}$$

and our assumption $|\mathrm{Re}\lambda_R| >> |\mathrm{Im}\lambda_R|$ becomes $|k_R a| >> |\beta_R|$. Using Eq. (30) in the exponentials and γ dependence of Eq. (27) and ignoring terms of $O(\beta_R^2)$ and $O(\beta_R/ka)$ we find that

$$f_R \approx -G_R\, J_0(kb_R\gamma)\, e^{-\beta_R(2\pi-2\theta_R)}\, e^{i\eta_R} \sum_{m=0}^{\infty} e^{im(2\pi k_R a-\pi)}\, e^{-2\pi m\beta_R} \tag{31}$$

$$\eta_R \approx -2\,ka\cos\theta_R + k_R a\,(2\pi - 2\theta_R) - \pi/2 \tag{32}$$

where we define $b_R = a\sin\theta_R$. This expression for f_R may be interpreted in terms of a Rayleigh wave coupled onto the sphere at a local angle of incidence θ_R. This wave repeatedly circumnavigates the sphere while shedding energy back into the liquid. Figure 5 illustrates the interpretation of f_R. The ray AA' in Fig. 5 may be attributed to the $m = 0$ term of f_R. AA' includes a ray traversing the surface of the sphere from B to B'. Evidently k_R is the

propagation constant of BB' and η_R is the phase delay of AA' relative to a hypothetical ray following the path in water $C'' \rightarrow C' \rightarrow C \rightarrow C' \rightarrow C''$; η_R includes a $\pi/2$ phase advance due to the caustic at K. The exponential decay $\exp[-\beta_R(2\pi-2\theta_R)]$ is due to continual reradiation of energy back into the liquid; i.e., radiation damping. Reradiation at any point along BB' occurs at angle θ_R with respect to the normal to the sphere's surface at that point. To understand the γ dependence of the m=0 term, one must examine the dashed rays to either side of A'B'. These dashed lines represent radiation slightly away from backscattering. Tracing the dashed lines and A'B' backward locates the point F_R from which they appear to originate. The spherical symmetry of the situation then allows the rotation of the figure around the C'C axis in which case F_R traces out a ring of radius b_R. In Eq. (31) the $J_0(kb_R\gamma)$ angular dependence followed from the SWT; however, we previously derived this radiation pattern of virtual ring-like sources by other methods of approximation.[14,16-18]

The $m > 0$ contributions to f_R are due to the continuation of the ray BB' around the sphere with radiation in the backscattering direction each time it arrives at B'. The $\exp[-2\pi m\beta_R]$ term in Eq. (31) accounts for radiation damping associated with m circumnavigations of the sphere. The factor $\exp(-im\pi)$ accounts for the phase advances due to caustics at C' and K. The on-axis magnitude of the contribution to f_R by the mth term in Eq. (31) is

$$A_m = |G_R|\, e^{-2\beta_R(\pi - \theta_R)}\, e^{-2\pi m\beta_R} \tag{33}$$

This interpretation of the SWT is consistent with the analysis and measurements of the axially-focused Rayleigh wave contributions to the scattering presented in Ref. 14. The absence of a γ-dependent phase factor in

Eq. (31) indicates that the virtual focal circle lies in a plane which contains the center of the sphere (see discussion below Eq. (37) of Ref. 17 for the case in which $\alpha_n = a$). This agrees with the location given by geometric methods.[14] The on-axis amplitudes were left unspecified in Ref. 14.

The SWT yields the following high-frequency approximation to the total form function away from the forward direction

$$f \simeq f_S + f_{tw} + f_R + \sum_{\ell=WG,F} f_{\lambda_\ell} \tag{34}$$

where the summation is over all whispering gallery and Franz poles. The $f_{\lambda_{WG}}$ will be of the same form as Eq. (31) except that parameters are to be calculated from the λ_{WG}.

3.3 Experimental confirmation of Rayleigh backscattering amplitudes

In this section tungsten carbide spheres are used to test the Rayleigh backscattering amplitudes of Eq. (33) for the cases $m = 0,1$. We first outline the methods used to obtain numerical results from Eq. (33). We then briefly summarize the experimental procedure. Last, we compare analytical and experimental results. The reader is referred to Refs. 14, 16, and 18 for a description of the experimental apparatus.

The backscattering amplitudes A_m of Eq. (33) are functions of ka. As a first step in calculating $A_0(ka)$ and $A_1(ka)$ for tungsten carbide we determined the Rayleigh pole's ka dependence. A computer program was developed based on the "winding number formula"[3,20] to find the complex zeros of $\mathfrak{D}^+_{\lambda-\frac{1}{2}}$ in Eq. (12). The program was used to find λ_R for a tungsten carbide sphere for 25 values of ka between $19 < ka < 83$. The ka values used and λ_R values obtained are given in Table I. Also given in Table I are the material parameters used for the tungsten carbide sphere. The motivation for the particular ka values chosen in Table I comes from our previous work[14]

Table I. The Rayleigh roots (λ_R) of $\mathfrak{D}_\nu^+(x, x_S, x_L, \rho_o, \rho_E) = 0$ for 25 values of x ($19 < x < 83$) using material parameters appropriate for a tungsten carbide sphere in water. The material parameters used for the tungsten carbide sphere were[a]: density = 13.80 g/cm^3, longitudinal wave speed = 6.860×10^5 cm/s, shear wave speed = 4.185×10^5 cm/s. Those for water were: density = 1 g/cm^3, longitudinal wave speed = 1.4760×10^5 cm/s.

x	λ_R^b	x	λ_R^b	x	λ_R^b
19.7231	5.9996 + 10.0616	43.6421	14.9996 + 10.1145	67.1333	23.9991 + 10.1635
22.4472	6.9995 + 10.0679	46.2612	15.9996 + 10.1207	69.7353	24.9991 + 10.1688
25.1401	7.9995 + 10.0747	48.8774	16.9996 + 10.1262	72.3364	25.9991 + 10.1741
27.8130	8.9995 + 10.0805	51.4907	17.9988 + 10.1316	74.9370	26.9991 + 10.1794
30.4712	9.9995 + 10.0864	54.1021	18.9988 + 10.1371	77.5366	27.9991 + 10.1847
33.1196	10.9995 + 10.0923	56.7114	19.9988 + 10.1418	80.1353	28.9991 + 10.1900
35.7583	11.9995 + 10.0981	59.3189	20.9988 + 10.1473	82.7329	29.9988 + 10.1948
38.3910	12.9995 + 10.1040	61.9253	21.9996 + 10.1527		
41.0190	13.9996 + 10.1090	64.5298	22.9988 + 10.1582		

[a]Reference 11.

[b]All λ_R values have uncertainties of $\pm$ (0.0005 + 10.0005).

using Resonance Scattering Theory (RST). In RST one deals with the partial wave series of Eq. (1) directly.[8] In Ref. 14 we found the complex ka zeros of D_n in Eq. (1) for integer values of n from $n = 0$ to $n = 30$. The ka values used in Table 1 are the real parts of the complex ka zeros found in Ref. 14. It is not necessary that the ka values be chosen in this manner; however, we have done so to facilitate discussion in a subsequent paper. The quantities $\mathrm{Re}\,\lambda_R = k_R a$ and $\mathrm{Im}\,\lambda_R = \beta_R$ were found as continuous functions of ka by curve fitting the discrete values of Table 1.

The fitted curves for $k_R a$ and β_R facilitated the numerical evaluation of A_0 and A_1 in the range $20 < ka < 80$. The evaluation of G_R in Eq. (28) requires the evaluation of Bessel functions of complex order (see Eq. (A5)). The procedure used in this evaluation was based in part on the analysis given in Ref. 22.

Figure 6 gives a conceptual diagram of the apparatus used to test the SWT predictions. A piston-like transducer produces a sinusoidal tone burst 4 cycles in duration. This tone burst is scattered from either a 1.27 cm or 2.54 cm diameter tungsten carbide sphere. In this experiment the needle hydrophone which picks up the resulting echo was set at $\gamma = 0$; i.e., along the backscattering axis. Figure 7 shows the structure of the backscattered echo for the case $ka = 49.1$. The figure displays the amplified voltage from the hydrophone averaged over repeated echoes. After the specular echo, the principal contributions are the Rayleigh echoes.[14] The frequency of the incident burst could be varied from 800 kHz up to 1.5 mHz. The corresponding range of accessible ka is from 25 to 80.

The experimental procedure was to measure the peak-to-peak voltage of the central cycle for each echo structure of interest. These voltages will be designated as V_S for the specular echo and as V_m for the first ($m = 0$) and

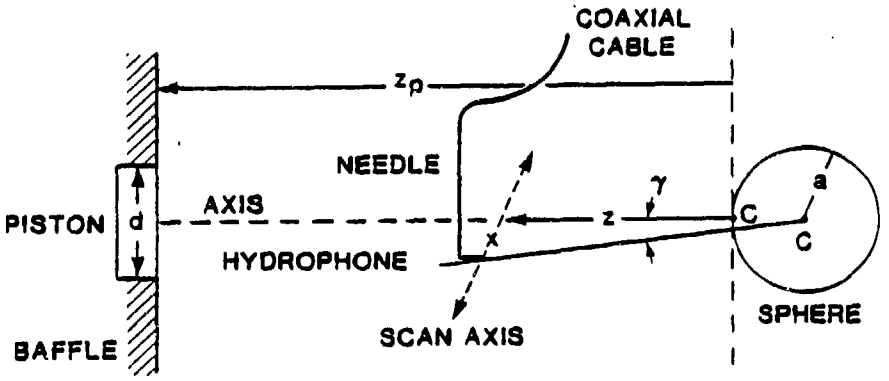

Simplified diagram of the scattering experiment. The backscattering angle γ is zero in the present experiment. The diagram is not drawn to scale. In all the experiments described in Section II, $z_p = 160$ cm, while $z = 33$ cm for experiments with the 2.54 cm diameter tungsten carbide sphere and $z = 19$ cm for experiments with 1.27 cm sphere.

Fig. 6.

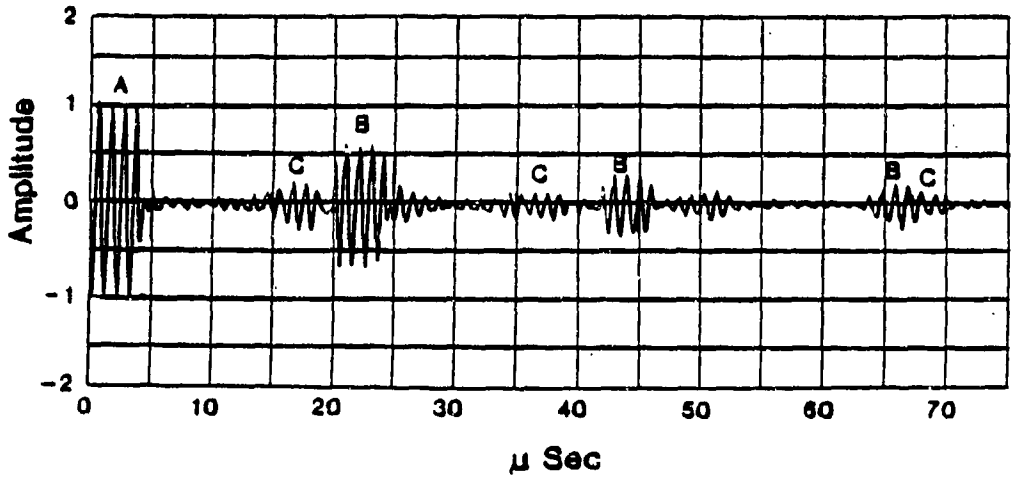

An oscilloscope trace of the backscattering echo from a tungsten carbide sphere ensonified by a tone burst. The ka of the sphere is approximately 49.1. The individual echoes are labeled as follows: A - specular reflection, B - Rayleigh surface wave echoes, C - echoes whose specific origin was not identified but which are conjectured to be other surface waves such as "Whispering Gallery" waves.

Fig. 7.

second ($m = 1$) Rayleigh echoes. The voltage measurements were made on the averaged echo from 256 bursts. An absolute calibration of the apparatus would require that signal attenuation associated with propagation through the water be accounted for. Instead of absolute scattering amplitudes, we will concern ourselves with the Rayleigh echo amplitudes relative to that of the specular reflection for the particular value of ka under consideration; these will be designated as $R_{0E} = V_0/V_S$ and $R_{1E} = V_1/V_S$.

In order to compare R_{0E} and R_{1E} with the SWT prediction for the A_0 and A_1, it was necessary to also evaluate the SWT predictions for the specular amplitude at $\gamma = 0$ as a function of ka. The required contribution to the form function is $|R_{S\lambda_s}|$ with $\lambda_S = 0$; see Eqs. (20) and (A8). We designate this quantity as R_{ST}. Evaluation of Eq. (A8) shows that as ka increases from 18 to 83, R_{ST} increases monotonically and approaches the specular reflection amplitude for a plane tungsten-carbide water interface, $|R_p| = 0.9693$ from Eq. (21). At ka = 20, R_{ST} was only 0.1% below $|R_p|$. Since R_{ST} varies by only about 0.1% in the ka region of interest, the theoretical echo amplitude ratios $R_{0T} = A_0/R_{ST}$ and $R_{1T} = A_1/R_{ST}$ are dominated by the ka dependences of A_0 and A_1. These ratios are plotted as the solid line in Fig. 8 together with the experimental amplitude ratios R_{0E} and R_{1E}. The general agreement appears to confirm the predictions of Eq. (33).

A couple of comments on the relation between the experimental and theoretical results are in order. First, the theoretical prediction uses material parameters from Ref. 11 since the elastic parameters of the actual spheres used could not be determined. The material parameters of the spheres used in the experiment may be slightly different. For example, the densities of the spheres used were measured to be 14.75 gm/cm^3 and 14.95 gm/cm^3 for the

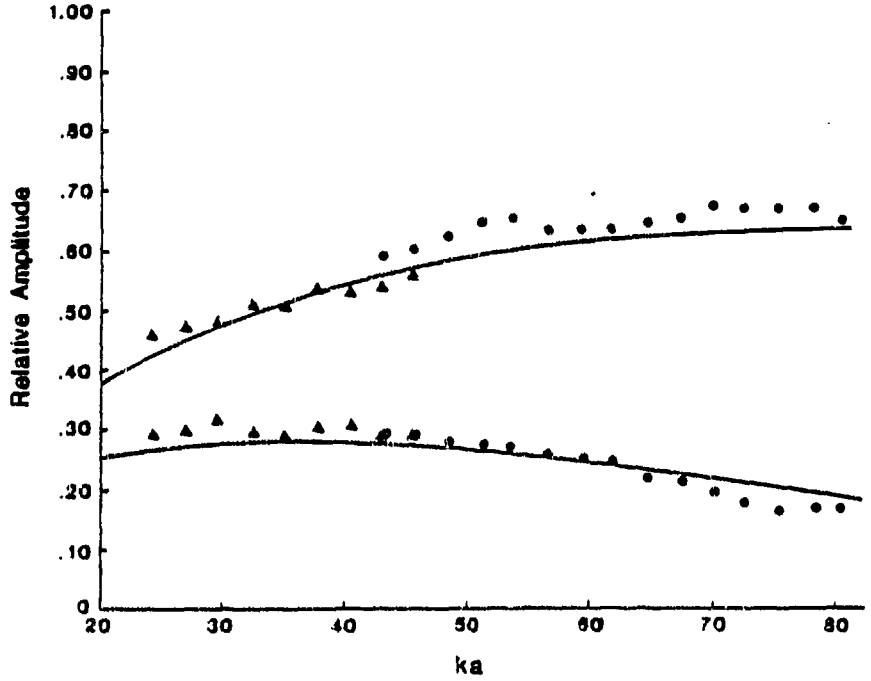

Experimental and theoretical results for the backscattering amplitudes of the first and second Rayleigh contributions as a function of ka. The amplitudes are normalized to the specular echo amplitude at the indicated value of ka. The dots are experimental results for the 2.54 cm diameter sphere, the triangles are results for the 1.27 cm diameter sphere, and the solid lines theoretical results using Eq. (33).

Fig. 8.

large and small spheres respectively. This may account for some of the difference between experiment and theory. Second, the SWT analysis is a steady state method. In the experiment, however, pulses must be used so that the Rayleigh contributions can be isolated in time. The validity of applying a steady-state analysis to experiments of the type described above has been examined[16,23] in connection with waves transmitted within the sphere. It was found that though focused tone bursts could be distorted, the peak-to-peak amplitude of the central cycle of a four-cycle burst should be well approximated by that of a steady state analysis. It is anticipated that a detailed analysis of the shapes of transient Rayleigh echoes would lead to similar conclusions.

It should also be noted that the receiver hydrophones were not always in the far-zone of the scattering. For example, in the far-zone condition $r \gg ka^2$, $a = 1.27$ cm and $ka = 50$ gives $ka^2 = 63.5$ cm. Fortunately, however, this is not a serious drawback. This is because the ratios of Rayleigh and specular echo amplitudes should be well approximated by $|A_m|/R_{ST}$ for distances much closer than the condition $r \gg ka^2$. The radiation from a virtual ring-like source of radius b_R is modeled in Section V of Ref. 16 for the region $r \gg b_R\,(kb_R/2)^{1/3} \equiv r_F$, the <u>Fresnel region</u>. This analysis may be applied to Rayleigh echoes in the present problem since these appear to originate from virtual ring-like sources; $ka = 50$ and $a = 1.27$ cm correspond to $kb_R \simeq 18$ and $r_F \simeq 0.7$ cm. The measurements were taken with $r = a + z \simeq 33$ cm. The near-field corrections required to predict the far-field amplitude ratios from the conditions of this measurement were estimated to be $< 2\%$.

3.4 Discussion

As was noted in Section II, the theoretical amplitude ratios R_{0T} and R_{1T} plotted in Fig. 8 have dependences on ka which are dominated by the Rayleigh echo amplitudes A_0 and A_1; the R_{mT} may be approximated to within 0.1% by $A_m/0.9693$. The qualitative features of these plots may be understood as follows. We have previously demonstrated[14] that the Rayleigh echoes are an example of axially focused scattering. Consequently, it is to be anticipated that over a range of ka (consistent with the phase matching condition[14]), the amplitude coupling factor, G_R in Eq. (38), increases with ka. Thus A_0 and A_1 are expected to increase with ka until the exponential factors in Eq. (33) are dominant. For tungsten carbide the damping parameter β_R also increases with ka. The dominance of radiation damping is evident in the plot of R_{1T} for $ka \geq 40$. The effects of damping are more significant in A_1 than in A_0 since $A_1 = A_0 \exp(-2\pi\beta_R)$.

The qualitative features mentioned above are clearly evident in the data. Some discussion of the discrepancies between observation and theory are in order. As noted in Sec. II, one plausible cause of error was the use of tabulated elastic parameters for tungsten carbide instead of the unknown parameters for the actual sphere studied. (There is other evidence that the parameters may depend on the manufacturing process of the tungsten carbide.) The differences between R_{0E} for the large and small spheres in the region of overlapping data (ka close to 45) is suggestive of the magnitude of systematic experimental uncertainties.

A further source of discrepancy may be inferred from the structure of the data. The deviation from the theoretical curve is not random but seems to have a structure (especially R_{0E} for $50 \leq ka \leq 80$). This is suggestive of possible interference of the Rayleigh wave with other small amplitude waves.

We have used the methods of Ref. 16-18 to find the amplitudes and times of the transmitted wave contributions. The most significant transmitted wave contributions have amplitudes which are between 0.1 and 0.15 times that of the specular reflection and are delayed by about 17.5 and 32.7 μsec relative to the specular reflection. The timing suggests these waves may be in part responsible for the two left most pulses labeled C in Fig. 7. The largest amplitude transmitted wave in the time windows of the first two Rayleigh contributions had an amplitude of about .07 times the specular reflection and could be a source of the structure of Fig. 8.

A related source of error may be the omission of whispering gallery waves. As noted earlier, the analysis of Sec. II for Rayleigh waves is also applicable to whispering gallery waves. We have not carried out the somewhat tedious computation of the whispering gallery amplitudes for tungsten carbide since an alternate analysis suggests their amplitudes are small in the ka region of the experiment. This alternate analysis involves approximating the <u>exact total form function</u> f_T for a tungsten carbide sphere by $f_A = f_S + f_R$; see Eq. (34). We have compared $|f_A|$ with $|f_T|$ computed using the PWS[11] and find that $|f_A|$ correctly reproduces $|f_T|$ except for a fine structure (superimposed on $|f_A|$) due to whispering gallery waves or other waves. Besides suggesting the whispering gallery contributions are small, this comparison is relevant to the interpretation of resonance scattering theory and a detailed discussion is beyond the scope of the present paper.

Another possible source of the experimental and theoretical differences as well as differences between the overlapping data for the two spheres is the sphere mounting system. Considerable time and effort was spent finding a mounting system which had a minimum effect on the scattering experiment. Even with this one must assume that the effect of the mounting

varied between the two spheres and had an impact on the attenuation of the Rayleigh waves at least locally in the region of contact between sphere and mount.

Finally, it is important to remember that below Eq. (4) we separated the pressure into contributions P_I and P_{II}. The analysis after Eq. (4) concentrated on P_I. P_{II} is known as the background pressure[3,4] and has been shown to be negligible in the fluid-loaded cylinder case.[4] The comparison of $|f_A|$ and $|f_T|$ discussed above implies P_{II} is small for tungsten carbide spheres. However, one cannot discount a priori the possibility of P_{II} contributions being responsible for part of the difference between experiment and theory. P_{II} is also important when interpreting f of Eq. (10): f must be interpreted as a high frequency approximation to f_T which excludes the contribution from P_{II}.

We have, within the limitations discussed in Sec. I, performed a SWT on a fluid-loaded elastic sphere. We paid particular attention to the specular reflection and Rayleigh contributions. Further, subject to the discussions in Sec. II and this section, we have experimentally tested the SWT prediction, Eq. (33), for the amplitude of the first two Rayleigh contributions to backscattering. The general agreement between experiment and theory appears to confirm this particular SWT result. The Bessel function angular dependence given by the SWT (cf. Eq. (31)) was experimentally confirmed in previous work.[14] It may be shown that $kb_R\gamma$ is equivalent to the argument of J_0 which was predicted and confirmed in Ref. 14.

Acknowledgment

This research was supported by the Office of Naval Research.

Appendix A

In this appendix we give the elements of the 3x3 determinants B_n and D_n of Eq. (1). We also manipulate the ratio B_ν/D_ν (where $\nu = \lambda - 1/2$) to obtain the results used in Eqs. (12) and (20).

From Ref. 11 we have that

$$B_n = \begin{vmatrix} -\tilde{\rho}\, x_s^2\, j_n(x) & d_{12}^n & d_{13}^n \\ x\, j_n'(x) & d_{22}^n & d_{23}^n \\ 0 & d_{32}^n & d_{33}^n \end{vmatrix} , \tag{A1}$$

$$D_n = \begin{vmatrix} \tilde{\rho}\, x_s^2\, h_n^{(1)}(x) & d_{12}^n & d_{13}^n \\ -x\, h_n^{(1)'}(x) & d_{22}^n & d_{23}^n \\ 0 & d_{32}^n & d_{33}^n \end{vmatrix} , \tag{A2}$$

$$\begin{aligned} d_{12}^n &= [2n(n+1) - x_s^2] j_n(x_L) - 4\, x_L\, j_n'(x_L) , \\ d_{13}^n &= 2n(n+1)[x_S\, j_n'(x_S) - j_n(x_S)] , \\ d_{22}^n &= x_L\, j_n'(x_L) , \quad d_{23}^n = n(n+1) j_n(x_S) , \\ d_{32}^n &= 2[j_n(x_L) - x_L\, j_n'(x_L)] , \\ d_{33}^n &= 2\, x_S\, j_n'(x_S) + [x_S^2 - 2n(n+1) + 2]\, j_n(x_S) . \end{aligned} \tag{A3}$$

In these expressions j_n and $h_n^{(1)}$ are spherical Bessel and Hankel functions respectively. The primes denote differentiation with respect to the argument. The definitions of all other variables are as listed below Eq. (1) with the additional definition that $\tilde{\rho} = \rho_o/\rho_E$.

The expression B_ν/D_ν is given by the ratio of Eq. (A1) and (A2) with n replaced by ν. By using the relations[24] $j_\nu(x) = 1/2[h_\nu^{(1)}(x) + h_\nu^{(2)}(x)]$ and $h_\nu^{(1,2)}(x) = (\pi/2x)^{1/2}\, H_\lambda^{(1,2)}(x)$ one can rewrite the ratio B_ν/D_ν as

$$B_\nu/D_\nu = -\tfrac{1}{2}\left(1 + \frac{H_\lambda^{(2)}(x)\mathfrak{D}_\nu^-}{H_\lambda^{(1)}(x)\mathfrak{D}_\nu^+}\right) \tag{A4}$$

$$\mathfrak{D}_\nu^{+,-} = z_{1,2} + \tilde{\rho}q \tag{A5}$$

where

$$\begin{aligned} q &= x_s^2(d_{22}^\nu d_{33}^\nu - d_{32}^\nu d_{23}^\nu)/(d_{12}^\nu d_{33}^\nu - d_{32}^\nu d_{13}^\nu) \\ z_i &= x\, h_\nu^{(i)\prime}(x)/h_\nu^{(i)}(x) \end{aligned} \tag{A6}$$

Equation (A5) is a convenient form for residue analysis leading to Eq. (22) and (23). However, for the saddle point analysis of Section I, $\mathfrak{D}_\nu^-/\mathfrak{D}_\nu^+$ must be rewritten. The object of developing an alternate expression for $\mathfrak{D}_\nu^-/\mathfrak{D}_\nu^+$ is to separate out a term which reduces (in the limit $ka \to \infty$) to the reflection coefficient of a plane solid, liquid interface. A related analysis was carried out by Brill[4] for the cylindrical case. Following Section II of Ref. 4 one can rewrite $\mathfrak{D}_\nu^-/\mathfrak{D}_\nu^+$ (after considerable algebra) as

$$\mathfrak{D}_\nu^-/\mathfrak{D}_\nu^+ = R_{s\lambda} - U_\lambda \tag{A7}$$

$$R_{s\lambda} = (z_2\, B_{22} + \tilde{\rho}A_{22})/(z_1\, B_{22} + \tilde{\rho}A_{22}) \tag{A8}$$

$$U_\lambda = -\frac{\tilde{\rho}(z_2 - z_1)}{(z_1 B_{22} + \tilde{\rho}A_{22})}\left[\frac{A_{22}Y_2 - B_{22}Y_1}{1 + (z_1 Y_2 + \tilde{\rho}Y_1)/(z_1 B_{22} + \tilde{\rho}A_{22})}\right]$$

$$A_{ij} = z_{iL}[(z_{jS} + 1)/(2x_s^2) + 1/4] - \nu(\nu+1)/(2x_s^2)$$

$$B_{ij} = [\nu(\nu+1)/x_s^2 - 1/(2\,x_s^2) - 1/4] + 2\nu(\nu+1)/x_s^4 - z_{jS}/(2x_s^2) +$$

$$z_{iL}[\nu(\nu+1)/x_s^4 - 2/x_s^4 - 1/x_s^2] + z_{jS}z_{iL}[\nu(\nu+1)/x_s^4 - 2/x_s^4]$$

$$Y_1 = A_{12}y_L + A_{21}y_S + A_{11}y_Ly_S$$

$$Y_2 = B_{12}y_L + B_{21}y_S + B_{11}y_Ly_S$$

$$y_A = h_\nu^{(1)}(x_A)/h_\nu^{(2)}(x_A),\ z_{\ell A} = x_A\, h_\nu^{(\ell)\prime}(x_A)/h_\nu^{(\ell)}(x_A)$$

where A = L or S. The significance of Eq. (A8) is discussed after Eq. (20) and in Appendix D.

Appendix B

In this appendix we want to show that the integrals

$$p_{\infty}^{(1,2,3)} = \int_{\Gamma_{\infty}^{(1,2,3)}} e^{-i\pi/4} \lambda\left(\frac{C_\nu}{D_\nu}\right) P_\nu(\mu) \frac{e^{-i\pi\lambda/2}}{\cos\pi\lambda} d\lambda \tag{B1}$$

are negligible. $\Gamma_{\infty}^{(1,2,3)}$ are the three contours at infinity shown in Fig. 3 and $C_\nu = D_\nu j_\nu(kr) + B_\nu h_\nu^{(1)}(kr)$. We first examine B_ν/D_ν in the limit $|\lambda| \to \infty$. To examine B_ν/D_ν we use the relations

$$j_\nu(x) = (\pi/2x)^{1/2} J_\lambda(x) , \qquad (\nu = \lambda - 1/2) \tag{B2}$$

$$h_\nu^{(i)}(x) = (\pi/2x)^{1/2} H_\lambda^{(i)}(x) \tag{B3}$$

between spherical and cylindrical functions and the result from Eq. (A6) of Ref. 15 that

$$J_\lambda(x) \to (2\pi\lambda)^{-1/2}(ex/2\lambda)^\lambda \quad \text{as} \quad |\lambda| \to \infty \tag{B4}$$

where $e = (2.718 \ldots)$. From Eq. (B2) and (B4) it follows that

$$\frac{j_\nu'(x)}{j_\nu(x)} \to \frac{\nu}{x} \quad \text{as} \quad |\lambda| \to \infty \tag{B5}$$

where the prime denotes differentiation with respect to x. This result can be used in the d_{ij}^{ν} of Eq. (A6) to find their limiting values as $|\lambda| \to \infty$. Using these limiting d_{ij}^{ν} values we find that $(d_{23}^{\nu}d_{33}^{\nu} - d_{32}^{\nu}d_{33}^{\nu}) \to 0$ as $|\lambda| \to \infty$. Finally, substituting this last result into Eqs. (A4) and (A5) we find

$$\frac{B_\nu}{D_\nu} \to -\frac{j_\nu'(x)}{h_\nu^{(1)\prime}(x)} \quad \text{as} \quad |\lambda| \to \infty \tag{B4}$$

for all regions in the complex λ plane.

Using Eq. (B2), (B3), (B4) and Fig. 15 of Ref. 15 one can also show that $j_\nu'(x)/h_\nu^{(1)'}(x) \to J_\lambda'(x)/H_\lambda^{(1)'}(x)$ as $|\lambda| \to \infty$. This and Eq. (B2) and (B3) allow us to write

$$p^{(1,2,3)} = \int_{\Gamma_\infty^{(1,2,3)}} e^{-i\pi/4} \left(\frac{\pi}{2kr}\right)^{\frac{1}{2}} \frac{L_\lambda(x,kr)}{H_\lambda^{(1)'}(x)} M_\lambda(\mu)\,d\lambda \tag{B5}$$

where

$$L_\lambda(x,kr) = H_\lambda^{(1)'}(x)\, J_\lambda(kr) - J_\lambda'(x) H_\lambda^{(1)}(kr)$$

$$M_\lambda(\mu) = \lambda P_\nu(\mu) \frac{\exp(-i\pi\lambda/2)}{\cos\pi\lambda}$$

Now, using Appendix A of Ref. 15 along with Eq. (2.21) and (2.24) of the same reference and the substitution $\lambda = R\exp(i\phi)$ one can establish on the contours $\Gamma_\infty^{(1,2,3)}$ (where $R \to \infty$) that: L_λ and M_λ behave no worse than $\exp(R)$, and $H_\lambda^{(1)'}(x)$ behaves as $\exp(R\ln R)$. Thus the integrand in Eq. (B5) vanishes on $\Gamma_\infty^{(1,2,3)}$ and therefore $p_\infty^{(1,2,3)} = 0$. In establishing this behavior it is important to note that the curve h_2 in Fig. 3 is the curve along which the zeros of $H_\lambda^{(2)}(x)$ are located.[15]

Appendix C

In this appendix we examine the integral

$$p_{inc} = -i \int_{\Gamma_M} e^{-i3\pi/4} F_2(\lambda,x)\, h_\nu^{(1)}(kr) Q_\nu^{(1)}(\cos\theta) e^{i\pi\lambda/2}\, d\lambda \tag{C1}$$

where the contour Γ_M is the portion of Γ_s in Fig. 4 which goes through the right hand saddle point. In identifying Γ_M the definition of Γ_L below Eq. (19) was used. We show, using the saddle point method, that Eq. (C1) represents the contribution to p_1 (cf. Eq. 14) from the incident plane wave.

To evaluate Eq. (C1) we must first find the saddle point location. To do so we rewrite the integrand of Eq. (C1) in a form valid when $x < \mathrm{Re}\lambda < kr$ (specifically part of region A in Fig. 15 of Ref. 15). In this region we can use the relation (Appendix A of Ref. 15)

$$H_\lambda^{(2)}(x) \simeq -H_\lambda^{(1)}(x) \tag{C2}$$

This relation, Eq. (A5) and (A6), and the definition $F_2(\lambda,x) = \lambda H_\lambda^{(2)}(x)\mathfrak{D}_\nu^-/H_\lambda^{(1)}(x)\mathfrak{D}_\nu^+$ allows one to show that $\mathfrak{D}_\nu^-/\mathfrak{D}_\nu^+ \simeq 1$ and

$$F_2(\lambda,x) \simeq -\lambda \tag{C3}$$

Also, when $|\lambda| \gg 1$, $\varepsilon \le \theta \le \pi - \varepsilon$, $|\lambda|\varepsilon \gg 1$ we can use the relation[15]

$$Q_\nu^{(1)}(\cos\theta) \simeq \frac{\exp[-i(\lambda\theta - \pi/4)]}{(2\pi\lambda\sin\theta)^{1/2}} . \tag{C4}$$

We return briefly to the requirement $|\lambda|\varepsilon \gg 1$ at the end of this appendix. The requirement $|\lambda| \gg 1$ is fulfilled in the region $\mathrm{Re}\lambda > x$ since at the outset of the paper we assumed $x \gg 1$. Finally, since we are examining the region where $\mathrm{Re}\lambda < kr$, we can rewrite $h_\nu^{(1)}(kr)$ using Eq. (B3) and (24).

With these results, and the change of variables $\lambda = kr \sin w$, p_{inc} becomes

$$p_{inc} = \int_{\Gamma'_M} S(w)\, e^{kr\, s(w)}\, dw \tag{C5}$$

$$S(w) = e^{-i\pi/4}\, [kr \sin w \cos w / 2\pi \sin\theta]^{1/2}$$

where $s(w) = i[(\frac{1}{2}\pi - \theta)\sin w + \cos w - (\frac{1}{2}\pi - w)\sin w]$ and Γ'_M is the transformed contour of Γ_M which passes through the saddle point $w = w_s$. One can evaluate Eq. (C5) using the saddle point method.[20,25] We find the saddle point at $w_s = \theta$ ($\lambda_s = kr \sin\theta$) which gives a value for p_{inc} of

$$p_{inc} = e^{[kr\, s(w_s)]} \left(\frac{-2\pi}{kr\, s''(w_s)}\right)^{1/2} S(w_s) \tag{C6}$$

where $s''(w_s)$ is d^2s/dw^2 evaluated at $w = w_s$. The right side reduces to $\exp(ikz)$ which corresponds to the incident plane wave as required.

The condition that Eq. (C4) is applicable at the saddle point is $|\lambda_s|\varepsilon = kr \sin\theta \gg 1$. Consequently, for points close to the backscattering axis, θ close to π, this proof is only strictly valid for large values of kr.

Appendix D

In this appendix we use the saddle point method to approximate the integral

$$f_S = \frac{2i}{ka} \int_{\Gamma_L} \lambda \, R_{S\lambda} \frac{H_\lambda^{(2)}(x)}{H_\lambda^{(1)}(x)} Q_\nu^{(1)}(\cos\theta) \, d\lambda \tag{D1}$$

where the contour Γ_L is that portion of Γ_s in Fig. 4 which passes through the left hand saddle point.

The saddle point analysis is similar to that carried out in Appendix C. To find the saddle point location we rewrite the integral in a form valid when $-x \leq \mathrm{Re}\lambda \leq x$ and $|\lambda - x| >> (\lambda)^{1/3}$. In this region we can use the Debye expansions of Eq. (24). This gives

$$\frac{H_\lambda^{(2)}(x)}{H_\lambda^{(1)}(x)} = i \exp[2i(-(x^2 - \lambda^2)^{1/2} + \lambda \arccos \lambda/x)] \tag{D2}$$

We can also use Eq. (C4) for $Q_\nu^{(1)}(\cos\theta)$ under the restrictions that $|\lambda| >> 1$, $\varepsilon \leq \theta \leq \pi - \varepsilon$, $|\lambda|\varepsilon >> 1$. Equations (C4) and (D2) and the substitution $\lambda = ka \sin w$ allow Eq. (D1) to be rewritten as

$$f_S = \int_{\Gamma_L'} T(w) \, e^{ka \, t(w)} \, dw \tag{D3}$$

$$T(w) = -e^{i\pi/4} R_{S\lambda} \cos w \, (2ka \sin w/\pi \sin\theta)^{1/2}$$

where $t(w) = i[-2 \cos w + (\pi - 2w)\sin w - \theta \sin w]$ and Γ_L' is the transformed contour of Γ_L which passes through the saddle point $w = w_s$. In writing Eq. (D3) use was made of the result that $R_{S\lambda}$ as given in Eq. (A8) will

contain no exponentials and is a slowly varying function of λ. Since $ka \gg 1$ the integral can be evaluated via the saddle point method.[20,25] In terms of the backscattering angle $\gamma = \pi - \theta$, the saddle point is at $w_s = \gamma/2$ for which $\lambda = ka \sin w_s \equiv \lambda_s$. The approximation of the integral in Eq. (D3) is given by the right side of Eq. (C6) with s, r, and S replaced by t, a, and T, respectively; the resulting approximation for f_S is given by Eq. (20).

References

1. J. W. S. Rayleigh, The Theory of Sound (Dover, New York, 1945).
2. J. J. Faran, Jr., "Sound Scattering by Solid Cylinders and Spheres," J. Acoust Soc. Am. 23, 405 (1951); R. Hickling, "Analysis of echoes from a solid elastic sphere in water," J. Acoust. Soc. Am. 34, 1582-1592 (1962).
3. R. D. Doolittle, H. Überall, and P. Ugincius, "Sound scattering by elastic cylinders," J. Acoust. Soc. Am. 43, 1-14 (1968).
4. D. Brill and H. Überall, "Acoustic waves transmitted through elastic cylinders," J. Acoust. Soc. Am. 50, 921-939 (1971).
5. L. R. Dragonette, R. H. Vogt, L. Flax, and W. G. Neubauer, "Acoustic reflection from elastic spheres and rigid spheres and spheroids. II. Transient analysis," J. Acoust. Soc. Am. 55, 1130-1137 (1974).
6. G. V. Frisk, J. W. Dickey, and H. Überall, "Surface wave modes on elastic cylinders," J. Acoust. Soc. Am. 58, 996-1008 (1975).
7. G. V. Frisk and H. Überall, "Creeping waves and lateral waves in acoustic scattering by large elastic cylinders," J. Acoust. Soc. Am. 59, 46-54 (1976).
8. L. Flax, G. C. Gaunaurd, and H. Überall, "Theory of resonance scattering," in Physical Acoustics, edited by W. P. Mason and R. N. Thurston (Academic, New York, 1981), Vol 15, pp. 191-294.
9. G. C. Gaunaurd, E. Tangles, H. Überall, and D. Brill, "Interior and exterior resonance in acoustic scattering. I: Spherical targets," Nuov. Cim. B 76, 153-175 (1983).
10. L. R. Dragonette, S. K. Numrich, and L. J. Frank, "Calibration technique for acoustic scattering measurements," J. Acoust. Soc. Am. 69, 1186-1189 (1981).

11. G. C. Gaunaurd and H. Überall, "RST analysis of monostatic and bistatic acoustic echoes from an elastic sphere," J. Acoust. Soc. Am. 73, 1-12 (1983).

12. H. M. Nussenzveig, "High frequency scattering by a transparent sphere. I. Direct reflection and transmission," J. Math. Phys. 10, 82-124 (1969).

13. H. M. Nussenzveig, "High frequency scattering by a transparent sphere. II. Theory of the rainbow and glory," J. Math. Phys. 10, 125-176 (1969).

14. K. L. Williams and P. L. Marston, "Axially-focused (glory) scattering due to surface waves generated on spheres: Model and experimental confirmation using tungsten carbide spheres," J. Acoust. Soc. Am. (accepted for publication).

15. H. M. Nussenzveig, "High-frequency scattering by an impenetrable sphere," Ann. Phys. 34, 23-95 (1965).

16. P. L. Marston, K. L. Williams, and T. J. E. Hanson, "Observation of the acoustic glory: High frequency backscattering from an elastic sphere," J Acoust. Soc. Am. 74, 605-618 (1983).

17. P. L. Marston and D. S. Langley, "Glory and rainbow enhanced acoustic backscattering from fluid spheres: Models for diffracted axial focusing," J. Acoust. Soc. Am. 73, 1464-1474 (1983).

18. K. L. Williams and P. L. Marston, "Mixed-mode acoustical glory scattering from a large elastic sphere: Model and experimental verification," J. Acoust. Soc. Am. 76, 1555-1563 (1984).

19. E. Kreyszig, Advanced Engineering Mathematics (John Wiley, New York, 1972), pp. 600-615.

20. V. I. Smirnov, A Course of Higher Mathematics (Pergamon Press, New York, 1964), Vol. III, Part two, pp. 84-87, 91.

21. G. Szegö, Orthogonal Polynomials (American Mathematical Society, New York, 1939), Theorem 8.21.6.

22. J. A. Cochran and J. N. Hoffspiegel, "Numerical techniques for finding -zeros of Hankel functions," Math. Comp. 24, 413-422 (1970).

23. P. L. Marston, "Half-order derivative of a sine-wave burst: Applications to two dimensional radiation, photoacoustics, and focused scattering from spheres and a torus," J. Acoust. Soc. Am. 76, 291-295 (1984).

24. M. Abramowitz and I. A. Stegun, Handbook of Mathematical Functions with Formulas, Graphs, and Mathematical Tables (Dover, New York, 1965).

25. L. M. Brekhovskikh, Waves in layered Media (Academic Press, New York, 1960).

Chapter 4

RESONANCE SCATTERING THEORY REVISITED VIA THE SOMMERFELD-WATSON TRANSFORMATION FOR SCATTERING FROM SPHERES

4.1 Introduction

Resonance Scattering Theory (RST) originated from the application of nuclear scattering theory to classical scattering problems.[1,2] It has been used in addressing a number of different scattering situations. (Reference 2 discusses several specific problems which have been examined via RST). Because of these applications of RST an examination of the limitations of some of the basic concepts of RST is justified. We stress at the outset that these limitations do not affect the validity of most results obtained with RST but they do affect interpretation of these results.

RST achieves a separation between rapidly varying "resonance" portions of scattered signals and a slowly varying background. In particular, for an acoustical plane wave scattered from fluid-loaded elastic bodies such as spheres[3] or cylinders,[4] RST has been used to interpret the rapid fluctuations in the backscattered pressure as the ka of the bodies are varied (where k is the wave number of the acoustical plane wave in the fluid and a is the radius of the sphere). One of the important numerical tasks in RST is to find the complex "resonance" ka values which locate poles of the scattering amplitude. Two basic RST ideas are then used in interpreting scattered pressures. For a sphere these ideas translate into the following statements[3]: (a) each of the many resonance ka's can be labeled with the integers n and ℓ and at the $(n,\ell)^{th}$ resonance $n + (1/2)$ wavelengths of the ℓth surface wave fit onto the circumference of the sphere, (b) that any rapid fluctuation in the scattered pressure is due to the in-phase adding of a specific surface wave and these fluctuations are thus associated in a simple fashion with the set of modal resonances of the target. Two of the major goals of this paper are to examine the limitations of these ideas.

Our examination uses the particular problem of an acoustical plane wave scattered from a fluid-loaded elastic sphere. We use a recently completed[5] Sommerfeld-Watson transform (SWT) analysis as an aid in investigating RST. The SWT allows separation of the contributions to scattering from reflected waves, transmitted bulk waves, and surface waves.

Section I contains an examination of the relation between the resonance ka's and the rapid fluctuations in the backscattering form function of an elastic sphere. To perform the examination we use the case of backscattering from a tungsten carbide sphere with $10 \leq ka \leq 80$. We approximate the exact partial wave series (PWS) solution for the backscattering form function of the tungsten carbide sphere by using a portion of the SWT results. This process allows a check of the SWT. Once checked the SWT results are useful in understanding the relation between resonance ka's and the backscattering form function fluctuations.

Throughout the paper we define <u>physical resonances</u> as the real ka values for which an integer plus one-half wavelengths of any surface wave fit on the sphere. In Section I we assume that the real part of the RST resonances give the physical resonance values of the sphere. In Section II we show that these RST results actually only approximate the physical resonance values. The error inherent in this RST approximation is small enough for tungsten carbide that it has no effect on the discussion of Section I. We conclude in Section II that, when one approximates the physical resonance values by using RST results, the numerical and conceptual significance of the approximation should be understood and related to the problem at hand.

A special note on notation is appropriate. In past RST work the parameter ℓ was an integer where $\ell = 1$ for the Rayleigh surface wave and $\ell = 2,3$, etc. for whispering gallery surface waves.[2] In previous SWT analyses

ℓ took on the value $\ell = R$ for the Rayleigh wave and $\ell =$ WG1, WG2, etc. for whispering gallery waves.[5] Throughout this paper we shall use both the RST and SWT definition of ℓ and imply from the previous work that $\ell = 1$ is equivalent to $\ell = R$ and $\ell = 2$ is equivalent to $\ell =$ WG1 for tungsten carbide spheres.

4.2 The backscattering form function via SWT and RST

In this section we discuss the relation between the resonances of RST and fluctuations in the magnitude of the backscattering form function of a fluid loaded elastic body as ka is varied. This relation is examined through the specific case of backscattering from a tungsten carbide sphere in water. Section IA is devoted to comparing the PWS with the SWT approximations for the backscattering form function of the tungsten carbide sphere.[3,5,6] Besides this comparison several intermediate SWT results are discussed. Some of these intermediate results introduce terminology and ideas useful in Section IB. Section IA serves the dual purpose of partially checking the SWT of Ref. 5 and laying the groundwork for the discussion of RST and form function fluctuations in Section IB. A comment is appropriate on the computer programs used in generating many of the figures of this section. In evaluating SWT results, we use subroutines which calculate Bessel functions of complex order and argument (see Ref. 5 for further discussion of subroutines). These subroutines have an error of less than (0.00001 + i0.00001) when the modulus of the Bessel function order $|\nu|$ is greater than 3. With $|\nu| < 3$ the error increases rapidly. SWT results for the tungsten carbide sphere below ka = 20 are affected by this inaccuracy. In some figures SWT results below ka = 20 are plotted since the qualitative features agree with PWS results even though quantitative accuracy cannot be assured. The PWS calculations have no such limitations. The maximum ka range plotted for SWT results is $10 \leq ka \leq 80$ and

for PWS results is $1 \leq ka \leq 80$. The methods used to obtain SWT results are similar to those discussed in Ref. 5. The material parameters used for tungsten carbide were: density = 13.80 g/cm^3, longitudinal wave speed = 6.860×10^5 cm/s, shear wave speed = 4.185×10^5 cm/s. Those for water were: density = 1 g/cm^3, longitudinal wave speed = 1.4760×10^5 cm/s.

A. PWS and SWT form functions

When a plane acoustic wave is scattered from a fluid-loaded elastic sphere and we use the coordinate system shown in Fig. 1 the total pressure in the far field of a fluid-loaded sphere can be written as the real part of[3,5]

$$p_T(x,\theta) = e^{ikz} + \frac{ae^{ikr}}{2r} f(x,\theta) \tag{1}$$

where $x \equiv ka$. On the right-hand-side the first term represents a unit amplitude incident plane wave and the second term the scattered pressure. The f in this expression is a form function descriptive of scattering when $r \gg ka^2$.

The PWS backscattering form function $f(x,\pi) = f^{PWS}(x,\pi)$ is[3]

$$f^{PWS} = \frac{2}{ix} \sum_{n=0}^{\infty} (-1)^n (2n+1) \frac{B_n(x)}{D_n(x)} \tag{2}$$

where B_n and D_n are 3 x 3 determinants given in Ref. 3. The complex resonances of RST fulfill the condition $D_n(x_{n\ell}) = 0$. It is important for the discussion in Section II to note that the RST resonances (the $x_{n\ell}$) are "located" in a complex x plane. The value x_{n1} corresponds to a Rayleigh resonance of the nth term of Eq. (2) while the values $x_{n\ell}$ with $\ell \geq 2$ correspond to any of the many whispering gallery resonances of the nth term. In the RST of a sphere[3,7] it is asserted that when the ka of the sphere equals

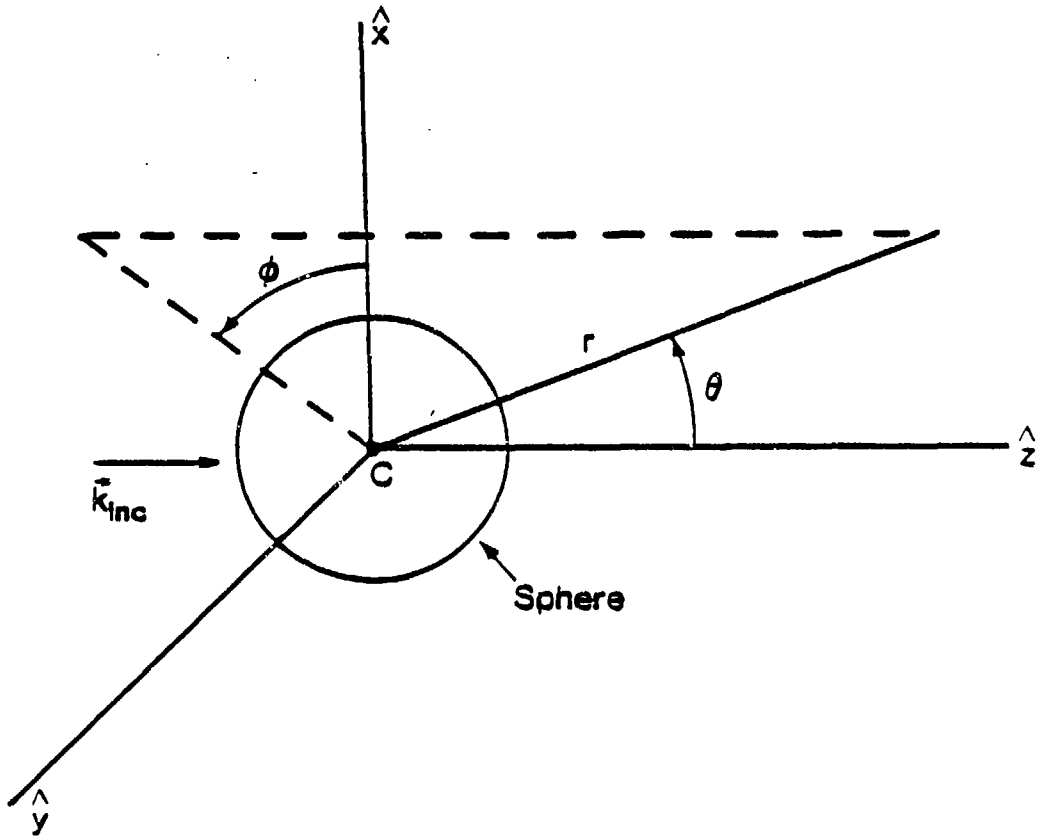

The r, θ, φ coordinate system shown above was used in writing the partial wave series (PWS) solution to plane wave scattering from an elastic sphere. The plane wave is assumed to be traveling in the +z direction.

Fig. 1.

$Re(x_{n\ell})$ then $n + (1/2)$ wavelengths of the ℓth surface wave fit on the sphere.

The SWT may be used to find an alternate representation for f. In the SWT one rewrites the PWS for the total pressure in terms of a contour integral in a complex ν plane.[5] The contour used can be deformed to surround complex poles whose residues given the contribution from Franz, Rayleigh, and whispering gallery waves. Furthermore, the contour passes through saddle points whose evaluation gives contributions from specular reflection and transmitted bulk waves. After a considerable effort one can write the far field pressure as shown in Eq. (1) with $f \approx f^{SWT}$ where $ka \gg 1$ and f^{SWT} can be separated into the sum of several contributions.[5] Here we consider only the contributions from the specular reflection, Rayleigh wave, and the slowest whispering gallery wave which we label f_S, f_R, f_{WG1} respectively. The analysis of Ref. 5 gives the essential details of the derivation, interpretation, and numerical implementation of the results for f_S, f_R, f_{WG1}. We will only briefly summarize their form for the case $\theta = \pi$; i.e., backscattering.

When $\theta = \pi$ the specular reflection contribution f_S has the form

$$f_S(x,\pi) = - R_{S(\lambda_s=0)}(x)\, e^{-i2x} \tag{3}$$

where $R_{S\lambda_s}$ is the coefficient of reflection from the front of the sphere and $(-2x)$ is the phase of the specular reflection relative to a ray traveling in the liquid to and from a reference point corresponding to the spheres center. The full expression for $R_{S\lambda_s}$, which was used in the calculations, is derived in Appendix A of Ref. 5.

The contributions f_R and f_{WG1} are found from a residue analysis using the Rayleigh pole ν_R and the appropriate whispering gallery pole

ν_{WG1}. The expressions for f_R and f_{WG1} have the same form and at $\theta = \pi$ they become

$$f_\ell(x,\pi) = -G_\ell\, e^{i\eta_\ell}\, e^{-2(\pi-\theta_\ell)\beta_\ell} \sum_{m=0}^{\infty} e^{-im\pi}\, e^{i2\pi m(\alpha_\ell+\frac{1}{2})}\, e^{-2\pi m\beta_\ell} \tag{4}$$

where ℓ equals R or WG1 for the Rayleigh or whispering gallery contribution and we have used the substitution $\nu_\ell = \alpha_\ell + i\beta_\ell$. We note that θ_ℓ, η_ℓ, β_ℓ, α_ℓ, G_ℓ are all functions of x and that f_ℓ is actually the appropriate form for <u>any</u> whispering gallery contribution to f^{SWT}. Equation (4) can be interpreted in terms of surface waves in which case the variables and summation have the following physical significance[5]: G_ℓ is a complex amplitude factor that accounts for the coupling efficiency of the ℓth surface wave onto the sphere as well as the effect of axial focusing, θ_ℓ is the local angle of incidence where the surface wave and incident acoustic wave are phase matched,[8] the terms $\exp(i\eta_\ell)$ and $\exp[-2(\pi-\theta_\ell)\beta_\ell]$ are the phase delay (relative to the same reference wave as used for Eq. (3)) and attenuation due to radiation damping the first time the wave radiates energy in the backscattering direction, the sum over m accounts for the surface wave circumnavigating the sphere an infinite number of times, the $\exp[i2\pi m(\alpha_\ell + \frac{1}{2})]$ and $\exp[-2\pi m\beta_\ell]$ are the propagation phase delay and attenuation of the surface wave for m circumnavigations the sphere, the $\exp[-im\pi]$ accounts for phase shifts due to caustics at $\theta = 0$ and $\theta = \pi$. We note for future reference that the results above show that the propagation phase delay for one complete trip around the sphere is $\exp[i2\pi(\alpha_\ell + \frac{1}{2})]$. This implies that α_ℓ is related to the number of cycles of the surface wave which fit on the sphere. For instance if the value of x is such that α_ℓ equals an integer n then $n + (1/2)$ cycles of the surface wave would fit on the sphere. Explicit expressions for G_ℓ and η_ℓ can be found in Ref. 5.

By inspecting Eq. (4) one can see that the backscattering amplitude of the mth term of the ℓth surface wave is

$$A_{m,\ell} = |G_\ell| \, e^{-2(\pi-\theta_\ell)\beta_\ell} \, e^{-2\pi m\beta_\ell} \tag{5}$$

The ability to calculate the coupling efficiencies G_ℓ and backscattering amplitudes $A_{m,\ell}$ can prove useful in transient scattering situations where one may want to determine the physical origin of various echoes seen in the scattered return.[5,9] The coupling efficiencies may also be useful in investigating more complex shapes such as cylinders with hemispherical endcaps. With these types of applications in mind Figure 2 gives $|G_R|$, $|G_{WG1}|$, $A_{0,R}$, $A_{0,WG1}$ for a tungsten carbide sphere. Throughout the ka range of Fig. 2, $|f_S| = 0.9693$ (see Ref. 5) and comparison with $A_{0,R}$ from Fig. 2 suggests that f_R will strongly influence the total form function. This supposition proves to be correct in what follows.

An alternate expression for $f_\ell(x,\pi)$ can be found by applying a relation used in the analysis of optical Fabry-Perot resonators[10,11]

$$\sum_{m=0}^{\infty} e^{mz} = \frac{1}{1 - e^{z}} , \quad |e^{z}| < 1 . \tag{6}$$

Using Eq. (6) we can write Eq. (4) as

$$f_\ell(x,\pi) = \frac{-G_\ell \exp[-2(\pi-\theta_\ell)\beta_\ell + i\eta_\ell]}{\{1 + \exp[-2\pi\beta_\ell + i2\pi(\alpha_\ell + \frac{1}{2})]\}} \tag{7}$$

This closed-form result is more convenient for steady state computations. Examination of the form of Eq. (7) shows that if the x value of the sphere is such that $\mathrm{Re}\,\nu_\ell \equiv \alpha_\ell$ equals n (where n is an integer) the magnitude of the denominator is close to a minimum and we have a resonance type behavior. We have discussed previously the idea that when $\alpha_\ell = n$ we have $n + (1/2)$

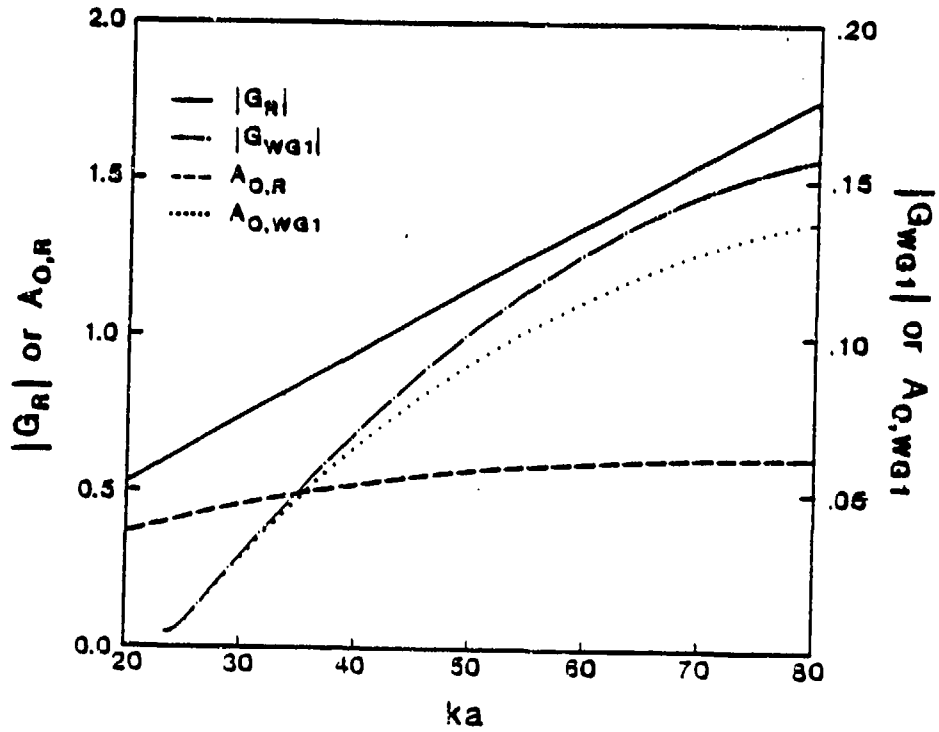

The Rayleigh and slowest whispering gallery coefficients G_R and G_{WG1} for coupling onto a tungsten carbide sphere are shown (cf. Eq. 4). Also shown are the backscattering amplitudes $A_{0,R}$ and $A_{0,WG1}$ for the first time the Rayleigh and whispering gallery waves return energy (cf. Eq. (5)). The different scales needed in this plot are an indication of the much larger coupling and backscattered amplitude of the Rayleigh wave in the case of a tungsten carbide sphere.

Fig. 2.

cycles of the ℓth surface wave on the sphere; i.e., a physical resonance as defined in the introduction. One way to understand the resonance when $n + (1/2)$ cycles fit on the sphere is through the use of Eq. (4). Each time the surface wave completes a trip around the sphere (each of the individual terms in sum of Eq. (4)) it is in phase with contributions from previous circumnavigations (the other terms of the sum). In phase addition occurs when $n + (1/2)$ cycles fit on the sphere instead of n as would be the case for a cylinder[2] because of the phase advance due to caustics at $\theta = 0$ and $\theta = \pi$. To see the resonance behavior of Eq. (7) we have plotted $|f_R(x,\pi)|$ for a tungsten carbide sphere in Fig. 3. The resonance behavior is clearly evident. We have also plotted as vertical dotted lines the real part of the RST Rayleigh resonances $Re(x_{n1})$ for $5 \leq n \leq 28$. The values of $Re(x_{n1})$ were taken from Table I of Ref. 8. The RST concept of $n + (1/2)$ cycles of the ℓth surface wave fitting on the sphere when the ka of the sphere equals $Re(x_{n\ell})$ is confirmed to within the resolution of this figure. Indeed we will show in Section II that the approximation inherent in the use of this concept is not detectable in any of the figures of this section for the particular case at hand. Therefore, for the remainder of this section we use the $Re(x_{n1})$ to indicate when $n + (1/2)$ cycles of the Rayleigh wave fit on the tungsten carbide sphere.

The results to this point can now be used to obtain curves for the magnitude of the backscattering form function of a tungsten carbide sphere immersed in water as a function of ka. The PWS result for $|f^{PWS}(x,\pi)| \equiv f_b$ was calculated using computer programs referenced in previous work.[6] We first compare f_b with a SWT result using only the specular reflection and Rayleigh contributions to f^{SWT} and given by $|f_S(x,\pi) + f_R(x,\pi)| \equiv f_{SR}$. Figure 4 shows f_b in the range $1 \leq ka \leq 80$ and f_{SR} in the range $10 \leq ka \leq 80$.

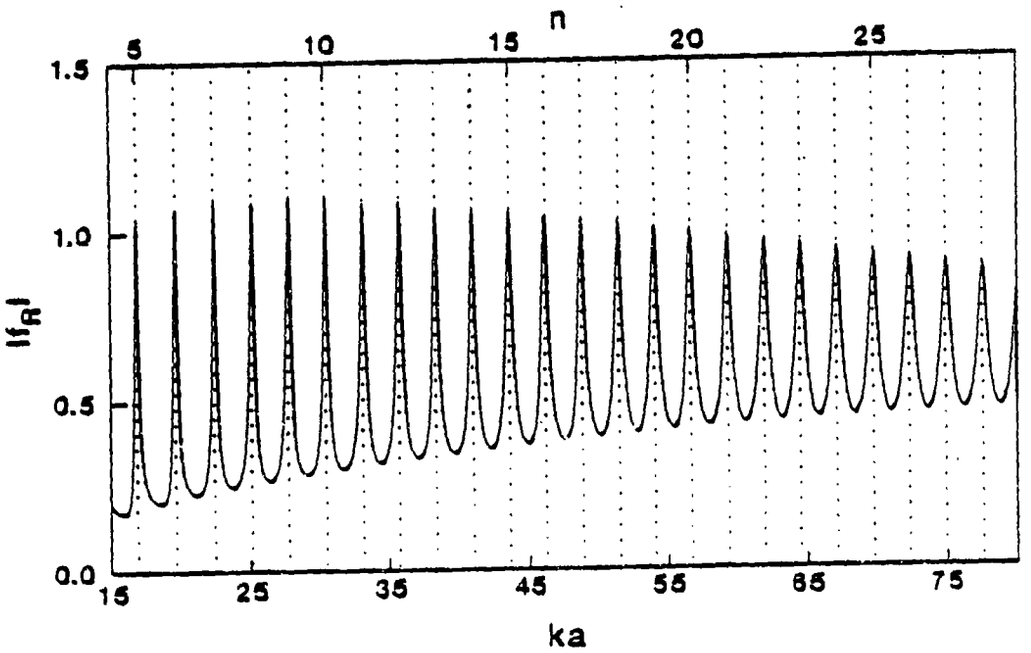

The absolute value of the Rayleigh contribution f_R to the backscattering form function $f(ka,\pi)$ of a tungsten carbide sphere is shown. Also indicated as vertical lines are the RST Rayleigh resonances $Re(x_{n1})$ for $5 \leq n \leq 28$. The value of n for each resonance is given at the top of the figure. One notes that within the resolution of this graph $|f_R|$ has a peak at $ka = Re(x_{n1})$.

Fig. 3.

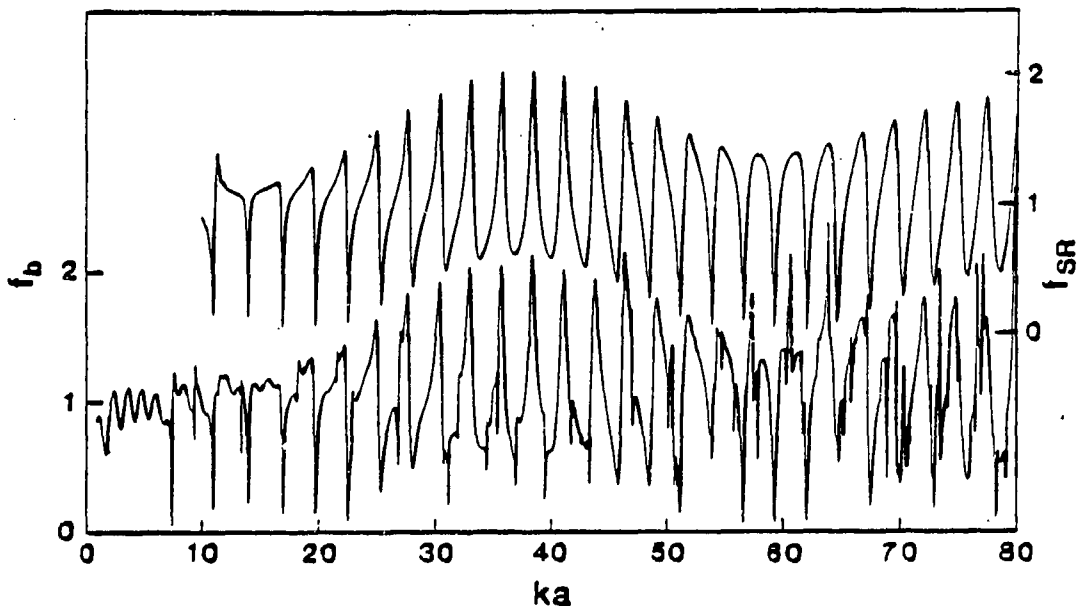

In this figure f_b is the absolute value of the backscattering form function for a tungsten carbide sphere as calculated using the PWS and f_{SR} is an approximation to f_b obtained using the SWT results for the specular reflection and Rayleigh surface wave contributions to backscattering. The vertical scale for f_{SR} has been shifted since the two curves are not easily distinguished otherwise.

Fig. 4.

We have offset f_{SR} vertically since when the curves are superimposed they cannot be easily distinguished. In Fig. 5 the ka scale has been expanded and f_b and f_{SR} are shown without offset. This facilitates a better view of the agreement between the two curves which is typical throughout the range $10 \leq ka \leq 80$. These figures show that f_{SR} correctly reproduces f_b except for a fine structure (superimposed on f_{SR}) due to other waves.

Though f_{SR} is the final result needed for the discussion of Section IIB it is appropriate to further test the SWT results of Ref. 5 by adding in the contribution from the slowest whispering gallery wave. The addition of this wave gives an approximation $|f_S(x,\pi) + f_R(x,\pi) + f_{WG1}(x,\pi)| \equiv f_{SRWG}$. Figures 6 and 7 show f_b and f_{SRWG}. From these figures one sees that some of the fine structure absent from f_{SR} has been recaptured. The increased agreement is especially obvious in Fig. 7. Presumably the rest of the fine structure could be obtained by adding in contributions from other whispering gallery waves. This method of adding one surface wave at a time to the approximate form function allows one to ascertain the effect of each surface wave by inspection.

It is appropriate to make some further comments on these results. One can understand the why G_R is approximately linear in ka over the range displayed in Fig. 2 by the following argument. The ka dependence results from the product of two factors. One factor is proportional to $\sqrt{ka}$ because of axial focusing.[12] The other $\sqrt{ka}$ factor can be attributed to the increased coupling efficiency of surface waves with increase of ka. This last $\sqrt{ka}$ factor can be obtained using energy conservation arguments similar to those of Ref. 13. One can find this $\sqrt{ka}$ factor due to increased coupling efficiency in cylindrical SWT results. Casting the SWT for cylinders[14] in a form similar to that for spheres gives a coupling factor for Rayleigh waves with a form

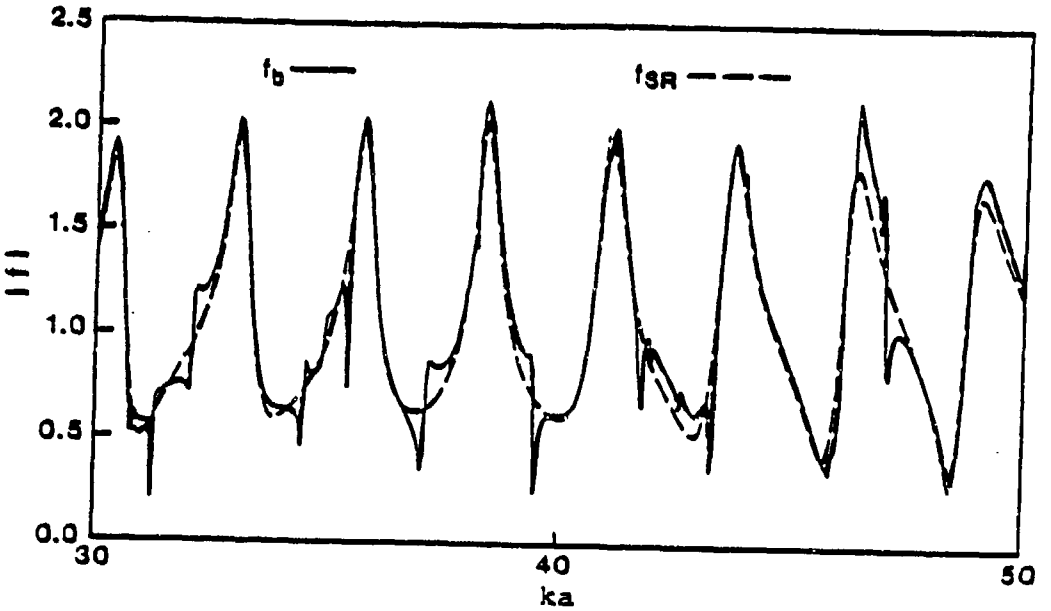

Shown on an expanded scale is part of f_b and f_{SR} from Fig. 4. In this figure the vertical scale of f_{SR} is no longer offset. This figure allows one to better examine the agreement between f_b and f_{SR} which is typical throughout the region $10 \leq ka \leq 80$.

Fig. 5.

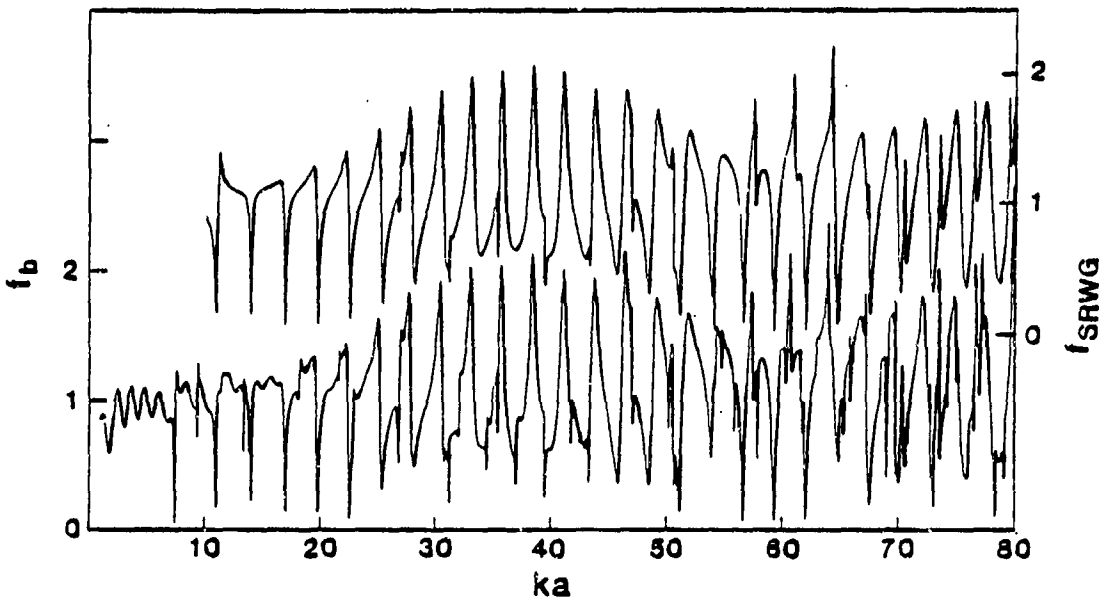

This figure is similar to Fig. 4 except that f_{SRWG} includes the contributions to backscattering from the slowest whispering gallery wave as well as the contributions from specular reflection and the Rayleigh wave included in f_{SR}. The inclusion of the whispering gallery wave in f_{SRWG} adds some fine structure to f_{SR} thus giving better agreement with f_b.

Fig. 6.

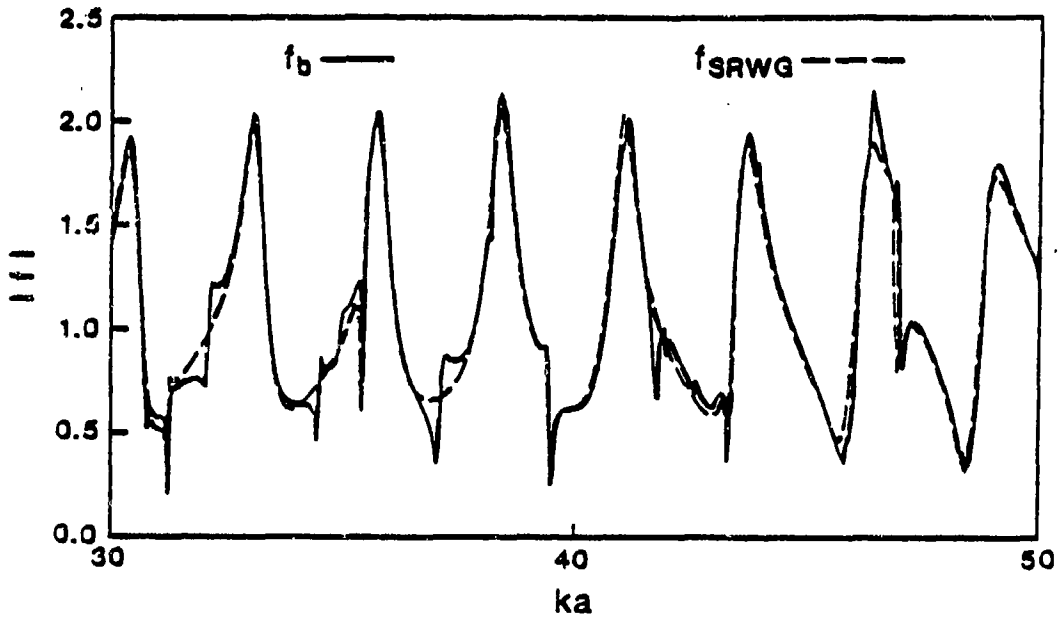

Shown on an expanded scale is part of f_b and f_{SRWG} from Fig. 6 but without vertical scale offset. As in Fig. 5 this allows a better view of the agreement between f_b and the SWT result.

Fig. 7.

like G_R but divided by $\sqrt{ka}$ due to the fact there is no axial focusing. This implies an approximate $\sqrt{ka}$ dependence for the cylindrical counterpart to G_R. The surface wave's phase velocity dispersion may alter this ka dependency for coupling efficiency. The above arguments are therefore only valid in ka regions where the surface wave of interest is weakly dispersive.

Finally we should discuss why our synthesis of f_b in Figs. 6 and 7 works as well as it does. It was not necessary to include transmitted bulk waves such as those described in Ref. 12 for a fused silica sphere. This is because for tungsten carbide, the contributions due to transmitted waves are estimated to be negligible in comparison to those due to specular reflection, the Rayleigh wave, and the leading whispering gallery waves near resonance in the ka region of interest.[8] It is significant in this regard that the density of tungsten carbide is much greater than that of water.

The reformulation of the m series of Eq. (4) into the closed form of Eq. (7) is similar, in principle, to Felsen's "Hybrid Synthesis" technique.[15] The form of Eq. (4) is useful for transient analysis[5] while that of Eq. (7) is more convenient for describing the steady state scattering.

B. Interpreting RST using f_{SR}

The physical nature of f_{SR} is relatively simple. The discussion of this section elucidates the physical interactions which produce the structure of f_{SR} and in doing so allows an excellent opportunity for examining RST. The main topics of discussion in this section are the significance of the phase between the specular reflection and first Rayleigh wave contribution in determining the structure of f_{SR} and the relation between the Rayleigh resonances x_{n1} of RST and the maxima and minima of f_{SR}.

The phase between the specular reflection and the first Rayleigh contribution can be determined from Eq. (3) and the $m = 0$ term of Eq. (4) to

be $\eta_1 \equiv 2x + \eta_R + \arg(G_R)$ where $\arg(G_R)$ is defined as $\arctan(\mathrm{Im}G_R/\mathrm{Re}G_R)$. In Figs. 8 and 9 both f_{SR} and $\eta_1^m \equiv \eta_1$ Modulo 2π are plotted as functions of ka. Figure 9 is an enlargement of the region $35 \leq k \leq 65$ of Fig. 8. In addition we have indicated values of $\mathrm{Re}(x_{n1})$ for $3 \leq n \leq 28$ by the position of vertical lines. These lines are labeled with the appropriate value of n at the top of the figures.

The vertical lines allow one to determine η_1^m at the point where the Rayleigh wave contributions all add in phase. By examination of [illegible] 8 and 9 one can make several statements about the η_1^m and its relation to the structure of f_{SR}. We see that the value of η_1^m at the point where $n + (1/2)$ Rayleigh wavelengths fit on the sphere is not the same for all n. Furthermore, the value of η_1^m at these points dictates what kind of structure f_{SR} will have in the local region. For instance $\eta_1^m = 0$ when $n = 13,28$ and f_{SR} has a maximum right at these points. Likewise $\eta_1^m = \pi$ when $n = 4,21$ and f_{SR} has a minimum at these points. However, it is obvious from Figs. 8 and 9 that in most cases η_1^m does not equal 0 or π and the maximum and minimums of f_{SR} do not coincide with the in phase adding of the Rayleigh contributions.

The ideas and results to this point can be used to reexamine and qualify the recent RST analysis of the backscattering form function of a tungsten carbide sphere.[3] First, the Rayleigh waves are responsible not only for the quasinulls in the (summed) form function but are also responsible for many of the maximums. Indeed, the interference of the specular reflection and Rayleigh contributions are responsible for the overall structure of the form function in a much more encompassing way than the RST discussion implies. Furthermore, the statement that the quasinulls of the form function are "at the roots x_{n1},"[3] is only true for $n = 4,21$ which points $\eta_1^m = \pi$. Last,

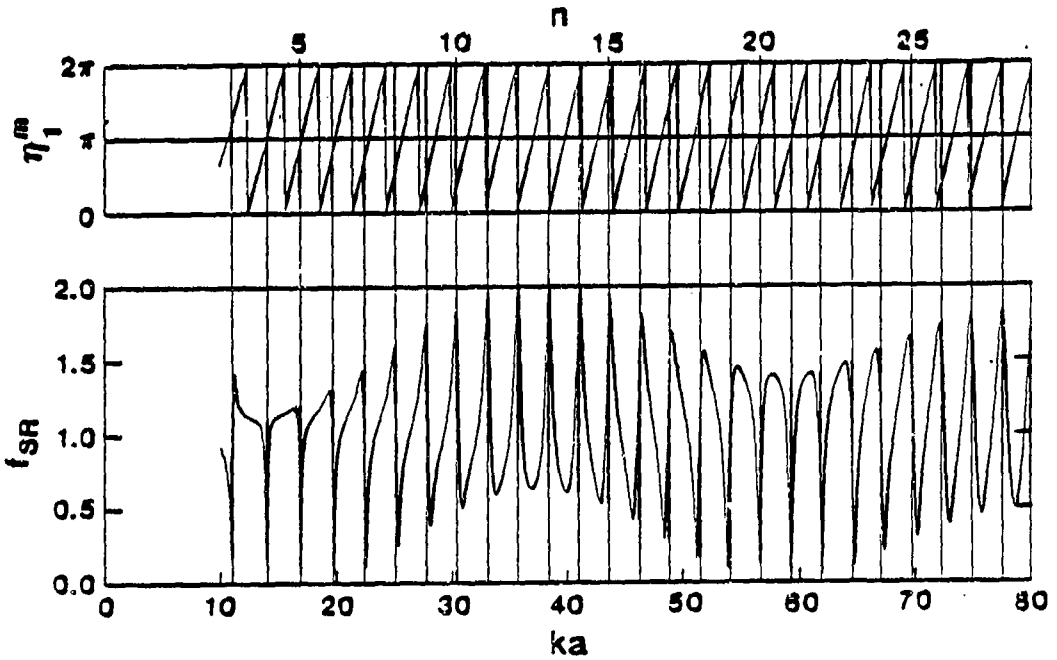

The phase η_1^m between the specular reflection and first Rayleigh wave contribution to backscattering is shown in the upper part of the figure. In the lower part f_{SR} from Fig. 4 is given. As in Fig. 3 the vertical lines indicate the position of the real part of the Rayleigh resonances $\mathrm{Re}\, x_{n1}$ where n is given at the top of the figure. To within the resolution of this graph the vertical lines allow one to find the phase between the first Rayleigh waves contribution and specular reflection when $n + (1/2)$ cycles of the Rayleigh wave fit on the sphere; i.e., at resonance. Note that f_{SR} does not always have a maximum or minimum at the $\mathrm{Re}(x_{n1})$ values.

Fig. 8.

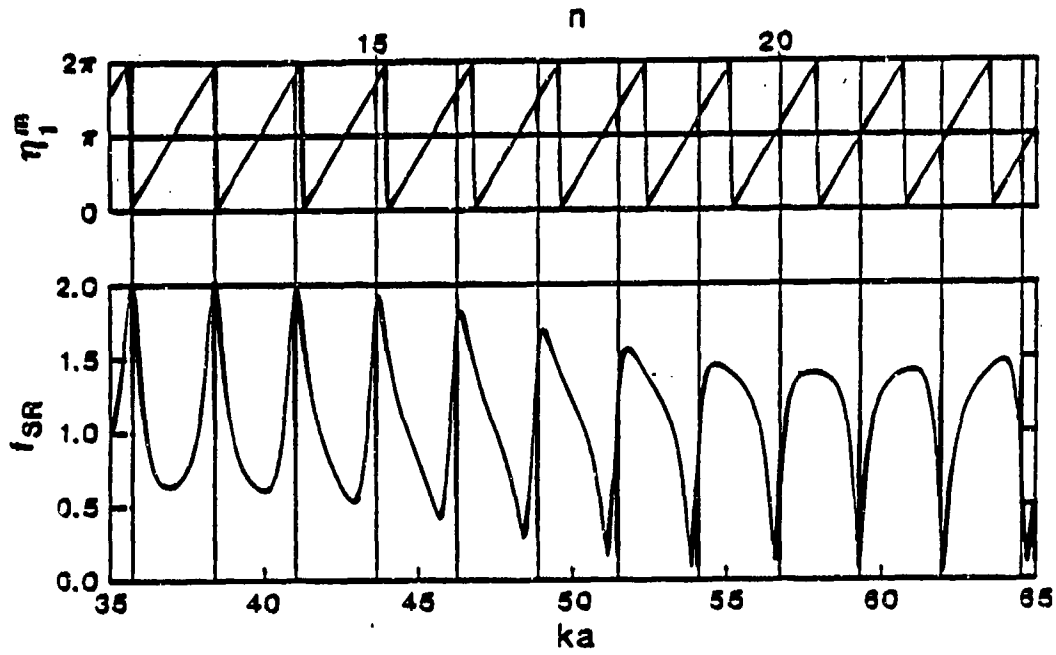

An expanded view of part of Fig. 8 is shown here so that one can obtain a more detailed look at how the phase η_1^m at the $Re(x_{n1})$ effects the local structure of f_{SR}.

Fig. 9.

Figs. 8 and 9 imply that the Rayleigh wave may be responsible for a local minimum or maximum in the form function even though the minimum or maximum may not be at one of the x_{n1} of the Rayleigh waves. This implies that some care may be needed in using the labeling in Fig. 4 of Ref. 3 to understand fluctuations in f_b. The labeling may correspond to the numerical values of $x_{n\ell}$; however, to understand the effect of a resonance on the form function, the coupling efficiency onto the sphere as well as the interference between the specular reflection and the surface waves must be taken into account.

4.3 Resonance conditions from RST and the SWT

In this section the condition for resonances given by the SWT (the "physical resonances") are compared with that of RST ("RST resonances"). The RST and SWT treatments of resonance differ. The RST $x_{n\ell}$ are found by allowing x to take on complex values while n remains an integer; i.e., RST resonances are located in a complex x plane. In the SWT, however, x remains real and one allows n to take on continuous complex values (i.e., the ν values) and the poles are located in a complex ν plane. It is the poles in this complex ν plane which lead to the idea of damped surface waves. In Sec. IIA we use Eq. (7) to examine the SWT and RST resonance conditions and then in Sec. IIB we arrive at the same results through a more formal channel.

A. <u>A first look</u>

Using again the definition $\nu_\ell = \alpha_\ell + i\beta_\ell$, Eq. (7) can be written as

$$f_\ell(x,\pi) = \frac{-G_\ell \exp[i\eta_\ell - 2\beta_\ell(\pi-\theta_\ell)]}{[1 - \exp(i2\pi\nu_\ell)]} \tag{8}$$

This equation resulted from the SWT and it is obvious that the resonance behavior is related to the complex value of ν_ℓ where we must remember that

ν_ℓ is a function of the real $ka \equiv x$. By varying x we can locate the values ν_ℓ^n in the complex ν plane where $\nu_\ell^n = n + i\beta_\ell^n$ and $n + (1/2)$ wavelengths of the surface wave fit on the sphere (cf. Sec. I). The value of x at which $\mathrm{Re}(\nu_\ell^n) = n$ are the resonance conditions given by the SWT. These x are real valued and are designated as x_ℓ^n.

To examine the RST resonance behavior of f we can expand ν_ℓ locally around the point x_ℓ^n giving

$$\nu_\ell = n + i\beta_\ell^n + \nu_\ell'(x-x_\ell^n) + \ldots \tag{9}$$

where $\nu_\ell' = \mathrm{Re}\nu_\ell' + i\,\mathrm{Im}\nu_\ell'$ and the prime denotes differentiation with respect to x evaluated at x_ℓ^n. Substituting Eq. (9) into Eq. (8) gives

$$f_\ell(x,\pi) = \frac{-G_\ell \exp[i\eta_\ell - 2\beta_\ell(\pi - \theta_\ell)]}{\{1 - \exp[i2\pi\nu_\ell'(x - (x_\ell^n + \Delta x) + i\tfrac{1}{2}\Gamma_\ell)]\}} \tag{10}$$

where $\Delta x = -\beta_\ell{}^n(\mathrm{Im}\nu_\ell')/|\nu_\ell'|^2$ and $\Gamma_\ell = 2\beta_\ell^n(\mathrm{Re}\nu_\ell')/|\nu_\ell'|^2$. Note that Δx is negative real. This approximation is valid near resonance when $|\nu_\ell''(x - x_\ell^n)^2| \ll |\nu_\ell'(x - x_\ell^n)|$. From Eq. (10) we can look at the RST resonance condition by allowing x to take on complex values. The pole in f_ℓ is located at $x = (x_\ell^n + \Delta x) - i\tfrac{1}{2}\Gamma_\ell = x_{n\ell}$.

Recall that the usual RST resonance condition is $x = \mathrm{Re}(x_{n\ell})$. We see that this differs from the SWT result $(x = x_\ell^n)$ by an error Δx. The magnitude of the error obviously depends on the pole in the complex ν plane associated with the resonance. We have calculated numerical values of Δx for the Rayleigh pole and one whispering gallery pole in both tungsten carbide and fused silica. The values of Δx at $ka \approx 40$ ranged from $\Delta x \approx -0.0007$

for the whispering gallery pole of tungsten carbide to $\Delta x \simeq -0.1$ for the Rayleigh pole of fused silica. The Δx shift for the Rayleigh pole of tungsten carbide was less than -0.003 throughout the ka range of the figures of Sec. I and is not detectable for any of the plots of that section.

For a given value of x, the phase velocity c_ℓ of a surface wave may be calculated using the SWT from the location of the ν pole. The result, which follows from Eq. (30) of Ref. 5 and the phase matching condition $\sin\theta_\ell = c_\ell/c$, is $c_\ell/c = x/[\alpha_\ell + (1/2)]$. Letting $x = x_\ell^n$ so that $\alpha_\ell = n$ gives

$$c_\ell/c = x_\ell^n/[n + (1/2)] \tag{11}$$

Since $x_\ell^n = \mathrm{Re}(x_{n\ell}) - \Delta x$, we also have

$$c_\ell/c = [\mathrm{Re}(x_{n\ell}) - \Delta x]/[n + (1/2)] \tag{12}$$

Equation (12) allows one to properly calculate surface wave phase velocity from the RST resonance condition.

Previous work[2,16] in RST relating the ν and x complex planes for cylinders and spheres started in the x plane and then carried out an expansion of $x_{n\ell}$ equivalent to the expansion of ν_ℓ in Eq. (9). By examination of these expansions one finds an implicit assumption in Ref. 2 that $d(\mathrm{Im}x_{n\ell})/d\nu = 0$. This is analogous to assuming $\mathrm{Im}\nu_\ell' = 0$ in Eq. (9) in which case Δx would equal zero. One should note that the relation between the complex ν and x planes was previously examined[17,18] for applications of the SWT to quantum mechanical scattering, especially Ref. 18, pp. 106-113.

B. A more formal approach

The results of Sec. IIA can be derived using the general expressions for the form function f^{PWS} and f^{SWT}. The expressions used for f^{PWS} and f^{SWT} in this section are less specific than given in Sec. I since detailed forms are not necessary in the derivation. The approach of this section is similar to that described by Newton for quantum mechanical scattering.[17]

The PWS result f^{PWS} can be written as

$$f^{PWS}(x,\theta) = \sum_{n=0}^{\infty} A_n(x) \cdot P_n(\mu) \tag{13}$$

where $\mu = \cos\theta$, P_n is the Legendre polynomial, and $A_n(x)$ is a complicated function[3] of x; A_n diverges at the complex $x_{n\ell}$ of RST.

As discussed in Sec. I, f^{SWT} can be written as a sum of contributions from specular reflection, transmittad bulk waves and surface waves. (For completeness one must also include a possible contribution[5] from a "background integral" and that due to forward diffraction in the case of near forward scattering.) One can write

$$f^{SWT}(x,\theta) = f_1 + \sum_{\ell=R,WG} f_\ell \tag{14}$$

where f_1 includes all contributions to f^{SWT} except those due to the Rayleigh and all whispering gallery waves which are accounted for by the sum.

For purposes of the present discussion it is convenient to rewrite the sum of Eq. (14) in slightly more detail. Using Eqs. (22) and (23) of Ref. 5 we can write

$$f^{SWT}(x,\theta) = f_1 + \sum_{\ell=R,WG} \frac{B_{\nu_\ell}(x)\, P_{\nu_\ell}(-\mu)}{\sin\pi\nu_\ell} \tag{15}$$

where P_{ν_ℓ} is now a Legendre function of the first kind. When x is large we may take $f^{PWS} = f^{SWT}$. Thus we have

$$\sum_{n=0}^{\infty} A_n(x)P_n(\mu) = f_1 + \sum_{\ell=R,WG} \frac{B_{\nu_\ell}(x)\, P_{\nu_\ell}(-\mu)}{\sin\pi\nu_\ell} \tag{16}$$

Now multiply both sides of Eq. (16) by $P_{n'}(\mu)$ were n' is a nonnegative integer and integrate from $\mu = -1$ to $\mu = 1$. Using the relations[19,20]

$$\int_{-1}^{1} P_{n'}(\mu)P_n(\mu)d\mu = \frac{2}{(2n+1)}\,\delta_{nn'} \tag{17}$$

$$\int_{-1}^{1} P_{n'}(\mu)P_{\nu_\ell}(-\mu)d\mu = \frac{2}{\pi}\,\frac{\sin\pi\nu_\ell}{(\nu_\ell-n')(\nu_\ell+n'+1)} \tag{18}$$

we find that

$$A_n(x) = \sum_{\ell=R,WG} \frac{C_{\nu_\ell}}{(\nu_\ell-n)(\nu_\ell+n+1)} + E_n \tag{19}$$

$$E_n = \left(\frac{2n+1}{2}\right) \int_{-1}^{1} f_1 P_n(\mu)d\mu \tag{20}$$

where $C_{\nu_\ell} = (2n+1)B_{\nu_\ell}/\pi$ depends on x and $\delta_{nn'}$ in Eq. (17) is the Kronecker delta. It is apparent from the form of the summation that $A_n(x)$ (and therefore the form function) exhibits resonance behavior at x near x_ℓ^n, which is the resonance condition from the SWT. Recall that $\mathrm{Re}(\nu_\ell) = n$ when

$x = x_\ell^n$. (There may also be some resonance behavior due to E_n but we will not address this.) Applying the expansion given by Eq. (9) to $(\nu_\ell - n)$ in Eq. (19) gives

$$A_n(x) = \sum_{\ell=R,WG} \frac{C_{\nu_\ell}}{\nu_\ell'(\nu_\ell+n+1)(x-(x_\ell^n+\Delta x)+i\frac{1}{2}\Gamma_\ell)} + E_n \tag{21}$$

where Δx and Γ_ℓ are as defined below Eq. (10). We now see poles in the complex x plane at the values $x_{n\ell} = (x_\ell^n + \Delta x) - i\frac{1}{2}\Gamma_\ell$ as before and the discussion and cautions subsequent to Eq. (10) apply.

This paper has reexamined some of the central concepts of RST. Though the specific case of a fluid-loaded sphere was used, the results have more general ramifications. The usefulness and power of the SWT for understanding acoustical scattering problems has been illustrated. It is appropriate to note that the present research was completed on the centenary of Rayleigh's original analysis[21] of surface waves on the flat surface of an elastic solid.

Acknowledgment

This research was supported by the Office of Naval Research. The authors thank Dr. R. C. Chivers for supplying the programs[6] used to calculate the PWS results of Sec. I.

References

1. L. Flax, L. R. Dragonette, and H. Überall, "Theory of elastic resonance excitation by sound scattering," J. Acoust. Soc. Am. 63, 723-731 (1978).
2. L. Flax, G. C. Gaunaurd, and H. Überall, "Theory of resonance scattering," in Physical Acoustics, edited by W. P. Mason and R. N. Thurson (Academic, New York, 1981), Vol. 15, pp. 191-294.
3. G. C. Gaunaurd and H. Überall, "RST analysis of monostatic and bistatic acoustic echoes from an elastic sphere," J. Acoust. Soc. Am. 73, 1-12 (1983).
4. D. Brill and G. C. Gaunaurd, "Acoustic resonance scattering by a penetrable cylinder," J. Acoust. Soc. Am. 73, 1448-1455 (1983).
5. K. L. Williams and P. L. Marston, "Backscattering from an elastic sphere: Sommerfeld-Watson transformation and experimental confirmation," J. Acoust. Soc. Am. (accepted for publication).
6. R. C. Chivers and L. W. Anson, "Calculations of the backscattering and radiation force functions of spherical targets for use in ultrasonic beam assessment," Ultrasonics 20, 25-34 (1982).
7. H. Überall, et al., "Dynamics of acoustic resonance scattering from spherical targets: Application to gas bubbles in fluids," J. Acoust. Soc. Am. 66, 1161-1172 (1979).
8. K. L. Williams and P. L. Marston, "Axially-focused (glory) scattering due to surface waves generated on spheres: Model and experimental confirmation using tungsten carbide spheres," J. Acoust. Soc. Am. (accepted for publication).
9. L. R. Dragonette, S. K. Numrich, and L. J. Frank "Calibration technique for acoustic scattering measurements," J. Acoust. Soc. Am. 69, 1186-1189 (1981).

10. E. Hecht and A. Zajac, Optics (Addison-Wesley, Massachusetts, 1974) p. 305.

11. I. S. Gradshteyn and I. M. Ryzhik, Table of Integrals, Series, and Products (Academic Press, New York, 1980).

12. P. L. Marston, K. L. Williams, and T. J. Hanson," Observation of the acoustic glory: High frequency backscattering from an elastic sphere," J. Acoust. Soc. Am. 74, 605-618 (1983).

13. J. B. Keller and F. C. Karal, Jr., "Geometrical theory of elastic surface wave excitation and propagation," J. Acoust. Soc. Am. 36, 32-40 (1964).

14. G. V. Frisk and H. Überall, "Creeping waves and lateral waves in acoustic scattering by large elastic cylinders," J. Acoust. Soc. Am. 59, 46-54 (1976).

15. L. B. Felsen, "Progressing and oscillatory waves for hybrid synthesis of source excited propagation and diffraction," IEEE Trans. Antennas Propag. AP-32, 775-796 (1984).

16. The reader is cautioned that the $x_{n\ell}$ in Eq. (37) of Ref. 2 is equal to $\mathrm{Re}(x_{n\ell})$ in the notation of our paper. It is the x_p of Eq. (19) of Ref. 2 which is given by our $x_{n\ell}$.

17. R. G. Newton, Scattering Theory of Waves and Particles (Springer-Verlag, New York, 1982).

18. R. G. Newton, The Complex j-Plane (W. A. Benjamin, New York, 1964).

19. J. D. Jackson, Classical Electrodynamics (Wiley & Sons, New York, 1975).

20. P. Roman, Advanced Quantum Theory (Addison-Wesley, Massachusetts, 1965).

21. Lord Rayleigh, "On waves propagated along the plane surface of an elastic solid," Proc. London Math. Soc. XVII, 4-11 (1885).

APPENDIX--COMPUTER PROGRAMS

ZNU and ZKA

The program ZNU calculates the SWT poles of a tungsten carbide sphere in the complex ν plane given the real ka value of the sphere. Parts of the program were adapted from a program written by Brad Brim as part of a master's degree project (Ref. 21 of Chapter 2). The program requires that you input a guess (GUESS) of the pole position. It also asks for the region in the complex plane where it is supposed to look (HEIGHT), the precision required in pole location (ERROR), and the ka value of the sphere. The program assumes a complex value for ka but one need only set the Im ka = 0 to find SWT poles. The program uses the winding number theorem to find the poles. There is a commentary (written by Brad Brim) within the program on the winding number theorem. Within this commentary the other parameter you are asked to input (Npnts) is discussed. The program finds the SWT poles by seeking the zeros of the function D_ν defined in Appendix A of Chapter 3.

The subroutine OLVER (which is called within the program) is given later in this appendix. This subroutine limits the accuracy of finding the SWT poles to no better than 0.000001 + i0.00001. Furthermore, this accuracy is only applicable under the conditions given in Section 4.2.

This program was used to generate the numbers found in Table I of Chapter 3. That table can be used to check that the program is working properly. If used for other isotropic spheres the material parameters must be changed.

The program ZKA (not listed here) is like ZNU except that it locates the zeros of $D_n(ka)$ as defined in Chapter 2. Here $n = Re(NU)$ is a specified integer and $Im(NU) = 0$. The complex ka for which $D_n(ka) = 0$ are obtained. The principal modification to ZNU is in the subprogram for the function f. The program was used to generate Table I of Chapter 2.

```
cccccccccccccccc
c              c
c     ZNU      c
c              c
cccccccccccccccc

cccccccccccccccccccccccccccccccccccccccccccccccccccccccccccccccccccccccccc
c                                                                        c
c      The calling program and subroutine ZROOT was originally           c
c    written by Brad Brim of the EE department.It has been altered       c
c    to apply to the scattering problem at hand.ZROOT locates the        c
c    complex zeros and poles of the function F which the user defines.   c
c    At present F is Dn of the fraction Bn/Dn discussed in the text.     c
c    This version of the program can be used to find the zeros in the    c
c    complex lamda (or nu) plane given a real value of ka.This program   c
c    was used to find the Rayleigh poles given in Table I of chapter 3   c
c    .To do spheres of material other than tungsten carbide you must     c
c    change the material parameters in the function F.                   c
c      The function F calls the subroutine OLVER which is given          c
c    in a seperate part of this appendix.I make no claims that this      c
c    program as altered is "efficient" in the sense of computer time     c
c    or program length.                                                  c
c      The program includes a discussion of how ZROOT works.             c
c                                                                        c
cccccccccccccccccccccccccccccccccccccccccccccccccccccccccccccccccccccccccc


C*********************************************************************
C*                                                                   *
C*    This is a very general calling program associated with the     *
C*    routine "ZROOT".  It handles all the input of parameters and   *
C*    output of results.                                             *
C*                                                                   *
C*********************************************************************
C*                                                                   *
C*    SEE the subroutine "ZROOT" for the requirements on F(z) and the *
C*    input parameters.  Contained therein is a fairly thorough      *
C*    description of the algorithm and numerical considerations.     *
C*                                                                   *
C*********************************************************************


      REAL*8      RADII(10),X,Y,HEIGHT,ERROR
      INTEGER     ORDER(10)
      COMPLEX*16  ZERCS(10),GUESS,KA
      COMMON KA


 1    WRITE (1,10)
   10 FORMAT(/////,' REAL PART OF GUESS',T35,' _')
      READ  (1,*) X

      WRITE (1,20)
```

```
   20 FORMAT(' IMAG PART OF GUESS',T35,' _')
      READ  (1,*) Y

      GUESS = CMPLX(X,Y)


      WRITE (1,30)
   30 FORMAT(/,' DESIRED HEIGHT',T35,' _')
      READ (1,*) HEIGHT

      WRITE (1,40)
   40 FORMAT(/,' DESIRED ERROR',T35,' _')
      READ (1,*) ERROR
      ERROR = DMAX1(ERROR,1.0D-07)

      Npnts = 100
      WRITE (1,50)
   50 FORMAT(/,' POINTS PER QUADRANT SIDE',T35,' _')
      READ (1,*) Npnts

      WRITE(1,53)
 53   FORMAT(/,'REAL PART OF KA',T35,'_')
      READ(1,*) X

      WRITE(1,54)
 54   FORMAT(/,'IMAG PART OF KA',T35,'_')
      READ(1,*) Y

      KA=CMPLX(X,Y)

      WRITE (1,60)
   60 FORMAT(5X,/////)


      CALL ZROOT(GUESS,HEIGHT,ERROR,Npnts,
     +           Nzero,ZEROS,RADII,ORDER)



      IF (Nzero .EQ. 0) THEN
           WRITE (1,70)
   70      FORMAT(/,' **********  THERE WERE NO ZEROES  **********')
      ELSE
           WRITE (1,80)
   80      FORMAT(/,' **********    THE ZEROES WERE     **********')
           DO 100 I=1,Nzero
                WRITE (1,90) I,ZEROS(I),RADII(I),ORDER(I)
   90           FORMAT(/,/,I4,7X,2E16.7,7X,E14.7,7X,I4)
  100      CONTINUE
      ENDIF

      GO TO 1

      END
```

```
      SUBROUTINE ZROOT(CENTR,HITE,ERROR,Npnts,
     +                 Nzero,ZEROS,RADII,ORDER)

C*********************************************************************
C***** by BRADLEY L. BRIM                final revisions  7/24/83 *****
C*********************************************************************
C*                                                                   *
C*      This routine searches the complex plane for the roots of the *
C*    function F(z). F(z) must be an externally defined COMPLEX*16   *
C*    function subroutine.  The variable z must also be COMPLEX*16.  *
C*      This routine is easily modified for    F(z)  ->  F(z,(Xn))  *
C*    where  (Xn)  is a set of n parameters independant of z.        *
C*                                                                   *
C*********************************************************************
C*                                                                   *
C*    This routine is based on the "WINDING NUMBER" theorem, found   *
C*    in any complex variables book.                                 *
C*                                                                   *
C*    This theorem basically says .....                              *
C*       "The integral around any simply closed contour (evaluated   *
C*        in the clockwise direction) of the function [F'(z)/F(z)]   *
C*        will be equal to  2*pi*i*(#P-#Z)."                         *
C*           where ...  #Z = number of zeroes within the contour     *
C*                      #P = number of poles  within the contour     *
C*                                                                   *
C*                                                                   *
C*                                                                   *
C*                                SIDE #4                            *
C*                                                                   *
C*                                                                   *
C*     CORNER #4 ____________________________________ CORNER #1      *
C*               |          >          :          >          |       *
C*               |                     :                     |       *
C*               |                     :                     |       *
C*               |                     c                     |       *
C*               |                     r                     |       *
C*               |                     o                     |       *
C*               |                     s                     |       *
C*               |     QUADRANT        s     QUADRANT        |       *
C*               |       # 4           :       # 1           |       *
C*               |                     #                     |       *
C*               |                     1                     |       *
C*               |                     :                     |       *
C*               |                     :                     |       *
C*        \      |                     :                     |      /  *
C*   S    |      |                     :                     |      | S *
C*   I #  |      |....cross.#4.....CENTR.....cross.#2....|      | I # *
C*   D 3  |      |                     :                     |      | D 1 *
C*   E    |      |                     :                     |      | E   *
C*        /      |                     :                     |      \  *
C*               |                     c                     |       *
C*               |                     r                     |       *
C*               |                     o                     |       *
C*               |                     s                     |       *
```

```
C*              |      QUADRANT      s      QUADRANT      |                 *
C*              |        # 3         :        # 4         |                 *
C*              |                    #                    |                 *
C*              |                    3                    |                 *
C*              |                    :                    |                 *
C*              |                    :                    |                 *
C*              |                    :                    |                 *
C*              |                    :                    |                 *
C*     CORNER #3_____________________________________CORNER #2              *
C*                        <                    <                             *
C*                                                                           *
C*                                 ___________                               *
C*                                /           \                              *
C*                                 SIDE #2                                   *
C*                                                                           *
C*                                                                           *
C*                                                                           *
C*     This routine was written especially to determine the location         *
C*   of ALL the roots in a specified square region, to a specified           *
C*   accuracy.  Other routines may claim to be more efficient, but           *
C*   all other complex root search routines this author knows of will       *
C*   terminate after finding the location of only the first root that       *
C*   the routine happens upon.                                               *
C*                                                                           *
C*   The parameters of this program are .....                                *
C*                                                                           *
C*     INPUT  :   CENTR      [C*16]    Center of the square region           *
C*                                     in which to search for roots.         *
C*                HITE       [R*08]    Half the length of a side of          *
C*                                     this square. (Quadrant height)        *
C*                ERROR      [R*08]    The maximum quadrant height           *
C*                                     of the root location(s).              *
C*                Npnts      [I*02]    Number of points per quadrant         *
C*                                     side in numerical integration.        *
C*                                                                           *
C*     OUTPUT :   ZEROS(10)  [C*16]    Center(s) of square region(s)         *
C*                                     containing the root(s).               *
C*                RADII(10)  [R*08]    Acutal quadrant height of the         *
C*                                     corresponding region(s).              *
C*                ORDER(10)  [I*02]    Order of the root(s)                  *
C*                                       +N  ->  Nth order ZERO              *
C*                                       -N  ->  Nth order POLE              *
C*                                                                           *
C*     The winding number basis for this routine allows one to find          *
C*   the location of both zeros and/or poles.  The problem with this         *
C*   is, if a region is searched which contains an equal number of           *
C*   poles and zeros, this is interpreted as a region with no roots.         *
C*   Thus, it is recommended that this routine be used with functions       *
C*   which has only zeros OR poles.  The exception is of course when         *
C*   one has some knowledge a priori of the location of both types of        *
C*   roots and regions where they occur mutually exclusively.                *
C*     This routine starts out by calculating the winding number of          *
C*   the given "initial square region".  If it's non-zero the routine        *
C*   next looks at the quadrants of that region in ascending order.          *
C*   If the winding number is zero, it goes on to the next quadrant.         *
C*   If the winding number is non-zero and the error is small enough,        *
C*   the information is recorded.  If the error is too large, this           *
```

```
C*    quadrant becomes the new "initial square region" and the routine *
C*    will start over.  When the routine has done enough "splits" to   *
C*    locate a root to the desired accuracy, it begins to work its way *
C*    back to larger regions, by checking quadrants of previous splits.*
C*      The variable Nsplit keeps track of how many times the original *
C*    initial square region has been split up.  A maximum of twenty-   *
C*    four splits are allowed, which should always be sufficient.      *
C*    Since a subroutine in FORTRAN may not call itself, the arrays    *
C*    CENTER,HEIGHT,QDRNTS,INTGRL,INSIDE are used to store information *
C*    calaculated in previous splits so it does not have to be redone. *
C*                                                                     *
C*    The function   [F'(z)/F(z)]*dz   is approximated as .....        *
C*                                                                     *
C*     ([F(z2)-F(z1)]/[z2-z1]) / (0.5*[F(z1)+F(z2)]) * (z2-z1)         *
C*                                                                     *
C*    OR, by reducing                                                  *
C*                      2*(1-2*(F(z1)/[F(z1)+F(z2)]))                  *
C*                                                                     *
C*    Integrating this over Npnts points                               *
C*                                                                     *
C*        integral =  2 * (Npnts - 2*SUM)                              *
C*                                                                     *
C*    where       z = (z1+z2)/2                                        *
C*              SUM = the sum for each z   F(z1)/[F(z1)+F(z2)]         *
C*                                                                     *
C*      This author found it both numerically accurate and efficient   *
C*    in time to calculate the quantity "SUM" and then apply the       *
C*    above integration formula.                                       *
C*      The subroutine "EXACT" is called if F(.) happens to be exactly *
C*    equal to zero.  That fact is printed and the routine stops.      *
C*      The subroutine "BETWN" is called if Fsum = F(z1)+F(z2) happens *
C*    to be exactly equal to zero.  There,  F(z) [z as defined above]  *
C*    is calculated.  If F(z) is non-zero, Fsum is replaced by twice   *
C*    F(z) and the numerical integration continues.  If F(z) is also   *
C*    zero, that fact is printed and the routine stopped.              *
C*      The reason that the routine is stopped if a zero is found is   *
C*    because numerical problems are very likely.  If a root is        *
C*    located "near" the contour of integration (relative to the step  *
C*    and quadrant sizes) then this root will contribute approximately *
C*    half its normal value to the winding number.  The contribution   *
C*    is almost always greater than half of normal if the root is just *
C*    inside the contour, and less if just outside.  Similarly, for a  *
C*    root located near a corner in the contour, the contribution will *
C*    be approximately one quarter normal.  These two facts tend to    *
C*    help the program work, even if the root is close to the contour. *
C*      The required "Npnts" will vary with the behavior of F(z)  It's *
C*    recommended that for large "HITE" and large "Npnts" one not use  *
C*    a small "ERROR".  Then, it saves time to do two call sequences.  *
C***********************************************************************
      COMPLEX*16 ZEROS(10),CENTR,dSIDE(4),CORNER(4),
     +           CENTER(24),INTGRL(24,0:8),INSIDE(24,5),
     +           Zcornr,Zend,F,Fz1,Fz2,Fsum,SUM,WIND
      INTEGER    ORDER(10),QDRNTS(24),SIDE,HALF,WINDno,CROSS,QUAD,
     +           start,end
      REAL*8     RADII(10),HEIGHT(24),HITE,ERROR,delta
```

```
      EXTERNAL F

      dSIDE(1)  = ( 0.0D0,-1.0D0)
      dSIDE(2)  = (-1.0D0, 0.0D0)
      dSIDE(3)  = ( 0.0D0, 1.0D0)
      dSIDE(4)  = ( 1.0D0, 0.0D0)

      CORNER(1) = ( 1.0D0, 1.0D0)
      CORNER(2) = ( 1.0D0,-1.0D0)
      CORNER(3) = (-1.0D0,-1.0D0)
      CORNER(4) = (-1.0D0, 1.0D0)

      Nsplit = 0
      Nzero  = 0
      CENTER(1) = CENTR
      HEIGHT(1) = HITE


 1    Nsplit = Nsplit+1
      delta  = HEIGHT(Nsplit)/Npnts


      DO 103 SIDE=1,4
         Zcornr = CENTER(Nsplit)+HEIGHT(Nsplit)*CORNER(SIDE)
         Fz2    = F(Zcornr)
         IF (ABS(Fz2) .EQ. 0.0D0)
     +      CALL EXACT(Zcornr)
         DO 102 HALF=1,2
            SUM   = (0.0D0,0.0D0)
            start = 1+(HALF-1)*Npnts
            end   = HALF*Npnts
            DO 101 LOOPS=start,end
               Fz1  = Fz2
               Fz2  = F(Zcornr+LOOPS*delta*dSIDE(SIDE))
               Fsum = Fz1+Fz2
               IF (ABS(Fz2) .EQ. 0.0D0)
     +            CALL EXACT(Zcornr+LOOPS*delta*dSIDE(SIDE))
               IF (ABS(Fsum) .EQ. 0.0D0)
     +         CALL BETWN(Zcornr+(LOOPS-0.5)*delta*dSIDE(SIDE),Fsum)
               SUM = SUM + Fz1/Fsum
 101        CONTINUE
            INTGRL(Nsplit,(SIDE-1)*2+HALF) = 2*(Npnts-2*SUM)
 102     CONTINUE
 103  CONTINUE
      INTGRL(Nsplit,0) = INTGRL(Nsplit,8)


      WIND = (0.0D0,0.0D0)
      DO 200 LOOPS=1,8
           WIND = WIND+INTGRL(Nsplit,LOOPS)/(0.0D0,-6.283185308D0)
 200  CONTINUE
      WINDno = NINT(REAL(WIND))

      IF (WINDno .EQ. 0) GO TO 6
```

```
      WRITE (1,10) Nsplit,WIND,CENTER(Nsplit),HEIGHT(NSPLIT)*.5
   10 FORMAT(5X,/,X,I4,'  *****',2F11.5,'  *****',2F11.5,E12.5)

      IF (HEIGHT(Nsplit) .LE. ERROR) GO TO 3


      DO 302 CROSS=1,4
         Zend = CENTER(Nsplit)-HEIGHT(Nsplit)*dSIDE(CROSS)
         Fz2  = F(Zend)
         IF (ABS(Fz2) .EQ. 0.0D0)
     +      CALL EXACT(Zend)
         SUM  = (0.0D0,0.0D0)
         DO 301 LOOPS=1,Npnts
            Fz1  = Fz2
            Fz2  = F(Zend+LOOPS*delta*dSIDE(CROSS))
            Fsum = Fz1+Fz2
            IF (ABS(Fz2) .EQ. 0.0D0)
     +         CALL EXACT(Zend+LOOPS*delta*dSIDE(CROSS))
            IF (ABS(Fsum) .EQ. 0.0D0)
     +         CALL BETWN(Zend+(LOOPS-0.5)*delta*dSIDE(CROSS),Fsum)
            SUM = SUM + Fz1/Fsum
 301     CONTINUE
         INSIDE(Nsplit,CROSS) = (2.D0,0.D0)*(Npnts-(2.D0,0.D0)*SUM)
 302  CONTINUE
      INSIDE(Nsplit,5) = INSIDE(Nsplit,1)

      QUAD = 0
2        QUAD = QUAD+1
         QDRNTS(Nsplit)    = QUAD
         HEIGHT(Nsplit+1)  = HEIGHT(Nsplit)/2.0D0
         CENTER(Nsplit+1)  = CENTER(Nsplit)+HEIGHT(Nsplit+1)*CORNER(QUAD)
         WIND = (INTGRL(Nsplit,2*QUAD-2)+INTGRL(Nsplit,2*QUAD-1)
     +           -INSIDE(Nsplit,QUAD)+INSIDE(Nsplit,QUAD+1))
     +           /(0.0D0,-6.283185308D0)
         WINDno = NINT(REAL(WIND))


         WRITE (1,20) QUAD,WIND,WINDNO,CENTER(NSPLIT+1)
   20    FORMAT(6X,I4,2X,2F11.5,X,I4,2X,2F11.5)


         IF (WINDno .EQ. 0) GO TO 5

         IF (HEIGHT(Nsplit+1) .GT. ERROR) GO TO 1

3              WRITE (1,30)
   30          FORMAT(5X,///)
               Nzero  = Nzero+1
               ZEROS(Nzero) = CENTER(Nsplit+1)
               RADII(Nzero) = HEIGHT(Nsplit+1)
               ORDER(Nzero) = WINDno
4        QUAD = QDRNTS(Nsplit)

5        IF (QUAD.LT.4) GO TO 2
```

```
 6    Nsplit = Nsplit-1
      IF (Nsplit .NE. 0) GO TO 4
      RETURN
      END



      SUBROUTINE BETWN(z,Fsum)

      COMPLEX*16 z,F,Fsum,Fnew

      WRITE (1,10) z
   10 FORMAT(' BETWEEN two points at',2E21.14,'  the function was zero')

      Fnew = (2.0D0,0.0D0)*F(Z,m,X)
      IF (ABS(Fnew) .EQ. 0.0D0) THEN
         WRITE (1,20)
   20    FORMAT(' and it was also zero AT THAT POINT !!')
         STOP 06
      ELSE
        Fsum = Fnew
        RETURN
      ENDIF

      END



      SUBROUTINE EXACT(z)

      COMPLEX*16 z

      WRITE (1,10) z
   10 FORMAT(' WE HIT A POINT WHERE THE FUNCTION IS EXACTLY ZERO',
     +       /,2E21.14)
      STOP 07
      END

      COMPLEX*16 FUNCTION F(NU)
      COMPLEX*16 X,XL,XT,EXPO,J,Y,JP,YP,JL,JLP,YL,YLP,JT,JTP,YT,YTP,
     +           JLP1,JLPP1,YLP1,YLPP1,JTP1,JTPP1,YTP1,YTPP1,NU,NUP1,
     +           D11,D12,D13,D21,D22,D23,D32,D33,JP1,JPP1,YP1,YPP1

      COMPLEX*8 XC,XLC,XTC,JC,JPC,YC,YPC,JLC,JLPC,YLC,YLPC,JTC,JTPC,
     +          YTC,YTPC,JLP1C,JLPP1C,YLP1C,YLPP1C,JTP1C,JTPP1C,YTP1C,
     +          YTPP1C,NUC,NUP1C,JP1C,JPP1C,YP1C,YPP1C


      REAL*4 SJ,SY,SJL,SYL,SJLP1,SYLP1,SJT,SYT,SJTP1,SYTP1,SJP1,SYP1

      REAL*8 DENO,DENI,SPEEDO,SPEEDL,SPEEDT,PI

      COMMON X
```

```
      EXPO=(0.0D0,1.0D0)
      PI=3.141592654

cccccccccccccccccccccccccccccccccccccccccccccccccccccccccccccccccccccccc
C   Set the material parameters of the sphere here.                    C
cccccccccccccccccccccccccccccccccccccccccccccccccccccccccccccccccccccccc

      DENO=1.0
      DENI=13.800
      SPEEDO=1.4760
      SPEEDL=6.860
      SPEEDT=4.185


      NU=NU+(.5D0,0.0D0)
      NUP1=NU+(1.0D0,0.0D0)
      NUC=(NU)
      NUP1C=(NUP1)
      XC=(X)
      XL=X*(SPEEDO/SPEEDL)
      XLC=(XL)
      XT=X*((SPEEDO/SPEEDT))
      XTC=(XT)


      CALL OLVER(NUC,XC,JC,JPC,SJ,YC,YPC,SY)
      CALL OLVER(NUP1C,XC,JP1C,JPP1C,SJP1,YP1C,YPP1C,SYP1)
      CALL OLVER(NUC,XLC,JLC,JLPC,SJL,YLC,YLPC,SYL)
      CALL OLVER(NUP1C,XLC,JLP1C,JLPP1C,SJLP1,YLP1C,YLPP1C,SYLP1)
      CALL OLVER(NUC,XTC,JTC,JTPC,SJT,YTC,YTPC,SYT)
      CALL OLVER(NUP1C,XTC,JTP1C,JTPP1C,SJTP1,YTP1C,YTPP1C,SYTP1)


      J=(JC*EXP(SJ))
      Y=(YC*EXP(SY))
      JP1=(JP1C*EXP(SJP1))
      YP1=(YP1C*EXP(SYP1))
      JL=(JLC*EXP(SJL))
      YL=(YLC*EXP(SYL))
      JLP1=(JLP1C*EXP(SJLP1))
      YLP1=(YLP1C*EXP(SYLP1))
      JT=(JTC*EXP(SJT))
      YT=(YTC*EXP(SYT))
      JTP1=(JTP1C*EXP(SJTP1))
      YTP1=(YTP1C*EXP(SYTP1))

cccccccccccccccccccccccccccccccccccccccccccccccccccccccccccccccccccccccc
C      The elements below are given in appendix A of chapter 3.     C
C      They are the elements of Dn.                                 C
cccccccccccccccccccccccccccccccccccccccccccccccccccccccccccccccccccccccc

      D11=((DENO*SPEEDO**2.)/(DENI*SPEEDT**2.))*(X**2.)
      D11=D11*CSQRT(PI/(2.*X))*(J+EXPO*Y)
```

```
      NU=NU*(.5D0,0.0D0)
      D12=(2.*NU*(NU+1.)-XT**2.)*JL-4.*(NU*JL-XL*JLP1)
      D12=D12*CSQRT(PI/(2.*XL))

      D13=2.*NU*(NU+1.)*CSQRT(PI/(2.*XT))
      D13=D13*((NU-1.)*JT-XT*JTP1)

      D21=CSQRT(PI/(2.*X))
      D21=D21*(X*(JP1+EXPO*YP1)-NU*(J+EXPO*Y))

      D22=CSQRT(PI/(2.*XL))*(NU*JL-XL*JLP1)

      D23=NU*(NU+1.)*CSQRT(PI/(2.*XT))*JT

      D32=2.*CSQRT(PI/(2.*XL))*((1.-NU)*JL+XL*JLP1)

      D33=2.*CSQRT(PI/(2.*XT))*(NU*JT-XT*JTP1)
      D33=D33+CSQRT(PI/(2.*XT))*(XT**2.-2.*NU*(NU+1)+2.)*JT

      F=D11*D22*D33-D11*D32*D23-D21*D12*D33+D21*D32*D13



      RETURN
      END
```

SLOPE3

This program generates a polynomial curve fit. It fits input data to a polynomial of up to and including order 5. The program was obtained from the Shock Dynamics Laboratory of Washington State University. It is based in part on subroutine LSQF1T obtained from the Stanford Accelerator Center by P. Marston.

The program was used to fit discrete values of the phase velocity, group velocity, and attenuation of the Rayleigh and slowest whispering gallery waves on tungsten carbide spheres. Polynomial expressions were obtained for these parameters as a function of the ka of the sphere (cf. Chapters 2 and 3). It was also used to curve fit discrete data for the coupling parameter G_{WG1} discussed in Chapter 3 and later in the appendix for the program WS.

The program is not listed here since polynomial fit programs are common. If the reader wishes a copy of the program he should request a copy of internal report SDL 78-02 from the Shock Dynamics Laboratory of Washington State University.

WS

This program calculates the SWT approximation for the magnitude of the backscattering form function of a tungsten carbide sphere. It outputs the ka value and the form function magnitude for that ka in the range $10 \leq ka \leq 80$. As it is given here the program results can be plotted to give f_{SRWG} of Chapter 4. This again offers a check that the program has been entered properly. By changing the ℓ do loop limits to $\ell = 1,1$ one can obtain f_{SR} of Chapter 4. By adding write statements one can generate numbers for plotting the coupling parameters G_ℓ and the backscattering amplitudes used in Fig. 8 of Chapter 3 or Fig. 2 of Chapter 4.

A comment is important on the way the program calculates the coupling parameters G_R and G_{WG1} of Chapter 4. The G_R is calculated using the curve fit results for the phase velocity and attenuation of the Rayleigh wave resulting from using the program SLOPE3. This was adequate for the Rayleigh wave but when done for the whispering gallery wave WG1 it was inaccurate. This was because those results were much more sensitive to small errors in the values of the phase velocity. Therefore, for the whispering gallery waves WS was first altered so that instead of a do loop over i and ℓ one just entered results for the ka of the sphere and the SWT pole location ν_{WG1} from program ZNU and outputed an "exact" value for G_{WG1}. This was done for 20 values of ka then a complex curve fit for G_{WG1} using the program SLOPE3 was generated. This curve-fit result is used in WS. In retrospect the method for obtaining G_{WG1} is more efficient from the standpoint of computer run time then the current method for calculating G_R within WS. From the standpoint of accuracy, however, G_R was calculated both ways and was found to give the same results so the program was not altered.

The subroutine BD of this program calls the subroutine OLVER given next in this appendix. To do other isotropic spheres one must use ZNU and SLOPE3 to generate the appropriate curve fits for phase velocity, attenuation, and coupling parameters and alter WS accordingly.

```
cccccccccccccc
c            c
c    WS      c
c            c
cccccccccccccc

cccccccccccccccccccccccccccccccccccccccccccccccccccccccccccccccccccccccc
c                                                                      c
c    This program calculates an approximate form function for a        c
c  tungsten carbide sphere using sommerfeld-watson theory.It           c
c  appropriately includes the specular reflection,Rayleigh wave,       c
c  and slowest whispering gallery wave.By including further write      c
c  statements one can get the coupling coefficients for the surface c
c  waves as well as the waves amplitudes each time they circum-        c
c  navigate the sphere.One thing to note is that the coupling          c
c  coefficient is calculted differently for the Rayleigh and           c
c  whispering gallery wave.The Rayleigh calculation uses curve fits c
c  of the wave speed and attenuation to find the coupling coeffi-      c
c  cient .This procedure was not accurate enough for the whisper-      c
c  ing gallery wave so the exact result for the coupling coeffi-       c
c  cient was calculated at several ka values and then these results c
c  were curve fit to give continuous values.                           c
c     The subroutine BD of this program uses the subroutine OLVER      c
c  which is given elsewhere in this appendix.                          c
c                                                                      c
cccccccccccccccccccccccccccccccccccccccccccccccccccccccccccccccccccccccc

      dimension fabs(1000),kam(1000),cupla(1000,2),speca(1000)
      dimension fabst(1000)
      real*4 vel,svel,lvel,theta,beta,thetm,thetp,dens,denl,dum,
     &       ray1,ray2,ray3,ray4,kam,fabs,ka,rvel,aspec,betp,betm
     &       ,fabst
      complex*8 nu,dminus,dplus,phase1,phase2,x,xs,xl,num,nup,
     &          ddplus,dplusm,dplusp,cn,sn,couple,decay1,decay2,
     &          spec,cthetm,cthetp,ctheta,cfabs,cupl,cupla,speca

      pi=3.141592654
      lud=1

cccccccccccccccccccccccccccccccccccccccccccccccccccccccccccccccccccccccc
c Set material parameters for the sphere.These parameters are same as  c
c those used by Gaunaurd in JASA Jan. 1983.                            c
cccccccccccccccccccccccccccccccccccccccccccccccccccccccccccccccccccccccc

      numb=1000
      vel=1.4760
      svel=4.185
      lvel=6.860
      dens=13.8
      denl=1.0
      a=12.7

cccccccccccccccccccccccccccccccccccccccccccccccccccccccccccccccccccccccc
c The i do loop calculates the required Sommerfeld-Watson theory (SWT) c
c results for a particular surface wave for a range of ka.The l do     c
c loop selects the particular surface wave;l=1 for the Rayleigh wave,  c
```

```
c l=2 for the whispering gallery wave.                                  c
cccccccccccccccccccccccccccccccccccccccccccccccccccccccccccccccccccccccc

      do 301 l=1,2
      do 100 i=1,numb

cccccccccccccccccccccccccccccccccccccccccccccccccccccccccccccccccccccccc
c    This part of the loop calculates surface wave speeds and atten-    c
c    uations.The calculations use results of a program which curve      c
c    fits data to a polynomial of up to (ka)**5.                        c
cccccccccccccccccccccccccccccccccccccccccccccccccccccccccccccccccccccccc

              ka=10.+((i-1)*70.)/numb
              kam(i)=ka
              x=cmplx(ka,0.0)
              if (l.eq.2) go to 211
              beta=.0322154+.210487e-2*ka
              rvel=3.40415-.249972e-1*ka+.331109e-3*ka**2
     &              -.157333e-5*ka**3
              go to 213
 211         beta=.246128e-1-.306817e-2*ka+.123060e-3*ka**2
     &              -.166263e-5*ka**3+.752955e-8*ka**4
 423          if (ka .lt. 45.2) go to 417
              rvel=5.480848912*exp(-.00437092*ka)
              go to 213
 417          if (ka .lt. 29.0) go to 418
              rvel=5.498195789*exp(-.00428319*ka)
              go to 213
 418          rvel=5.51968062*exp(-.00447460*ka)
              go to 213
 211          continue

cccccccccccccccccccccccccccccccccccccccccccccccccccccccccccccccccccccccc
c  This section calculates the coupling coeffcients for the surface    c
c  wave.Note again that the coupling coefficient is calculated diff-   c
c  erently for the two surface waves.In retrospect it is probably      c
c  more efficient to calculate exact results for the coupling coeff-   c
c  icients at several ka values and then curve fit those results.This  c
c  assures accuracy and decreases computer run time.The Rayleigh       c
c  calculation was done both ways and the same accuracy was found      c
c  but this is not generally found to be the case.Showing the two      c
c  different methods here allows a comparison of techniques.In any     c
c  case one still needs the curve fits for the surface wave speeds     c
c  and attenuations given above for further calculation.               c
cccccccccccccccccccccccccccccccccccccccccccccccccccccccccccccccccccccccc

              dum=ka*vel/svel
              xs=cmplx(dum,0.0)
              dum=ka*vel/lvel
              xl=cmplx(dum,0.0)

              div=1000.
              theta=asin(1./rvel)
              thetm=theta-theta/div
              thetp=theta+theta/div
```

```
            if (l .eq. 2) go to 707
            dum=ka*sin(theta)-.5
            nu=cmplx(dum,beta)
            dum=ka*sin(thetm)-.5
            num=cmplx(dum,beta)
            dum=ka*sin(thetp)-.5
            nup=cmplx(dum,beta)

            call bd(x,xs,xl,num,dens,denl,dminus,dplusm)
            call bd(x,xs,xl,nup,dens,denl,dminus,dplusp)
            call bd(x,xs,xl,nu,dens,denl,dminus,dplus)


            ddplus=(dplusp-dplusm)/(nup-num)

  707       continue
            if (l.eq.2) go to 703
            couple=(4.*pi*cmplx(0.0,1.0)*(nu+.5)*dminus)/(ddplus*ka)
            go to 704
  703       dum1=-.132352+.644651e-2*ka-.353597e-4*ka**2
            dum2=.021110-.844136e-3*ka+.672282e-5*ka**2
            couple=cmplx(dum1,dum2)

cccccccccccccccccccccccccccccccccccccccccccccccccccccccccccccccccccccccc
c  The exponenial decay and propagation phase shifts are calculated    c
c  here using the appropriate curve fits.                              c
cccccccccccccccccccccccccccccccccccccccccccccccccccccccccccccccccccccccc

  704       dum=exp((2.*pi-2.*theta)*(-1.)*beta)
            decay1=cmplx(dum,0.0)
            dum=exp((-1.)*2.*pi*beta)
            decay2=cmplx(dum,0.0)

            a1=cos(2.*ka*(1.-cos(theta))+ka*sin(theta)*
     &         (2.*pi-2.*theta)-pi/2.0)
            a2=sin(2.*ka*(1.-cos(theta))+ka*sin(theta)*
     &         (2.*pi-2.*theta)-pi/2.0)
            phase1=cmplx(a1,a2)

            a1=cos(2.*pi*ka*sin(theta)-pi)
            a2=sin(2.*pi*ka*sin(theta)-pi)
            phase2=cmplx(a1,a2)

cccccccccccccccccccccccccccccccccccccccccccccccccccccccccccccccccccccccc
c  The specular reflection is calculated at this point.                c
cccccccccccccccccccccccccccccccccccccccccccccccccccccccccccccccccccccccc

            nu=cmplx(-.5,0.0)
            call refl(x,xs,xl,nu,dens,denl,dminus,dplus)
            spec=dminus/dplus
            speca(i)=spec
            aspec=cabs(spec)

cccccccccccccccccccccccccccccccccccccccccccccccccccccccccccccccccccccccc
c  The SWT terms for the surface wave contributions to the form        c
c  function are calculated using the results above.                    c
```

```
cccccccccccccccccccccccccccccccccccccccccccccccccccccccccccccccccccccccc

              cupl=phase1*decay1*couple/(1.-decay2*phase2)
              cupla(i,1)=cupl


 100          continue
 301          continue

cccccccccccccccccccccccccccccccccccccccccccccccccccccccccccccccccccccccc
c    The approximate form function is calculated.Since the SWT       c
c  results for the whispering gallery wave are not accurate below    c
c  ka=21 its contribution is not included for 10<ka<21.              c
cccccccccccccccccccccccccccccccccccccccccccccccccccccccccccccccccccccccc

      do 302 i=1,numb
              if (kam(i) .lt. 21.0) go to 303
              fabst(i)=cabs(speca(i)+cupla(i,1)+cupla(i,2))
              go to 304
 303          fabst(i)=cabs(speca(i)+cupla(i,1))
 304          write(lud,315) kam(i),fabst(i)
 315          format(3x,3f12.5)
 302          continue

              end
```

```
cccccccccccccccccccccccccccccccccccccccccccccccccccccccccccccccccccccccccccc
c The subroutine bd calculates the D- and D+ of the SWT.It uses the      c
c subroutine olver which can calculate bessel functions of complex       c
c order and arguement.                                                   c
cccccccccccccccccccccccccccccccccccccccccccccccccccccccccccccccccccccccccccc

      subroutine bd(x,xs,xl,nu,dens,denl,dm,dp)

          complex*8 x,xs,xl,dm,dp,r1,r2,rs,rl,nu,e2,es2,el2,z,
     &              ai,aip,cdum,j,jp,y,yp
          real*4  dens,denl,kas,r,s,kal,dum,sj,sy

           e2=(nu+.5)
           call olver(e2,x,j,jp,sj,y,yp,sy)
           jp=jp*exp(sj)
           j=j*exp(sj)
           yp=yp*exp(sy)
           y=y*exp(sy)
           r1=(jp+cmplx(0.0,1.0)*yp)/(j+cmplx(0.0,1.0)*y)-(2.*x)**(-1.)
           r2=(jp-cmplx(0.0,1.0)*yp)/(j-cmplx(0.0,1.0)*y)-(2.*x)**(-1.)
           call olver(e2,xs,j,jp,sj,y,yp,sy)
           j=j*exp(sj)
           jp=jp*exp(sj)
           rs=jp/j-(2.*xs)**(-1)
           call olver(e2,xl,j,jp,sj,y,yp,sy)
           j=j*exp(sj)
           jp=jp*exp(sj)
           rl=jp/j-(2.*xl)**(-1)



           dm=(denl/dens)*xs*xs*((xl*rl)*(2.*xs*rs+(xs*xs-2.*nu*
     &        (nu+1.)+2.))-(2.*(1.-xl*rl)*nu*(nu+1.)))
           dm=dm+x*r2*(((2.*nu*(nu+1.)-xs*xs)-4.*xl*rl)*(2.*xs*rs+
     &        (xs*xs-2.*nu*(nu+1.)+2.))-(2.*(1.-xl*rl))*(2.*nu*
     &        (nu+1.)*(xs*rs-1.)))

           dp=(denl/dens)*xs*xs*((xl*rl)*(2.*xs*rs+(xs*xs-2.*nu*
     &        (nu+1.)+2.))-(2.*(1.-xl*rl)*nu*(nu+1.)))
           dp=dp+x*rl*(((2.*nu*(nu+1.)-xs*xs)-4.*xl*rl)*(2.*xs*rs+
     &        (xs*xs-2.*nu*(nu+1.)+2.))-(2.*(1.-xl*rl))*(2.*nu*
     &        (nu+1.)*(xs*rs-1.)))

            return
            end

cccccccccccccccccccccccccccccccccccccccccccccccccccccccccccccccccccccccccccc
c The subroutine refl calculates the reflection coefficient from the     c
c front of the sphere.It does not use olver since olver is not accur-    c
c ate for order of less then 3 and for backscattering we need answers    c
c for order 0.This subroutine uses large arguement expansions for        c
c the bessel and hankel functions and neglects terms of O(ka**-2).       c
cccccccccccccccccccccccccccccccccccccccccccccccccccccccccccccccccccccccccccc

      subroutine refl(x,xs,xl,nu,dens,denl,dm,dp)
```

```
      complex*8 x,xs,xl,nu,dm,dp,z2,zl,z2s,z2l,b22,a22,
     &          e2,es2,el2,j,jp,y,yp
      real*4 dens,denl,sj,sy


      e2=(nu+.5)*(nu+.5)/(x*x)
      es2=(nu+.5)*(nu+.5)/(xs*xs)
      el2=(nu+.5)*(nu+.5)/(xl*xl)

      z2=x*(cmplx(0.,-1.)*sqrt(1.-e2)-(2.-e2)/(2.*x*
     &   (1.0-e2)))
      zl=x*(cmplx(0.,1.)*sqrt(1.-e2)-(2.-e2)/(2.*x*
     &    (1.0-e2)))
      z2s=xs*(cmplx(0.,-1.)*sqrt(1.-es2)-(2.-es2)/
     &      (2.*xs*(1.-es2)))
      z2l=xl*(cmplx(0.,-1.)*sqrt(1.-el2)-(2.-el2)/
     &      (2.*xl*(1.-el2)))


      a22=z2l*(1./4.+1./(2.*xs*xs)+z2s/(2.*xs*xs))
     &      -nu*(nu+1.)/(2.*xs*xs)
      b22=(-1./4.-1./(2.*xs*xs)+(nu+1.)*nu/(xs*xs))+
     &      (2.*nu*(nu+1.)/(xs*xs*xs*xs))-
     &      nu*nu*(nu+1.)*(nu+1.)/(xs*xs*xs*xs)
      b22=b22-
     &      z2s/(2.*xs*xs)+(nu*(nu+1.)/(xs*xs*xs*xs)
     &      -1./(xs*xs)-2./(xs*xs*xs*xs))*z2l
     &      +(nu*(nu+1.)/(xs*xs*xs*xs)-2./(xs*xs*xs*xs))
     &      *z2s*z2l

      dm=z2*b22+(denl/dens)*a22
      dp=zl*b22+(denl/dens)*a22

      return
      end
```

OLVER

This program calculates Bessel functions of the first and second kind $J_\nu(x)$ and $N_\nu(x)$ as well as their derivatives with respect to x for complex order ν and argument x. The program was obtained from J. A. Cochran of the Department of Mathematics at Washington State University. The program is asserted to have an error of less than (0.00001 + i0.00001) wherever $|\nu| \geq 3$ and $x/\nu \geq 10^{-6}$. There are some comments in Chapters 3 and 4 on the program as well as a reference to earlier work on the numerical computation of Bessel functions by Cochran et al. (Ref. 22 of Chapter 2). Much more extensive comments can be found in the Master degree paper (Ref. 21 of Chapter 2) by Brad Brim.

OLVER makes a decision of whether to scale the values of $J_\nu(x)$ and $J'_\nu(x)$ by exp(jscale) and the values of $N_\nu(x)$ and $N'_\nu(x)$ by exp(yscale) for convenient output. In the programs ZNU, ZKA, and WS the scale factors are included in all calculations. If one desires to use OLVER for other work the programs should be checked to see how to include the scale factors.

```
cccccccccccccccccc
c                c
c    OLVER       c
c                c
cccccccccccccccccc

      subroutine olver(argnu,argw,j,jprime,jscale,y,yprime,yscale)

c*********************************************************************
c*    large order routine to generate bessel functions of first and  *
c*    second kinds and their derivatives for complex values of order *
c*    argnu and argument argw.written by e.j.murphy 1970/71,revised  *
c*    by j.a. cochran 1/72, revised by e.r. kamgnia 7/1977.          *
c*********************************************************************

      common /info/ uc,vc,ac,bc,a,b,c,d,cos120,cos30,third

      complex*8  argnu,argw,j,jprime,y,yprime
      complex*16 w,nu,nuto13,nuto23,nuto43,nuto2,nuto4,nu23xz,
     +           a(6,2),b(6,2),c(6,2),d(6,2),ar(2),br(2),cr(2),dr(2),
     +           u(5),v(5),asum,bsum,csum,dsum,
     +           z,zeta,zeta12,ztam32,phiofz,tauinv,t1,t2,t3,t4,
     +           ai,aip,bi,bip,ai1,ai1p,ai2,ai2p,
     +           cos120,cos30,
     +           x,t,term1,term2
      real*8     uc(14),vc(14),ac(5),bc(5),theta,third,s1,s2,s3,
     +           realnu,imagnu,magnu
      real*4     jscale,yscale


c*********************************************************************
c*    initialization                                                 *
c*********************************************************************

      jscale = 0.0
      yscale = 0.0
      w      = argw
      nu     = argnu
      realnu =  real(nu)
      imagnu = imag(nu)

      z      = w/nu
      theta  = third*datan2(imagnu,realnu)
      magnu  = abs(nu)
      nuto13 = (magnu**third)*cmplx(dcos(theta),dsin(theta))
      nuto23 = nuto13*nuto13
      nuto43 = nuto23*nuto23
      nuto2  = nu*nu
      nuto4  = nuto2*nuto2
      nterms = 1
      if (magnu .lt. 25.0d0)  nterms = 2
```

```
c*********************************************************************
c*    compute   zeta                                                 *
c*********************************************************************

      call szeta(z,zeta12,phiofz,tauinv)

      zeta   = zeta12*zeta12


c*********************************************************************
c*    the magnitude of  z  determines how we compute ar,br,cr,dr     *
c*********************************************************************

      if (abs(z-1.d0) .gt. 0.1d0)  then

c     ******************************************************************
c     *    compute   ar,br,cr,dr  in the normal way                 *****
c     ******************************************************************
          t1     = (1.d0,0.d0)/tauinv
          t2     = t1*t1
          t      =  t2
          u(1)   = (1.d0,0.d0)
          v(1)   = (1.d0,0.d0)
          u(2)   = t1*(uc(1)-uc(2)*t)
          v(2)   =-t1*(vc(1)-vc(2)*t)
          u(3)   = t2*(uc(3)-t*(uc(4)-t*uc(5)))
          v(3)   =-t2*(vc(3)-t*(vc(4)-t*vc(5)))
          if (nterms .eq. 2)  then
            t3   = t1*t2
            t4   = t2*t2
            u(4) = t3*(uc(6)-t*(uc(7)-t*(uc(8)-t*uc(9))))
            v(4) =-t3*(vc(6)-t*(vc(7)-t*(vc(8)-t*vc(9))))
            u(5) = t4*(uc(10)-t*(uc(11)-t*(uc(12)-t*(uc(13)-t*uc(14)))))
            v(5) =-t4*(vc(10)-t*(vc(11)-t*(vc(12)-t*(vc(13)-t*vc(14)))))
          end if
          ztam32 = (1.0d0,0.0d0)/(zeta*zeta12)
          do 8 i=1,nterms
               ar(i) = (0.0d0,0.0d0)
               br(i) = (0.0d0,0.0d0)
               cr(i) = (0.0d0,0.0d0)
               dr(i) = (0.0d0,0.0d0)
               term1 = (1.0d0,0.0d0)
               term2 = (1.0d0,0.0d0)/zeta12
               do 6 k=1,2*i+1
                    l      = 2*(i+1)-k
                    ar(i) = ar(i)+bc(k)*u(l)*term1
                    dr(i) = dr(i)+ac(k)*v(l)*term1
                    term1 = term1*ztam32
  6            continue
               do 7 k=1,2*i
                    l      = 2*i+1-k
                    br(i) = br(i)-ac(k)*u(l)*term2
                    cr(i) = cr(i)-bc(k)*v(l)*term2
```

```
                    term2 = term2*ztam32
  7             continue
                cr(i) = cr(i)*zeta
  8         continue

        else

c       ******************************************************************
c       *    compute   ar,br,cr,& dr   by power series                 *****
c       ******************************************************************
            do 11 i=1,nterms
                ar(i)=a(6,i)
                br(i)=b(6,i)
                cr(i)=c(6,i)
                dr(i)=d(6,i)
                do 10 l=5,1,-1
                    ar(i)=ar(i)*zeta+a(l,i)
                    br(i)=br(i)*zeta+b(l,i)
                    cr(i)=cr(i)*zeta+c(l,i)
                    dr(i)=dr(i)*zeta+d(l,i)
  10            continue
  11        continue

        end if


c*********************************************************************
c*    compute airy functions                                         *
c*********************************************************************

        nu23xz = nuto23*zeta

        x = nu23xz
        call airy(x,ai,aip,s3)

        x = cos120*nu23xz
        call airy(x,ai1,ai1p,s1)

        x = conjg(cos120)*nu23xz
        call airy(x,ai2,ai2p,s2)


c*********************************************************************
c*    scaling                                                        *
c*********************************************************************

        s1     = s1-s2
        jscale =  s3
        yscale =  s2

        if (dabs(s1) .gt. 170.0d0) then

            if (s1 .gt. 0.0d0) then
                yscale = yscale+s1
```

```
            ai2     = (0.0d0,0.0d0)
            ai2p    = (0.0d0,0.0d0)
        else
            ail     = (0.0d0,0.0d0)
            ailp    = (0.0d0,0.0d0)
        endif

    else

        ail  =  ail*dexp(s1)
        ailp = ailp*dexp(s1)

    endif

    bi  =   cos30*ail+conjg(cos30)*ai2
    bip = -(conjg(cos30)*ailp+cos30*ai2p)


c*****************************************************************
c*    compute   a,b,c,& d  sums                                  *
c*****************************************************************

    asum  = (1.0d0,0.0d0) + ar(1)/nuto2
    bsum  = br(1)
    csum  = cr(1)
    dsum  = (1.0d0,0.0d0) + dr(1)/nuto2

    if (nterms .eq. 2)  then
      asum  = asum+ar(2)/nuto4
      bsum  = bsum+br(2)/nuto2
      csum  = csum+cr(1)/nuto2
      dsum  = dsum+dr(2)/nuto4
    endif


c*****************************************************************
c*    form    j,y,jprime,yprime    & then return the results    *
c*****************************************************************

    term1  = bsum/nuto43
    term2  = phiofz/nuto13
    j      = term2*(aip*term1+ai*asum)
    y      =-term2*(bip*term1+bi*asum)

    term1  = (2.d0,0.d0)/nuto23/z/phiofz
    term2  = csum/nuto23
    jprime =-term1*(ai*term2+aip*dsum)
    yprime = term1*(bi*term2+bip*dsum)


    return
    end
```

```
      subroutine szeta(z,zeta,phiz,r)
c ***
c *** double precision complex calculation of sqrt(zeta),phi(zeta),
c *** and sqrt(1-z*z).
c ***
      complex*16 z,zeta,phiz,r
      double precision pi2,al3,zr,zi,zm,az,argz
      data pi2/6.283185307179586d0/,al3/.3333333333333333d0/
      zr=z
      zi=(0.d0,-1.d0)*z
      if(zi.ne.0.d0) go to 1
      if(zr.eq.1.d0) go to 6
      if(zr.gt.1.1d0) go to 5
c ***
c *** z is not real or is real < 1.1
c ***
  1   r=sqrt(1.d0-z*z)
      if (real(r) .lt. 0.0d0) r = -r
      argz=datan2(zi,zr)
c ***
c *** compute zeta**1.5
c ***
      zeta=1.5d0*(log((1.d0+r)/z)-r)
      zm=abs(zeta)
      if(zm.le.1.d-12) go to 6
c ***
c *** place zeta**1.5 in the proper quadrant
c ***
      zr=zeta
      zi=(0.d0,-1.d0)*zeta
      az=datan2(zi,zr)
      if(zr.gt.0.d0) go to 4
      if(zi.le.0.d0) go to 3
      if(argz.lt.0.d0) go to 4
      az=az-pi2
      go to 4
```

```
  3   if(argz.gt.0.d0) go to 4
      az=az+pi2
c ***
c *** compute sqrt(zeta)
c ***
  4   az=az*al3
      zeta=(zm**al3)*cmplx(dcos(az),dsin(az))
c ***
c *** compute phi(zeta)
c ***
  2   phiz=sqrt(2.d0*zeta/r)
      if (real(phiz) .lt. 0.0d0) phiz = -phiz
      return
c ***
c *** z is real and >1.1
c ***
  5   zi=dsqrt(zr*zr-1.d0)
      r=cmplx(0.d0,-zi)
c ***
c *** compute zeta**1.5
c ***
      zm=dabs(1.5d0*(datan(zi)-zi))
      zeta=cmplx(0.d0,-zm**al3)
      go to 2
c ***
c *** zeta=0
c ***
  6   phiz=(1.2599210499d0,0.d0)
      zeta=(0.d0,0.d0)
      r=(0.d0,0.d0)
      return
      end
c ***
      subroutine airy(x,ai,aip,fexp)
      dimension iexp(2)
      double precision n,c(4,6),rspi,temp,fexp
      complex*16 x,z,f,g,h,l,term1,term2,z2,y(4),a(4),fc(2),t,ai,aip
      data rspi/.5641895835477563d0/,c/
     +1513.439537849732d0,274.0268600980441d0,-1605.281761546393d0,
     +-293.5892410223650d0,
     +54.73651753365000d0,12.08406751643030d0,-58.82238306494943d0,
     +-13.19452747124167d0,
     +3.015237035520228d0,.8518825830603329d0,-3.307648276323637d0,
     +-.9606547181952595d0,
     +.2830348387667181d0,.1109516996742113d0,-.3217286160943928d0,
     +-.1326922046467763d0,
     +.0550974151234568d0,.0355259773662552d0,-.0670090663580247d0,
     +-.0470357510288066d0,
     +.0347222222222222d0,.0694444444444444d0,-.0486111111111111d0,
     +-.0972222222222222d0/
c ***
c *** initialize
c ***
      fexp=0.d0
      z=x
      temp=z*conjg(z)
```

```
      if(temp.gt.25.d0) go to 2
c ***
c *** power series
c ***
      term1=(.3550280538887817d0,0.d0)
      term2=(.2588194037928 07d0,0.d0)
      f=term1
      l=term2
      term2=z*term2
      g=term2
      z2=z*z
      h=(0.d0,0.d0)
      n=1.d0
  1   n=n+1.d0
      term1=z2*term1/n
      h=h+term1
      n=n+1.d0
      term1=z*term1/n
      f=f+term1
      term2=z2*term2/n
      l=l+term2
      n=n+1.d0
      term2=z*term2/n
      g=g+term2
      temp=term1*conjg(term1)
      if(temp.gt.1.d-32) go to 1
      ai=f-g
      aip=h-l
      return
c ***
c *** phase amplitude expansions
c ***
  2   n=1.d0
      if(real(z).gt.0.) go to 3
      n=-1.d0
      z=-z
  3   h=sqrt(z)
      if (real(h) .lt. 0.0d0) h = -h
      l=sqrt(h)
      if (real(l) .lt. 0.0d0) l = -l
      f=z*h
      t=(1.5d0,0.d0)/f
      g=t*t*n
      fc(1)=cmplx(rspi,0.d0)/l
      fc(2)=cmplx(rspi,0.d0)*l
c ***
c *** compute phases and amplitudes
c ***
      do 5 i=1,4
      y(i)=(0.d0,0.d0)
      do 4 j=1,6
      y(i)=g*(y(i)+c(i,j))
  4   continue
      y(i)=y(i)+1.d0
  5   continue
      do 6 i=2,4,2
```

```
      y(i)=y(i)/t
  6   continue
      if(n.gt.0.d0) go to 7
c ***
c *** set values for cosine expansions
c ***
      y(2)=y(2)-(0.785398163397448d0,0.d0)
      y(4)=y(4)+(3.926990816987241d0,0.d0)
      n=1.d0
      go to 9
c ***
c *** set values for exponential expansions
c ***
  7   continue
      do 8 i=2,4,2
      y(i)=-y(i)
  8   continue
      n=2.d0
c ***
c *** form ai and aip
c ***
  9   continue
      do 10 i=2,4,2
      j=i-1
      k=i/2
      call func(n,y(i),f,iexp(k))
      a(k)=y(j)*f*fc(k)/n
  10  continue
      if(iexp(1).eq.0.and.iexp(2).eq.0) go to 11
      fexp=dble(float(iexp(1)))
      a(2)=a(2)*dexp(dble(float(iexp(2)-iexp(1))))
  11  ai=a(1)
      aip=a(2)
      if(n.ne.2.d0) return
      aip=-aip
      return
      end
c ***
      subroutine func(n,z,w,i)
      complex*16 z,w
      double precision n,x,y,r,u,v,textra
      textra=.9210340371976183d1
      if(n.eq.1.d0) go to 2
c ***
c *** calculate exponential
c ***
      i=int(real(z))
      w=exp(z-cmplx(dble(float(i)),0.d0))
      return
c ***
c *** calculate cosine
c ***
  2   x=z
      y=(0.d0,-1.d0)*z
      r=dabs(y)
      i=idint(r)
```

```
      v=dexp(r-dble(float(i)))*.5d0
      if(r.gt.textra) go to 4
      r=dexp(-2.d0*r)
      go to 6
 4    r=0.d0
 6    u=v*(1.d0+r)*dcos(x)
      v=v*(r-1.d0)*dsin(x)
      if(y.lt.0.d0) v=-v
      w=cmplx(u,v)
      return
      end


      block data

      common /info/ uc,vc,ac,bc,a,b,c,d,cos120,cos30,third

      complex*16 w,nu,nuto13,nuto23,nuto43,nuto2,nuto4,nu23xz,
     +           a(6,2),b(6,2),c(6,2),d(6,2),ar(2),br(2),cr(2),dr(2),
     +           u(5),v(5),asum,bsum,csum,dsum,
     +           z,zeta,zeta12,ztam32,phiofz,tauinv,t1,t2,t3,t4,
     +           ai,aip,bi,bip,ai1,ai1p,ai2,ai2p,
     +           cos120,cos30,
     +           x,t,term1,term2
      real*8     uc(14),vc(14),ac(5),bc(5),theta,third,s1,s2,s3,
     +           realnu,imagnu,magnu

      data uc/
     + .1250000000000000d 0, .2083333333333333d 0, .0703125000000000d 0,
     + .4010416666666667d 0, .3342013888888889d 0, .0732421875000000d 0,
     + .8912109375000000d 0, .1846462673611111d+1, .1025812596450617d+1,
     + .1121520996093750d 0, .2364086914062500d+1, .8789123535156248d+1,
     + .1120700261622300d+2, .4669584423426247d+1/

      data vc/
     + .3750000000000000d 0, .2916666666666667d 0, .1171875000000000d 0,
     + .5156250000000000d 0, .3949652777777778d 0, .1025390625000000d 0,
     + .1089257812500000d+1, .2130533854166667d+1, .1146496431327160d+1,
     + .1441955566406250d 0, .2793920898437500d+1, .9961006673177080d+1,
     + .1238668710214120d+2, .5075635242854613d+1/

      data ac/
     + .1000000000000000d+1, .1041666666666667d 0, .8355034722222222d-1,
     + .1282265745563271d 0, .2918490264641404d 0/

      data bc/
     + .1000000000000000d+1,-.1458333333333333d 0,-.9874131944444444d-1,
     +-.1433120539158950d 0,-.3172272026784[illegible] 0/

      data a/
     +(-.4444444643965860d-02, .1420578595950520d-15),
     +(-.1463707789139049d-02, .6540517965151910d-15),
     +( .7064169774714094d-03, .1150547373140440d-13),
     +( .6728874534333555d-03, .4501377701085880d-13),
     +( .1540024288054082d-03,-.1231413828621110d-11),
```

```
     +(-.5766054148891132d-04,-.4537867583220980d-11),
     +( .6937359165991589d-03, .1897333806124500d-12),
     +( .3686593402959254d-03,-.8371533582241440d-11),
     +(-.2698466000992447d-03,-.3102332528113870d-10),
     +(-.3512938924677978d-03, .2412173021438300d-09),
     +(-.1025787226230560d-03, .8114846206597060d-09),
     +( .3103622516889943d-04, .1779089985273050d-07)/

      data b/
     +( .1799887220844051d-01,-.1001796159871510d-16),
     +( .8888889036810635d-02, .6331537179006460d-16),
     +( .1625687328118995d-02, .3210068395633560d-15),
     +(-.3642847477297854d-03, .6316282866674010d-14),
     +(-.3020603907838276d-03, .2654113441221400d-13),
     +(-.5844387298607676d-04,-.6757485415387840d-12),
     +(-.1492829626703820d-02, .2157677521550440d-13),
     +(-.1394063233151223d-02, .8929927363489880d-13),
     +(-.3820961498708859d-03,-.2521380004952490d-11),
     +( .1690971426253441d-03,-.9523018697274750d-11),
     +( .1709979970784747d-03, .7370961265482400d-10),
     +( .4163922946834485d-04, .2503789308434250d-09)/

      data c/
     +( .1587401055816959d 00, .3756978606015920d-17),
     +( .2519842152827235d-01, .1852643775066890d-16),
     +(-.3301586923087801d-02,-.9331802487391570d-16),
     +(-.2356591754094817d-02,-.4468200793264190d-15),
     +(-.8674296486680654d-04,-.8205527812277570d-14),
     +( .2775244443466439d-03,-.3393508378723270d-13),
     +(-.2169219229636311d-02,-.1188771172507000d-14),
     +(-.3443422456221393d-03,-.2858562252390120d-13),
     +( .7803782532232625d-03,-.1035358884288060d-12),
     +( .3813588018215028d-03, .3058429677926410d-11),
     +(-.9395426299457243d-04, .1101306700814700d-10),
     +(-.1503912086220632d-03,-.8649848907871960d-10)/

      data d/
     +( .7301587529520868d-02,-.1444641035652920d-15),
     +( .3328274163318927d-02,-.6647230780883520d-15),
     +(-.2837940464100678d-03,-.1155671802714180d-13),
     +(-.7615127119290934d-03,-.4346463579853540d-13),
     +(-.2390070372062002d-03, .1244342572214570d-11),
     +( .4236746529272183d-04, .4472204080723670d-11),
     +(-.9372997840256660d-03,-.1904932268853110d-11),
     +(-.6275701960924115d-03, .8402555092305780d-12),
     +( .1849038863886771d-03, .3068433182874190d-10),
     +( .3795955396627962d-03,-.2415609997246610d-09),
     +( .1370678212350365d-03,-.7853812708782050d-09),
     +(-.2256873551578751d-04,-.1790520486266400d-07)/

      data cos120/(-.5000000000000000d 00, .8660254037844386d 00)/

      data cos30 /( .8660254037844386d 00, .5000000000000000d 00)/

      data third/ .3333333333333333d 00/
```

```
      end
```

CHIVER

This program calculates the partial wave series solution for the backscattering form function of a tungsten carbide sphere. The program was adapted from one written by R. C. Chiver et al. and referenced in the paper given at the beginning of the program. The program results were checked against those of G. C. Gaunaurd et al. in Ref. 11 of Chapter 3 in the ka region from $1 \leq ka \leq 70$. The form function of other spheres can be calculated by changing the material parameters.

```
CCCCCCCCCCCCCCC
C             C
C   CHIVER    C
C             C
CCCCCCCCCCCCCCC

CCCCCCCCCCCCCCCCCCCCCCCCCCCCCCCCCCCCCCCCCCCCCCCCCCCCCCCCCCCCCCCCCCCCCCCCCCC
C                                                                          C
C THIS PROGRAM CALCULATES FORM FUNCTIONS USING PROGRAMS REFERENCED IN      C
C R.C. CHIVERS AND L.W. ANSON "CALCULATIONS OF THE BACKSCATTERING          C
C AND RADIATION FORCE FUNCTIONS OF SPHERICAL TARGETS FOR USE IN ULTRA-     C
C SONIC BEAM ASSESSMENT."ULTRASONICS,JAN. 1982,PP.25-34.THE PROGRAM        C
C OUTPUTS THE KA OF THE SPHERE AND THE ABSOLUTE VALUE OF THE FORM          C
C FUNCTION AT THAT KA.I FOUND THAT THE PROGRAM REQUIRES HIGH PRECISION     C
C ARITHMETIC OR IT WILL HAVE NUMERICAL DIFFICULTIES.THE PROGRAM ALSO       C
C BECOMES EXPENSIVE IF YOU DESIRE TO GO TO VERY LARGE KA'S (>50).          C
C                                                                          C
CCCCCCCCCCCCCCCCCCCCCCCCCCCCCCCCCCCCCCCCCCCCCCCCCCCCCCCCCCCCCCCCCCCCCCCCCCC
      DIMENSION PB(300),PCB(300),PSB(300),KAM(2000),FABS(2000)
      REAL KAM
      COMPLEX CFAC
CCCCCCCCCCCCCCCCCCCCCCCCCCCCCCCCCCCCCCCCCCCCCCCCCCCCCCCCCCCCCCCCCCCCCCCCCCC
C                                                                          C
C   SET MATERIAL PARAMETERS FOR THE SPHERE.                                C
C                                                                          C
CCCCCCCCCCCCCCCCCCCCCCCCCCCCCCCCCCCCCCCCCCCCCCCCCCCCCCCCCCCCCCCCCCCCCCCCCCC
      DATA RHO,VC,VS /7.7,5960.0,3240.0/
      RH=1.0/(RHO*2.0)
      RAT1=1483.0/VC
      RAT2=1483.0/VS
      WRITE(6,5) RHO,VC,VS
  5   FORMAT(8X,5H RHO=,F6.2,4H C1=,F8.1,4H C2=,F8.1)
      WRITE(6,4)
  4   FORMAT(11X,3H KA,9X,3H /ff/)
      XMAX=50
      X=1.0
      K=0
  10  X=X+0.05
      K=K+1
      T=1.25*X
      X1=RAT1*X
      X2=RAT2*X
      X2S=X2**2
      XSN=SIN(X)
      XCS=COS(X)
      CALL BESS(X,PB,T)
      TERM=(XSN/X)/PB(1)
      BN1=PB(2)*TERM
      CALL BESS(X1,PCB,T)
      CBN1=PCB(2)/PCB(1)
      CALL BESS(X2,PSB,T)
      SNNO=-XCS/X
      XSIGN=1.0
      SBET=0.0
      SALP=0.0
```

```
      N=0
      SUM=0.0
      CALL STVAL(X,X1,X2,ALPN,BETN,CBN1,BN1,SNN1,RH,XSN,X2S,XCS)
   20 CONTINUE
      CBN1=1.0
      CBN2=PCB(N+3)/PCB(N+2)
      Q=FLOAT(N+1)
      ANUM=(Q*CBN1)-(X1*CBN2)
      ADEN=((Q-1.0)*CBN1)-(X1*CBN2)
      DNUM=(((X2S/2.0)-Q*(Q-1.0))*CBN1)-(2.0*X1*CBN2)
      SBN1=1.0
      SBN2=PSB(N+3)/PSB(N+2)
      BNUM=(2.0*Q*(Q+1))*SBN1
      EDEN=(((2.0*(Q**2))-(X2S+2.0))*SBN1)+(2.0*SBN2*X2)
      ENUM=2.0*Q*(Q+1.0)*(((1.0-Q)*SBN1)+(X2*SBN2))
      FN1=X2S*RH*((ANUM/ADEN)-(BNUM/EDEN))/((DNUM/ADEN)
     &-(ENUM/EDEN))
   30 CONTINUE
      BN2=PB(N+3)*TERM
      GN1=((FN1-Q)*BN1)+(X*BN2)
      BN1=BN2
      SNN2=(((2.0*Q)+1.0)*SNN1/X)-SNNO
      HN1=((FN1-Q)*SNN1)+(X*SNN2)
      SNNO=SNN1
      SNN1=SNN2
      DEN=(GN1**2)+(HN1**2)
      ALPN1=-(GN1**2)/DEN
      BETN1=-(GN1*HN1)/DEN
      ADD=Q*(ALPN+ALPN1+(2.0*ALPN*ALPN1)+(2.0*BETN*BETN1))
      FAC=XSIGN*(2.0*Q-1.0)
      SALP=SALP+FAC*ALPN
      SBET=SBET+FAC*BETN
      ALPN=ALPN1
      BETN=BETN1
      SUM=SUM+ADD
      IF ((ABS(ADD/SUM)).LT.1.0E-8) GO TO 90
      J=0
      N=N+1
      XSIGN=-XSIGN
      GO TO 20
   90 J=J+1
      IF (J.EQ.5) GO TO 100
      N=N+1
      XSIGN=-XSIGN
      GO TO 20
  100 YP=(-4.0/(X**2))*SUM
      FAC=-XSIGN*(2.0*Q+1.0)
      SALP=SALP+FAC*ALPN1
      SBET=SBET+FAC*BETN1
      CFAC=CMPLX(SBET,-SALP)*(2.0/X)
CCCCCCCCCCCCCCCCCCCCCCCCCCCCCCCCCCCCCCCCCCCCCCCCCCCCCCCCCCCCCCCCCCCCCCCCCCCC
C                                                                          C
C   THE VARIABLE FINF IS THE ABSOLTE VALUE OF THE BACKSCATTERING           C
C   FORM FUNCTION.THE VALUE OF (KA) AND (FINF) ARE OUTPUT BELOW.           C
C                                                                          C
CCCCCCCCCCCCCCCCCCCCCCCCCCCCCCCCCCCCCCCCCCCCCCCCCCCCCCCCCCCCCCCCCCCCCCCCCCCC
```

```
      FINF=CABS(CFAC)
      KAM(K)=X
      FABS(K)=FINF
      WRITE(6,40) KAM(K),FABS(K)
   40 FORMAT(5X,F10.2,2F14.4)
      IF(X.GE.XMAX) GO TO 50
      GO TO 10
   50 CONTINUE
      STOP
      END
C
C
C
      SUBROUTINE STVAL(X,X1,X2,ALPN,BETN,CBN1,BN1,SNN1,RH,XSN,X2S
     &,XCS)
      TERM=CBN1*X1
      FN=-X2S*RH*TERM/((X2S/2.0)-2.0*TERM)
      SNN1=-((XCS/(X**2))+(XSN/X))
      GN=(FN*(XSN/X))+(BN1*X)
      HN=(-(FN*XCS)/X)+(X*SNN1)
      DEN=(GN**2)+(HN**2)
      ALPN=-(GN**2)/DEN
      BETN=-(GN*HN)/DEN
      RETURN
      END
C
C
C
      SUBROUTINE BESS(X,PA,T)
      DIMENSION PA(300)
      L=IFIX(T)+15
      PA(L+2)=0.0
      PA(L+1)=1.0E-30
      DO 10 I=1,L
      M=(L+1)-I
      R=FLOAT(M)
      PA(M)=(((2.0*R)+1.0)*PA(M+1)/X)-PA(M+2)
   10 CONTINUE
      RETURN
      END
```